A Study of Multiple Guide Optical Couplers

Edward Milczarek

A Thesis in the Department of

Electrical and Computer Engineering

Presented in Partial Fulfillment of the Requirements

for the degree of Master of Applied Science at

Concordia University

Montréal,Québec,Canada

March 1993

ISBN 0-315-84633-X

Canada

ABSTRACT

A Study of Multiple Guide Optical Couplers

Edward Milczarek

This thesis introduces coupled mode theory and uses it to study the transfer characteristics of multiple guide optical couplers. Two and three guide couplers are examined to determine their effectiveness as power transfer devices, and the implementation of two and three guide switches is discussed.

A novel approach to designing a three guide coupler is introduced, where a feedback loop is placed around one of the guides. It is demonstrated that this device exhibits desirable characteristics that are not available by current passive coupler designs: splitting any fraction of a signal between two separate waveguides while maintaining a zero phase shift between the outputs, as well as combining two signals of arbitrary amplitude and phase. The wavelength dependence of this device is examined, and its potential as a wavelength selective filter or wavelength division multiplexer is demonstrated.

Various computer programs have been developed to aid in the analysis of optical couplers including one that animates the eigensolutions of the device as signals propagate though its length. The technique of eigensolution decomposition is used to illustrate the relationship between coupling parameters of multiple N-guide couplers such that they may either achieve complete transfer of power between guides or act as interferometers.

Contents

List of Figures

Chapter 1

Introduction

The transfer of power between guided modes of parallel waveguides is known as directional coupling. Directional coupling has long been a subject of interest in the field of integrated optics [1]. Directional couplers can serve as signal routing devices, switches, modulators, multiplexers and can perform various signal processing functions [2,3,4]. Directional couplers are key components in Mach-Zehnder, Michelson and Sagnac interferometers [5] used in a variety of optical communications and sensor applications [6]. Directional couplers are also employed in the fabrication of high power semiconductor lasers.

The most common tool of mathematical analysis used to study optical couplers is coupled mode theory, developed by J. R. Pierce [7,8] to analyze the interaction of electron beam waves with electromagnetic waves in travelling wave tubes. It was further developed by Yariv [9], and by Kogelnik

and Shank [10], for the analysis of the effect of coupling in optical waveguides and distributed feedback lasers. Kogelnik and Schmidt [11] proposed cascaded directional couplers consisting of sections having alternating phase mismatch in which complete conversion of light from one guide to another was achieved by applying a voltage to electrodes placed over the waveguides. These so called $\Delta\beta$ couplers allow the signal to be electrically switched between crossover and straight-through states, and provide the capability to electrically tune out residual crosstalk.

Although two guide (four port) couplers perform the basic functions of signal rerouting and combining, three guide (six port) couplers have properties, mainly relating to their phase characteristics, which overcome several limitations of four port systems, making six port couplers the preferred device for several applications [12,13,14,15,16,17,18]. For example, it has been demonstrated that a three guide coupler can be used to build a fiber-optic gyroscope without the need of a 90° phase bias required by conventional gyroscopes [19,20]. In addition, symmetrical three guide couplers can be used as power dividers and combiners, whereas their two guide counterparts are asymmetrical.

In the second chapter of this thesis, we discuss the fundamental concepts of optical coupling using the example of a four port coupler. To overcome some of the limitations of the ordinary four port coupler, the switched $\Delta\beta$

directional coupler is introduced. It is demonstrated how switched directional couplers can be implemented using sections of alternating differential phase constant.

The third chapter presents the properties of the 3 × 3 coupler [21,22, 23,24,25]. Although most researchers limit their discussions to cases where coupling takes place only between adjacent waveguides, or nearest neighbors, a completely general derivation of the transfer characteristics of the 3 × 3 couplers are presented. This general derivation permits the study of devices consisting of waveguides that do not all lie in the same plane, such as in the case where the three guides are placed in an equilateral triangle, and all three guides are coupled to each other. Both closed form and numerical solutions for the transfer function of the 3 × 3 device are presented. Equations describing the device dependent coupling parameters and the system transfer function are presented in matrix form. Properties of these matrices are also discussed. It is demonstrated how 3 × 3 couplers can be used to form switching systems that require fewer stages than conventional systems consisting of switched $\Delta\beta$ 2 × 2 couplers.

In chapter 4, a 3 × 3 coupler with feedback is introduced. A loop connecting together an output port with an input port reduces the coupler to a four port device with characteristics that alleviate the limitations of both 2 × 2 and conventional 3 × 3 couplers. Two important advantages of this novel device,

which cannot be achieved by any other passive coupler presently available, are emphasized. We demonstrate that an arbitrary fraction of power can be transferred between the two guides of this feedback assisted 3×3 coupler, while maintaining a constant phase difference between the two outputs. We prove that this device has the capability to transfer power completely between two dissimilar guides and show how an electrically tuned device can be designed to combine two signals of arbitrary magnitude and phase. Finally, the wavelength dependence of the device is examined and its potential as a wavelength division multiplexer is evaluated.

The fifth chapter of this thesis deals with devices built using an arbitrary number of waveguides [26]. The method of analysis developed earlier in the study is used to determine how such devices can be designed to exhibit predescribed transfer characteristics.

Polarization effects are not considered in this study; rather, it is assumed that the waves are purely linearly polarized, and remain in that state throughout the system. This is a good approximation for a family of devices which are inherently polarization maintaining.

Chapter 2

Fundamental concepts

2.1 The 2×2 coupler

Unlike the bound electromagnetic field propagating in metallic waveguides at microwave and millimeterwave frequencies, those associated with optical wave propagation in open dielectric waveguides extend beyond the core medium into the cladding. True guided modes decay exponentially with the distance from the core boundary and are therefore evanescent in the cross section of the external region. If two open waveguides are brought into proximity, their evanescent fields will overlap, and power is transferred between guides as the signals propagate along the structure. If the separation between the two guides is large, the interaction is negligible, and the individual guides remain unperturbed. However, as the distance between the guides is decreased, the coupling strength increases exponentially and the presence of the neighboring guide can no longer be ignored. Fig. 2.1 illustrates a 2×2

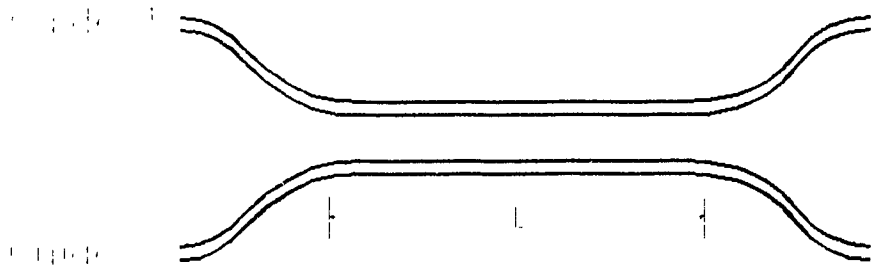

Figure 2.1: The 2 × 2 coupler.

directional coupler, where along the length L the guides are sufficiently close to interact. It will later be shown that, in the case of two identical guides, power between the guides is periodically completely exchanged. The minimum distance required to obtain complete crossover is referred to as the conversion or beat length, l.

A mathematical technique known as coupled mode theory can be used to solve for the interaction between weakly coupled guides. The analysis of the interaction that occurs between strongly coupled guides can be found in [27,28,29,30,31,32,33] . When the guides are sufficiently separated, the perturbation of one guide upon the other will be small, and the field distribution

of the coupled system can be represented as a superposition of the simpler, known solutions of the unperturbed systems.

The relationship between the perturbed and unperturbed field quantities which contribute to the coupled mode theory is governed by the Lorentz reciprocity theorem [34],

$$\iint_S \frac{\partial}{\partial z}(\mathbf{E}_t^* \times \mathbf{H}_t' + \mathbf{E}_t' \times \mathbf{H}_t^*) \cdot \hat{z}\, dS \qquad j\omega \iint_S (\epsilon' - \epsilon)\mathbf{E}' \cdot \mathbf{E}^* \, dS \qquad (2.1)$$

where z is the axial coordinate along which the signal travels, S represents the cross section of the system, the primed quantities refer to the perturbed fields, the unprimed quantities refer to the unperturbed fields, the asterisk denotes the complex conjugate, and the integration is over the entire cross section of the guide.

In this chapter coupled mode theory will be used to find solutions for the modal amplitudes in a 2×2 (two guide) system. The electric and magnetic fields for a single mode waveguide with constant permittivity along the propagation direction z are given by

$$\left.\begin{matrix} \mathbf{E}(x,y,z) & \mathbf{e}(x,y) \\ \mathbf{H}(x,y,z) & \mathbf{h}(x,y) \end{matrix}\right\} \exp(-j\beta z) \qquad (2.2)$$

where we use lower case symbols to represent normalized field distributions in the cross section of the guide, and where the $\exp(j\omega t)$ harmonic time dependence is suppressed.

The fields in the composite structure can be represented as:

$$\left\{ \begin{array}{c} \mathbf{E}'(x,y,z) \\ \mathbf{H}'(x,y,z) \end{array} \right\} = a_1(z) \left\{ \begin{array}{c} \mathbf{e}_1(x,y) \\ \mathbf{h}_1(x,y) \end{array} \right\} \exp(-j\beta_1 z) + a_2(z) \left\{ \begin{array}{c} \mathbf{e}_2(x,y) \\ \mathbf{h}_2(x,y) \end{array} \right\} \exp(-j\beta_2 z) \tag{2.3}$$

The fields represented by (2.2) and (2.3) are total fields, composed of both forward and backward propagating waves. However, we shall restrict our investigations in this thesis to uniform devices in which coupling from forward propagating waves to backward propagating waves does not occur. As a result, the field amplitudes $a_1(z)$ and $a_2(z)$ are those of forward propagating waves, where subscripts 1 and 2 denote the guides.

Substituting (2.2) and (2.3) into the Lorentz reciprocity theorem and invoking the orthogonality of the modal functions, we obtain the coupled mode equations. Considering guide 1 to be perturbed by guide 2 one obtains

$$\frac{da_1}{dz} = j[a_1(z)\kappa_{11} + a_2(z)e^{j(\beta_1-\beta_2)z}\kappa_{21}] \tag{2.4}$$

where the coupling coefficient is

$$\kappa_{m1} = \frac{\omega}{2}\iint_{S_2}(\epsilon_2 - \epsilon_s)\mathbf{e}_m \cdot \mathbf{e}_1^* dS \qquad m = 1,2 \tag{2.5}$$

The subscript 's' denotes the substrate, i. e. the region external to the guides. Integration is performed over the surface S_2, which encompasses the perturbing region, namely guide 2. Over this region of integration, $|\mathbf{e}_1|^2$ is negligible compared to $\mathbf{e}_2 \cdot \mathbf{e}_1^*$ and as a result κ_{11} is likewise negligible compared to κ_{12}. Thus, (2.4) can be approximated as

$$\frac{da_1}{dz} = -ja_2(z)\kappa_{21}e^{j(\beta_1 - \beta_2)z} \tag{2.6}$$

Similarly, in the case where guide 2 is perturbed by guide 1, we can write

$$\frac{da_2}{dz} = -ja_1(z)\kappa_{12}e^{-j(\beta_1 - \beta_2)z} \tag{2.7}$$

where

$$\kappa_{12} = \frac{\omega}{2}\iint_{S_1}(\epsilon_1 - \epsilon_s)\mathbf{e}_1 \cdot \mathbf{e}_2^* dS \tag{2.8}$$

Expressions (2.6) and (2.7) can be rewritten by defining the field amplitudes as

$$\begin{array}{rcl} E_1(z) & = & a_1(z)e^{-j\beta_1 z} \\ E_2(z) & = & a_2(z)e^{-j\beta_2 z} \end{array} \tag{2.9}$$

This definition transforms the set of differential equations governing the complex field amplitudes of signals propagating through the waveguides of a 2×2 coupler from (2.6) and (2.7) to

$$\frac{dE_1}{dz} = -j\beta_1 E_1 - j\kappa_{12}E_2 \tag{2.10}$$

$$\frac{dE_2}{dz} = -j\kappa_{21}E_1 - j\beta_2 E_2 \tag{2.11}$$

Conservation of power requires the total power flow in the system to be invariant of z. Thus for a forward coupler where power propagates in the $+z$ direction in both guides:

$$\frac{d}{dz}\left[E_1(z)E_1(z)^* + E_2(z)E_2(z)^*\right] = 0 \tag{2.12}$$

Forcing this condition on (2.10) and (2.11) results in the constraint for lossless systems: $\kappa_{12} = \kappa_{21}^*$.

2.2 Determining the transfer matrix

The set of differential equations described by (2.10) and (2.11) can be solved using methods of linear algebra as discussed in [35]. Casting these equations in matrix form we write

$$\frac{dE(z)}{dz} \quad j\mathbf{R}E(z) \tag{2.13}$$

where $\mathbf{R}$ is referred to as the coupling matrix:

$$\mathbf{R} \quad \begin{bmatrix} \beta_1 & \kappa_{12} \\ \kappa_{21} & \beta_2 \end{bmatrix} \tag{2.14}$$

The solution to (2.13) describes the field amplitudes at any position z along the system given an incident $E(0)$. Thus we can write,

$$E(z) \quad \mathbf{T}(z)E(0) \tag{2.15}$$

where, formally the transfer matrix $\mathbf{T}(z)$ can be expressed as [35]

$$\mathbf{T}(z) \quad \exp(\ j\mathbf{R}z) \tag{2.16}$$

Using the series expansion of the exponential matrix, the transfer matrix can also be written as

$$\mathbf{T}(z) = \mathbf{I} + j\mathbf{R}z - \frac{1}{2!}\mathbf{R}^2z^2 + j\frac{1}{3!}\mathbf{R}^3z^3 + \cdots \tag{2.17}$$

where $\mathbf{I}$ is the identity matrix. This formulation is convenient because the N^{th} power of a square matrix can easily be computed using Chebyshev polynomials of the second kind [36].

An alternate solution for the transfer matrix can be obtained by examining the properties of the eigenvectors and eigenvalues of the system. Denoting the eigenvectors of $\mathbf{T}(z)$ by $\bar{\mathsf{E}}_i$, $i = 1, 2$, and the eigenvalues by $p_{1,i}(z)$, the eigenvalue equation is

$$\mathbf{T}(z)\mathsf{E}_i = p_{1,i}(z)\mathsf{E}_i \tag{2.18}$$

In order to obtain the relationship between the eigenvalues and eigenvectors of $\mathbf{T}$ and $\mathbf{R}$, let us consider the input amplitude to coincide with an eigenvector, that is

$$\mathcal{E}(0) = \bar{\mathsf{E}}_i \tag{2.19}$$

From the nature of the eigenvector we obtain the amplitude at z as

$$E(z) \quad p_{Ti}(z)\mathsf{E}_i \tag{2.20}$$

Substituting (2.20) into (2.13) results in the eigenvalue equation for the coupling matrix, **R**:

$$j\frac{1}{p_{Ti}}\frac{dp_{Ti}(z)}{dz}\mathsf{E}_i \quad \mathbf{R}\mathsf{E}_i \quad p_{Ri}\mathsf{E}_i \tag{2.21}$$

which indicates that **R** and **T**(z) have a common set of eigenvectors, i.e. that they commute. From (2.21) the eigenvalues of **R**, p_{Ri}, are related to those of **T**(**z**) through [8]

$$p_{Ti}(z) \quad \exp(\ jp_{Ri}z) \tag{2.22}$$

The modal matrix **U** which diagonalizes **R** according to

$$\mathbf{U}^{-1}\mathbf{R}\mathbf{U} \quad \mathbf{P}_\mathbf{R} \quad diag\ p_{R1}\ \ p_{R2} \tag{2.23}$$

consists of the columns of the eigenvectors of the coupling matrix;

$$\mathbf{U} = [\mathsf{E}_1 \;\; \mathsf{E}_2] \tag{2.24}$$

Since $\mathbf{T}(z)$ and $\mathbf{R}$ have a common set of eigenvectors, U also diagonalizes $\mathbf{T}(z)$ according to

$$\mathbf{U}^{-1}\mathbf{T}(z)\mathbf{U} = \mathbf{P}_{\mathbf{T}}(z) \quad diag[\exp(-jp_{R1}z) \;\; \exp(-jp_{R2}z)] \tag{2.25}$$

Therefore $\mathbf{T}(z)$ can be evaluated from

$$\mathbf{T}(z) = \mathbf{U}\mathbf{P}_{\mathbf{T}}(z)\mathbf{U}^{-1} \tag{2.26}$$

The system is conservative if and only if the quadratic form [37] representing the power flow in the coupler

$$\sigma \quad E(z)^{\dagger}\mathbf{K}E(z) \tag{2.27}$$

is conserved. $\mathbf{K}$ is the so-called metric of the system, a 2×2 diagonal

matrix consisting of +1 elements for forward and −1 elements for backward propagating modes. Thus, conservation of power occurs when

$$\frac{d\sigma}{dz} = \frac{d\bar{E}(z)^\dagger}{dz}\mathbf{K}E(z) + E(z)^\dagger\mathbf{K}\frac{dE(z)}{dz} \quad jE(z)^\dagger(\mathbf{R}^\dagger\mathbf{K} \quad \mathbf{KR})E(z) \quad 0 \quad (2.28)$$

Since $\bar{E}(z)$ is arbitrary, we have

$$\mathbf{R}^\dagger\mathbf{K} \quad \mathbf{KR} \quad (2.29)$$

as the condition of energy conservation. Power conservation requires that the power flow entering and exiting the coupler be the same. In terms of the $\mathbf{T}(z)$ matrix, this requires

$$\bar{E}(0)^\dagger\mathbf{K}E(0) \quad E(z)^\dagger\mathbf{K}E(z) \quad E(0)^\dagger\mathbf{T}(z)^\dagger\mathbf{K}'\mathbf{T}(z)E(0) \quad (2.30)$$

to be valid for an arbitrary excitation vector $E(0)$, i. e. :

$$\mathbf{K} \quad \mathbf{T}(z)^\dagger\mathbf{K}\mathbf{T}(z) \quad (2.31)$$

For a forward coupler, $\mathbf{K} = \mathbf{I}$ the identity matrix, which means that in this case $\mathbf{R} = \mathbf{R}^t$ and $\mathbf{T}(z)\mathbf{T}(z)^\dagger = \mathbf{I}$. The consequences of this is that since the eigenvalues of a Hermitian matrix are real, therefore

$$\mathbf{U}\mathbf{U}^\dagger = \mathbf{I} \tag{2.32}$$

and the modulus of the transfer matrix eigenvalues must be unitary

$$\exp(-j\rho_{Bi}z) = 1 \tag{2.33}$$

2.3 Reduction of the coupling matrix

In general $\beta_1 \neq \beta_2$, so we can we denote the average propagation constant as

$$\beta_o = \frac{\beta_1 + \beta_2}{2} \tag{2.34}$$

and define the detuning parameters

$$\delta_i \quad \beta_i \quad \beta_o \qquad\qquad i \quad 1,2 \tag{2.35}$$

A linear transformation from the $E(z)$ basis to the $A(z)$ basis according to

$$A(z) \quad \begin{bmatrix} \exp(j\beta_o z) & 0 \\ 0 & \exp(j\beta_o z) \end{bmatrix} E(z) \tag{2.36}$$

will then produce the reduced coupling equation

$$\frac{dA(z)}{dz} \qquad j\mathbf{R}_{reduced}A(z) \tag{2.37}$$

where

$$\mathbf{R}_{reduced} \quad \begin{bmatrix} \delta_1 & \kappa_{12} \\ \kappa_{21} & \delta_2 \end{bmatrix}. \tag{2.38}$$

Using $\mathbf{R}_{reduced}$ often serves to simplify optical coupler analysis as it allows a common β_o term to be factored out. In cases where the device contains identical lines, $\mathbf{R}_{reduced}$ contains only zeros along the diagonal. When $\mathbf{R}_{reduced}$ is used to obtain the transfer characteristics of a coupler, the phase shift of the signals relative to the input is lost; however, magnitudes and relative

phase differences of signals in each of the guides are preserved. Actual phases (with respect to the input signals) are seldom needed but can nevertheless be regained using (2.36).

2.4 Transfer characteristics of a 2×2 coupler

The transfer matrix of a forward coupler defined by (2.14) with $\kappa = \kappa_{12} = \kappa_{21}^*$ and assuming β_i to be real, is

$$\mathbf{T}(z) = \begin{bmatrix} A & -jB \\ -jB^* & A^* \end{bmatrix} \tag{2.39}$$

Where

$$A \qquad \cos z\sqrt{|\kappa|^2 + (\Delta\beta/2)^2} + j(\Delta\beta/2)\left[\frac{\sin z\sqrt{|\kappa|^2 + (\Delta\beta/2)^2}}{\sqrt{|\kappa|^2 + (\Delta\beta/2)^2}}\right] \tag{2.40}$$

$$B \qquad \kappa\left[\frac{\sin z\sqrt{|\kappa|^2 + (\Delta\beta/2)^2}}{\sqrt{|\kappa|^2 + (\Delta\beta/2)^2}}\right] \tag{2.41}$$

and $\Delta\beta \quad (\beta_1 \quad \beta_2)$. As shown by (2.5), the coupling coefficients, κ, are obtained from an overlap integral that contains the difference of permittivities

and the product of field amplitudes. For the case of lossless media, these terms tend to be real. Section 3.5 provides an example of the parameters required to implement a 3×3 coupler in the case of a slab waveguide, and shows that the resultant coupling coefficient is indeed real. For brevity and without loss of generality, the remainder of this thesis will restrict κ to real values.

Examining (2.39) reveals that if and only if $\Delta\beta = 0$ can full transfer of power from one waveguide to the other be achieved. This transfer occurs periodically when the length of the coupler is

$$L_{cross} = (2\nu + 1)\frac{\pi}{2\kappa} \qquad \nu \quad integer \tag{2.42}$$

When all power is transferred from one guide to the other the coupler is said to be in the crossed state 'x'. In contrast, when no power is transferred to the neighboring guide the coupler is said to be in the bar state 'o'. The bar state occurs for a coupler length of

$$L_{bar} = \nu \frac{\pi}{\sqrt{\kappa^2 + (\Delta\beta/2)^2}} \qquad \nu \quad integer \tag{2.43}$$

The transfer characteristics of a 2×2 coupler with $\Delta\beta = 0$ is illustrated in Fig. 2.2 showing the output power of guides 1 and 2 as a function of

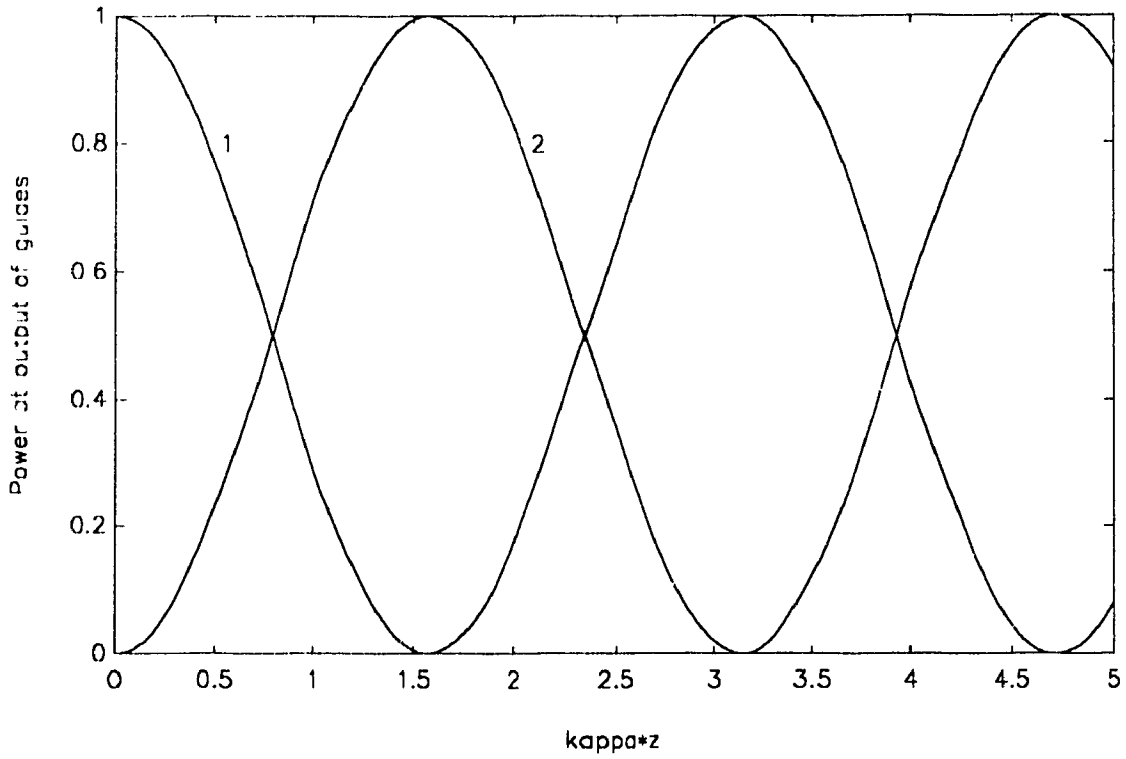

Figure 2.2: Transfer characteristics of the 2×2 coupler, with $\Delta\beta = 0$.

coupler length when unity power is applied to the input of guide 1. The figure demonstrates that, for a device with identical guides ($\Delta\beta = 0$), it is possible to achieve any ratio of power transfer between the two guides by fabricating a coupler of appropriate length. Note that if the guides are not identical, then complete power transfer cannot be achieved.

For the case of identical guides, A and B are real, and the transfer matrix (2.39) illustrates that the phase difference between the outputs of the two

guides remains identically 90°, regardless of the coupling state.

2.5 The principle of alternating $\Delta\beta$

Section 2.1 of this chapter introduced the basic 2 × 2 coupler. It was shown that a device consisting of identical waveguides can be designed to transfer a given fraction of the incident power to the coupled guide by choosing the appropriate coupling length. The major shortcoming of the 2 × 2 coupler is that once it is built, its length cannot be adjusted. If a fabrication error results in inaccurate device length, then power will not be coupled between guides in the desired proportion. For the particular case where the coupler was designed to achieve a cross state, an error in the uniformity, device length, or transverse distribution of material and geometrical parameters produces crosstalk, which is the residual power remaining in a guide that should have been depleted. In telecommunications applications, the level of permitted crosstalk is -20dB or lower, so one could potentially be left with a device that does not meet specification and must be rejected. Thus, accurate manufacturability is heavily dependent upon material and geometric exactitude.

Although the physical characteristics of a fabricated device cannot be ad

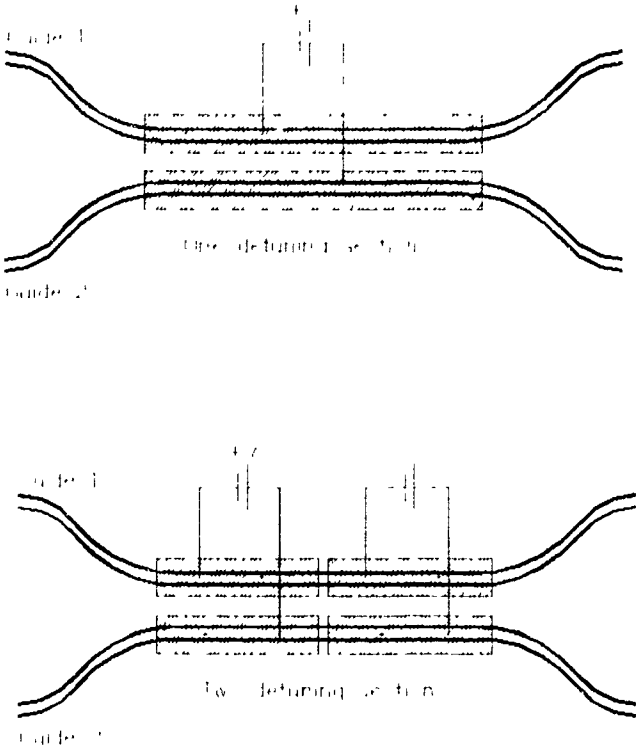

Figure 2.3: 2×2 couplers employing one and two tuning sections.

justed, it is possible to adjust the material parameters of the device through the electrooptic effect, by applying an electric field to the substrate using overlaid electrodes. This allows post-fabrication tuning of the device to perform as intended.

When a d .c. (or low frequency) electric field is applied to an electrooptic material, such as $LiNbO_3$, the refractive index varies with the strength of the applied field. This property can be used to electrically tune a coupling

device. If a voltage is applied across a pair of electrodes placed over one of the coupled guides, as illustrated by Fig. 2.3, the voltage creates an electric field (transverse to the z direction) which in turn induces a change in the refractive index and a change in the propagation constants of the guide, β_1 and β_2. This is referred to as a single detuning section. In the case where a single detuning section is employed, the applied voltage can be used to overcome differences in the propagation constants that occurred due to fabrication errors. Also, since the condition for a bar state is dependent upon the difference in propagation constants, application of a specific voltage may be used to switch from a cross state to a bar state. This allows the device to act as a switched directional coupler.

It will be shown that employing two detuning sections in cascade also allows the conversion length to be adjusted within a range of values. Thus, employing two detuning sections relaxes the restrictions on the fabrication parameters by compensating for fabrication errors in both the propagation constants as well as in the length of the device. In the case of two detuning sections, half the length of the coupler, from $z = 0$ to $z = L/2$, is exposed to a voltage inducing $\Delta\beta$, while the other half, from $z = L/2$ to $z = L$, is exposed to a voltage of opposite polarity, inducing $-\Delta\beta$ as illustrated in Fig. 2.3. This is referred to as detuning with sections of alternating $\Delta\beta$.

A device employing detuning sections has been analyzed [11,38] and

demonstrated experimentally [39]. The switching capability is best illustrated by a switching diagram. Fig. 2.4 shows the switching diagram of a directional coupler that employs a single detuning section. The abscissa is proportional to the phase mismatch created by the voltage, and the ordinate is the interaction length, L, normalized by the conversion length l.

Bar states are marked by o's, and cross states are marked by x's. States, either cross or bar, may be calculated by referring to the state equations introduced in the previous section. Cross states occur when $\kappa L = (2\nu+1)\pi/2$, which can be written in the form $L/l \quad 2\nu + 1$, since $l = \pi/2\kappa$. They occur at discrete points. The condition for a bar state is given by $(\kappa L)^2 + (\Delta\beta L/2)^2 = (\nu\pi)^2$, or, $(L/l)^2 + (\Delta\beta L/\pi)^2 = (2\nu)^2$. There are an infinite number of bar states, lying along the circles terminated by the o's. The diagram illustrates how a bar state can be reached for a device of arbitrary length by adjusting the $\Delta\beta$, which, in turn, is dependent on the voltage. However, stringent physical requirements on the length must still be met in order to achieve a cross state. Thus, fabrication errors cannot be completely compensated for by applying a single detuning voltage.

The requirements for cross states can be relaxed and the switching diagram can be fundamentally changed by using two detuning sections in cascade, featuring $\Delta\beta$'s of opposite signature. In this case, the transfer function from (2.39) must be modified to include the reversed $\Delta\beta$ section. The trans-

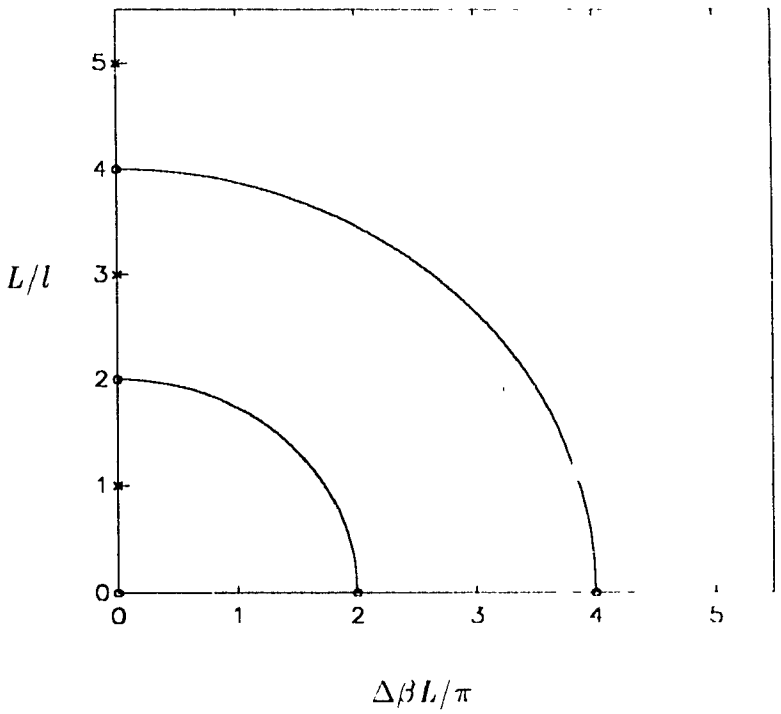

Figure 2.4: Switching diagram of a directional coupler employing a single tuning section.

fer function of the new system is simply the product of the transfer functions of each half section:

$$\begin{bmatrix} E_1(z) \\ E_2(z) \end{bmatrix} = \begin{bmatrix} A^* & jB \\ -jB^* & A \end{bmatrix} \begin{bmatrix} A & jB \\ jB^* & A^* \end{bmatrix} \begin{bmatrix} E_1(0) \\ E_2(0) \end{bmatrix}$$

$$\begin{bmatrix} |A|^2 & |B|^2 & j2BA^* \\ j2B^*A & |A|^2 & |B|^2 \end{bmatrix} \begin{bmatrix} E_1(0) \\ E_2(0) \end{bmatrix} \tag{2.44}$$

In this case, cross states occur when $|A|^2 - |B|^2 = 1 - 2B^2 = 0$, where A and B are described by (2.40) and (2.41), with $z = L/2$. This results in the cross state condition:

$$\frac{\kappa^2}{\kappa^2 + (\Delta\beta/2)^2} \sin^2\left(\frac{L}{2}\sqrt{\kappa^2 + (\Delta\beta/2)^2}\right) = \frac{1}{2} \tag{2.45}$$

The switching diagram of Fig. 2.5 depicts L/l as a function of $\Delta\beta L/2$ and illustrates that the cross state condition is translated into a family of curves that terminate on the vertical axis at the points $L/l = (2\nu + 1)$.

Bar states occur when $2A^*B = 0$, that is, either when $A = 0$ or when $B = 0$. Setting $\Delta\beta = 0$, $A = 0$ is satisfied when

$$\frac{L}{l} = 2(2\nu + 1) \qquad \nu = integer \tag{2.46}$$

This condition is represented by isolated points marked by o's on the vertical axis of the switching diagram. The second condition, $B = 0$, requires that

$$\left(\frac{L}{l}\right)^2 + \left(\frac{\Delta\beta L}{\pi}\right)^2 = (4\nu)^2 \qquad \nu = integer \tag{2.47}$$

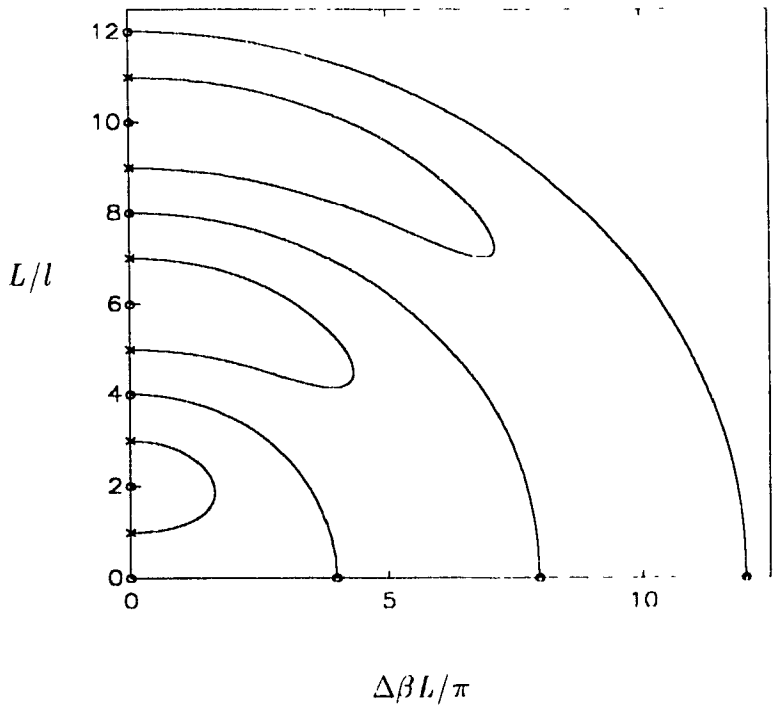

Figure 2.5: Switching diagram of an alternating $\Delta\beta$ coupler employing two tuning sections.

On Fig. 2.5 these points translate into the family of circles with radius 4ν.

Fig. 2.5 reveals that there exist ranges of L/l within which any desired amount of power transfer can be achieved by adjusting $\Delta\beta$. This is an important advantage, since it eliminates the restrictions on device length that make accurate fabrication difficult.

This method of applying two reversed $\Delta\beta$ sections can be extended to any number of cascaded alternating sections. As a result, the number of available switching states will increase with an increase in the number of alternating sections used.

Chapter 3

3×3 couplers

3.1 Introduction to 3×3 couplers

A device consisting of two waveguides in proximity of each other constitutes a four port 2×2 coupler. Similarly, when three guides are placed in proximity of each other, such as is illustrated in Fig. 3.1, a six port device known as a 3×3 coupler is formed. Three guide couplers can be implemented as integrated optical devices where the three guides lie in the same plane or as optical fiber devices where the guides form an equilateral triangle. Fig. 3.2 illustrates cross sectional views of these two configurations.

This chapter discusses how the 3×3 device can be used as a switch, a splitter, or a power combiner. We also examine how the three guide coupler can be used to overcome some of the limitations of two guide couplers. Because the three guide coupler has more ports than the two guide coupler, it has potentially more flexibility. When used in switching systems, the two

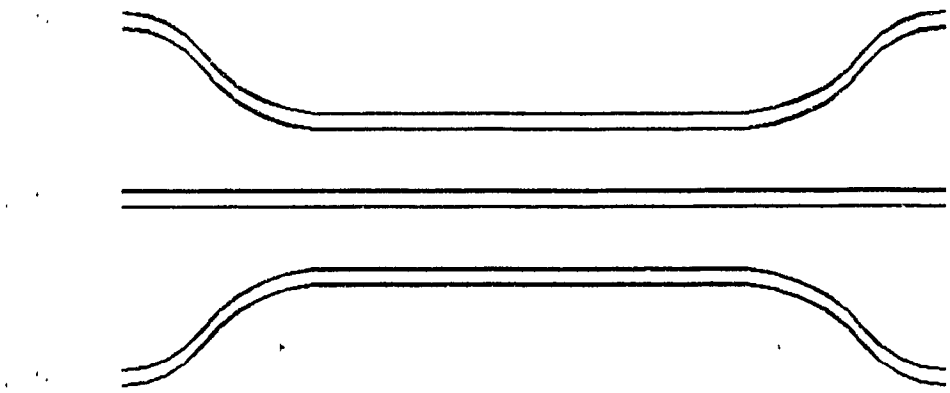

Figure 3.1: Schematic of a 3 × 3 coupler.

Figure 3.2: Cross sectional view of (a) integrated optical, and (b) optical fiber 3 × 3 couplers.

guide device acts on only two channels, whereas its three guide counterpart can act on three, resulting in a smaller switching system.

In the previous chapter, it was determined that although the 2 2 coupler is capable of splitting an input signal into two separate signals, the outputs will be 90° out of phase, requiring an external phase shifter for compensation. This chapter will discuss how the 3 · 3 coupler can act as a splitter with zero output phase difference.

In Section 3.2, the matrix method presented in Chapter 2 for determining the transfer function of the two guide coupler is extended for the 3 3 case. In Section 3.3 a Laplace transform solution to the coupled mode equations is presented. Section 3.4 examines the transfer characteristics of the 3 3 coupler when used to exchange power between the outer waveguides, as well as when used as a power combiner. In the former case, the effect of coupling between non-adjacent waveguides is considered. It is shown that complete power transfer between the outer guides is possible only when the coupling between them is neglegible. When used as a combiner, the signals propagating in the two outer guides can be combined in the center guide only when the applied input signals are of equal magnitude and phase. Section 3.5 discusses the implementation of a 3 · 3 coupler using the specific case of slab waveguides. In Section 3.6, it is shown that a 3 × 3 switch can be implemented using a 3 × 3 coupler with two sections of alternating phase

mismatch.

3.2 Coupling equations of a 3×3 coupler

In an integrated surface wave device the three guides all lie in the same plane. In optical fiber couplers the three guides are usually packed into an equilateral triangle. Since the distance between outside guides in an integrated surface wave device is relatively large, the coupling between those guides is often neglected. In contrast, in the case of the 3×3 optical fiber coupler, all coupling coefficients are equal and must be considered. Thus, in order to study the characteristics of three guide couplers, the coupled mode theory introduced in the previous chapter is used to determine the transfer matrix of a general 3×3 coupler having an arbitrary coupling matrix, constrained only by the assumptions of losslessness and co-directionality of propagation. Reciprocity does not constrain the elements of a coupling matrix ($\mathbf{R}$) of a uniform coupler, which admits coupling only among forward running waves. This can be shown by considering, for example, the scattering matrix of a six-port, such as that of a 3×3 coupler. When coupling occurs only in one direction, the scattering matrix of a reciprocal network is [40]

$$\mathbf{S} \quad \begin{bmatrix} 0 & \mathbf{S}_3^t \\ \mathbf{S}_3 & 0 \end{bmatrix} \tag{3.1}$$

where $\mathbf{S}_3$ is a 3×3 matrix relating the three output wave amplitudes to that of the three input amplitudes. There are no constraints among the elements of $\mathbf{S}_3$; $\mathbf{S}_3$ is exactly $\mathbf{T}$ as defined in (2.15).

The method that was used to obtain the set of differential equations governing the complex field amplitudes of signals propagating through the waveguides of a 2×2 coupler described by (2.10) and (2.11) can be extended to cover the case of three guides [41]. This results in

$$\frac{dE_1}{dz} \quad j\beta_1 E_1 \quad j\kappa_{12} E_2 \quad j\kappa_{13} E_3 \tag{3.2}$$

$$\frac{dE_2}{dz} \quad j\kappa_{12} E_1 \quad j\beta_2 E_2 \quad j\kappa_{23} E_3 \tag{3.3}$$

$$\frac{dE_3}{dz} \quad j\kappa_{13} E_1 \quad j\kappa_{23} E_2 \quad j\beta_3 E_3 \tag{3.4}$$

where β_i $(i = 1,2,3)$ is the propagation constant of the ith line and κ_{ij} is the coupling coefficient between the ith and jth lines.

A solution to the set of differential equations described by (3.2) (3.4) can be found using the methods of linear algebra that were outlined in Section

2.2. The equations are cast in their matrix form as in (2.13), where the coupling matrix is now given by

$$\mathbf{R} \quad \begin{bmatrix} \beta_1 & \kappa_{12} & \kappa_{13} \\ \kappa_{12} & \beta_2 & \kappa_{23} \\ \kappa_{13} & \kappa_{23} & \beta_3 \end{bmatrix} \tag{3.5}$$

T(z) is determined by evaluating (2.26). Since the order of the coupling matrix has increased to three, the system will generally have three distinct eigenvalues and three eigenvectors.

3.3 Laplace transform solution of the coupling equation

Although the solution to the coupled mode equations has been presented in Chapter 2, a Laplace transform solution to (3.2)-(3.4) is given here for completeness.

The differential equations (3.2) - (3.4) can be converted to a set of algebraic equations using their Laplace transforms,

$$E(z) \quad \mathcal{E}(s) \tag{3.6}$$

resulting in

$$s\mathcal{E}_1(s) \quad E_1(0) \quad j\beta_1\mathcal{E}_1(s) \quad j\kappa_{12}\mathcal{E}_2(s) \quad j\kappa_{13}\mathcal{E}_3(s) \tag{3.7}$$

$$s\mathcal{E}_2(s) \quad E_2(0) \quad j\kappa_{12}\mathcal{E}_1(s) \quad j\beta_2\mathcal{E}_2(s) \quad j\kappa_{23}\mathcal{E}_3(s) \tag{3.8}$$

$$s\mathcal{E}_3(s) \quad E_3(0) \quad j\kappa_{13}\mathcal{E}_1(s) \quad j\kappa_{23}\mathcal{E}_2(s) \quad j\beta_3\mathcal{E}_3(s) \tag{3.9}$$

In matrix form,

$$\mathbf{M}\mathcal{E}(s) \quad E(0) \tag{3.10}$$

where

$$\mathbf{M} = \begin{bmatrix} s + j\beta_1 & j\kappa_{12} & j\kappa_{13} \\ j\kappa_{12} & s + j\beta_2 & j\kappa_{23} \\ j\kappa_{13} & j\kappa_{23} & s + j\beta_3 \end{bmatrix} \tag{3.11}$$

The solution for $\mathcal{E}(s)$ is

$$\mathcal{E}(s) \quad \mathbf{M}^{-1}E(0) \tag{3.12}$$

The inverse of the matrix M is given by

$$\mathbf{M}^{-1}$$

$$\frac{1}{D}\begin{bmatrix} s^2+j\beta_2 s+j\beta_3 s-\beta_2\beta_3+\kappa_{23}^2 & \kappa_{12}\kappa_{23}-j\beta_1\kappa_{12}-\kappa_{13}\kappa_{23} & j\kappa_{12}s+\kappa_{13}\kappa_{23}-\kappa_{12}\beta_3 \\ \kappa_{12}\kappa_{23}-j\beta_1\kappa_{12}-\kappa_{13}\kappa_{23} & s^2+j\beta_1 s+j\beta_3 s-\beta_1\beta_3+\kappa_{13}^2 & -j\kappa_{12}s+\kappa_{13}\kappa_{23}-\kappa_{12}\beta_3 \\ j\kappa_{12}s+\kappa_{13}\kappa_{23}-\kappa_{12}\beta_3 & -j\kappa_{12}s+\kappa_{13}\kappa_{23}-\kappa_{12}\beta_3 & s^2+j\beta_1 s+j\beta_2 s-\beta_1\beta_2+\kappa_{12}^2 \end{bmatrix} \tag{3.13}$$

Where D is the determinant of M:

$$\begin{aligned} D \quad & s^3+js^2(\beta_1+\beta_2+\beta_3)+s(\kappa_{12}^2+\kappa_{13}^2+\kappa_{23}^2-\beta_1\beta_2-\beta_1\beta_3-\beta_2\beta_3) \\ & +j(\kappa_{12}^2\beta_3+\kappa_{13}^2\beta_2+\kappa_{23}^2\beta_1-\beta_1\beta_2\beta_3-2\kappa_{12}\kappa_{13}\kappa_{23}) \end{aligned} \tag{3.14}$$

Following algebraic simplification, the components of $\bar{\mathcal{E}}(s)$ can be expressed as

$$\mathcal{E}_i(s) \quad \frac{a_i s^2+b_i s+c_i}{(s-\bar{s}_1)(s-\bar{s}_2)(s-\bar{s}_3)} \qquad i=1..3 \tag{3.15}$$

where s_1, s_2, and s_3 are the three roots of $D=0$ and

$$a_i \quad E_i(0) \tag{3.16}$$

$$b_i = E_i(0)[j(\beta_{i+1} - \beta_{i-1}) + E_{i-1}(0)|-j\kappa_{i,i-1}| + E_{i+1}(0)|-j\kappa_{i,i+1}| \quad (3.17)$$

$$c_i = -E_i(0)\left[\kappa^2_{i+1,i-1} + \beta_{i+1}\beta_{i-1}\right] + E_{i-1}(0)[\kappa_{i,i-1}\beta_{i+1} - \kappa_{i,i+1}\kappa_{i+1,i-1}] + E_{i+1}(0)[\kappa_{i+1,i-1}\beta_{i-1} - \kappa_{i,i+1}\kappa_{i+1,i-1}] \quad (3.18)$$

($i = 1,2,3$ in cyclic order).

A trigonometric solution for the roots, s_i, of the cubic equation (3.14) is given by

$$s_i = -\frac{1}{3}u + C\cos\left[\theta + \frac{2}{3}\pi(i-1)\right] \quad (3.19)$$

where

$$C = 2\sqrt{\left(\frac{u}{3}\right)^2 - \frac{v}{3}} \quad (3.20)$$

$$\theta = \frac{1}{3}\cos^{-1}\left[\frac{uv}{3} - u^3 - 2\left(\frac{u}{3}\right)^3 - .25C^3\right] \quad (3.21)$$

and

$$u \quad j(\beta_1 + \beta_2 + \beta_3) \tag{3.22}$$

$$v \quad \kappa_{12}^2 + \kappa_{13}^2 + \kappa_{23}^2 \quad \beta_1\beta_2 - \beta_1\beta_3 - \beta_2\beta_3 \tag{3.23}$$

$$w \quad j(\kappa_{12}^2\beta_3 + \kappa_{13}^2\beta_2 + \kappa_{23}^2\beta_1 \quad \beta_1\beta_2\beta_3 - 2\kappa_{12}\kappa_{13}\kappa_{23}) \tag{3.24}$$

Once $\mathcal{E}_i(s)$ is known, $E_i(z)$ is obtained by taking the inverse Laplace transform of (3.15). The result is

$$\begin{aligned} E_i(z) \quad - \quad & \frac{a_i s_1^2 + b_i s_1 + c_i}{(s_1 \quad s_2)(s_1 - s_3)} \exp(s_1 z) + \\ & \frac{a_i s_2^2 + b_i s_2 + c_i}{(s_2 - s_1)(s_2 - s_3)} \exp(s_2 z) + \\ & \frac{a_i s_3^2 + b_i s_3 + b_i}{(s_3 \quad s_1)(s_3 - s_2)} \exp(s_3 z) \end{aligned} \tag{3.25}$$

($i \quad 1,2,3$ in cyclic order).

Result (3.25) describes the amplitude at z in guide i for an arbitrary input excitation $E(0)$. The elements of the transfer function, $\mathbf{T}(z)$, are obtained from (3.25) through

$$T_{ij}(z) \quad E_i(z) \Big|_{E_j(0)=1,\ E_{k\neq j}(0)=0} \tag{3.26}$$

This is to say that the element T_{ij} is computed by evaluating $E_i(z)$ in (3.25) with the input to guide j, $E_j(0)$, set to unity and the input to guides other than j set to zero.

In deciding whether the method given in (2.26) or in (3.26) should be used to compute $\mathbf{T}(z)$ it is important to consider the accuracy and the computation time required for their evaluation. The performance of a computer program using expression (3.25) can be evaluated by counting the number of floating point operations required in obtaining the result. This number is constant regardless of the number of system parameters. However, the method described in Section 3.2 requires calculating the eigenvalues and eigenvectors of the coupling matrix $\mathbf{R}$. Numerical methods used to determine these results employ successive iterations. The number of iterations required to obtain the result changes with the conditioning of the $\mathbf{R}$ matrix, which makes it difficult to make a good comparison between the two methods discussed. Tests have been performed to measure the number of floating point operations used by both methods, and the results indicate that finding the transfer function by computing the matrix exponential of $j\mathbf{R}z$ is up to 2 times faster than computing the closed form solution. In fact, software

packages, such as MATLAB [42], that are designed to deal with matrices very efficiently can improve calculation speed by as much as six times over that required by the method described in this section.

It should be noted that calculating the matrix exponential via eigenvalues and eigenvectors is not the only numerical method available. Many other methods exist, including one that uses a Taylor series approximation and another that uses the Padé approximation. Algorithms and discussions of these methods can be found in [43]. It was found that neither of the aforementionned methods were more efficient or more accurate than the direct computation of the matrix exponential.

The method employed in Section 2.3 can also be used to simplify the 3×3 system matrix; (2.13) can be reduced by factoring out the average β_o term from the propagation constants of the three guides using the transformation

$$A(z) = \tilde{E}(z)\exp(j\beta_o z) \tag{3.27}$$

where, for the case of three guides,the arithmetic average of the propagation constants is given by

$$\beta_o = \frac{\beta_1 + \beta_2 + \beta_3}{3} \tag{3.28}$$

Thus, the equivalent of $\mathbf{R}_{reduced}$ of (2.38) for the three guide case is

$$\mathbf{R}_{reduced} \quad \begin{bmatrix} \delta_1 & \kappa_{12} & \kappa_{13} \\ \kappa_{12} & \delta_2 & \kappa_{23} \\ \kappa_{13} & \kappa_{23} & \delta_3 \end{bmatrix}. \tag{3.29}$$

where

$$\delta_i \quad \beta_i \quad \beta_0 \tag{3.30}$$

This serves to simplify the analysis involving couplers because it allows a common β_0 term to be factored out early in the analysis.

3.4 Transfer characteristics of 3×3 couplers

The transfer characteristics of couplers are best studied by examining how complex wave amplitudes vary along the length of the device. It is often easier to examine amplitude and phase information separately, therefore, graphs illustrating the power in each guide as a function of device length are common in the study of optical couplers. Graphs describing the phase of the signal along one guide relative to a reference guide are also provided when phase information is relevant. Such graphs are used to analyze the

behavior of the 3 × 3 coupler when used to transfer power between guides, as well as when used as a combiner. In this study, complex amplitude plots have also been introduced, and a computer program has been developed that graphically animates the complex amplitudes of the signals as a function of length.

As a first example, consider a device consisting of three identical lines ($\beta_1 \quad \beta_2 \quad \beta_3 \quad \beta$) in a surface wave configuration as depicted by Fig. 3.1. The coupling between guides 1 and 3 is much smaller than the coupling between adjacent guides and will be ignored ($\kappa_{13} = 0$). The coupler is also assumed to be transversely symmetric, with ($\kappa_{12} = \kappa_{23} = \kappa$). As a result, the coupling matrix for the device is given by

$$\mathbf{R} = \begin{bmatrix} \beta & \kappa & 0 \\ \kappa & \beta & \kappa \\ 0 & \kappa & \beta \end{bmatrix} \tag{3.31}$$

The transfer matrix is determined by evaluating (3.26). After considerable algebraic manipulation, the transfer matrix is found to be

$$\mathbf{T} \quad \exp(-j\beta z) \begin{bmatrix} X + .5 & Y & X - .5 \\ Y & 2X & Y \\ X - .5 & Y & X + .5 \end{bmatrix} \tag{3.32}$$

where

$$X = \frac{1}{2}\cos(\sqrt{2}\kappa z) \tag{3.33}$$

and

$$Y = \frac{j}{\sqrt{2}}\sin(\sqrt{2}\kappa z) \tag{3.34}$$

The complex field amplitudes of the waves travelling within the device at any position z are described by

$$E(z) = \mathbf{T}(z)E(0) \tag{3.35}$$

For the case where only the first guide of the device is initially excited by a wave with unity amplitude,

$$E(0) = [1 \quad 0 \quad 0]^t \tag{3.36}$$

the output at $z = L$ is

$$E_1(L) = \frac{1}{2}\cos(\sqrt{2}\kappa L) + \frac{1}{2} \tag{3.37}$$

$$E_2(L) \qquad \frac{J}{\sqrt{2}} \sin(\sqrt{2}\kappa L) \tag{3.38}$$

$$E_3(L) \qquad \frac{1}{2}\cos(\sqrt{2}\kappa L) \quad \frac{1}{2} \tag{3.39}$$

These expressions reveal that the power is periodically exchanged as the signal travels within the device. The power in guide 2 never exceeds half the input power and a complete transfer of power into guide 3 occurs whenever

$$z \qquad \frac{(2n \cdot 1)\pi}{\sqrt{2}\kappa} \tag{3.40}$$

where n is any non-negative integer. The first occurrence of complete power transfer from one outside guide to the other occurs when $n \quad 0$, thus the shortest conversion length is

$$l \quad \pi \sqrt{2}\kappa \tag{3.41}$$

\ graph demonstrating these periodic oscillations of power exchange is provided in Fig. 3.3.

It is important to emphasize that *complete* transfer of power from one guide to another can only be achieved when the coupling between the outside

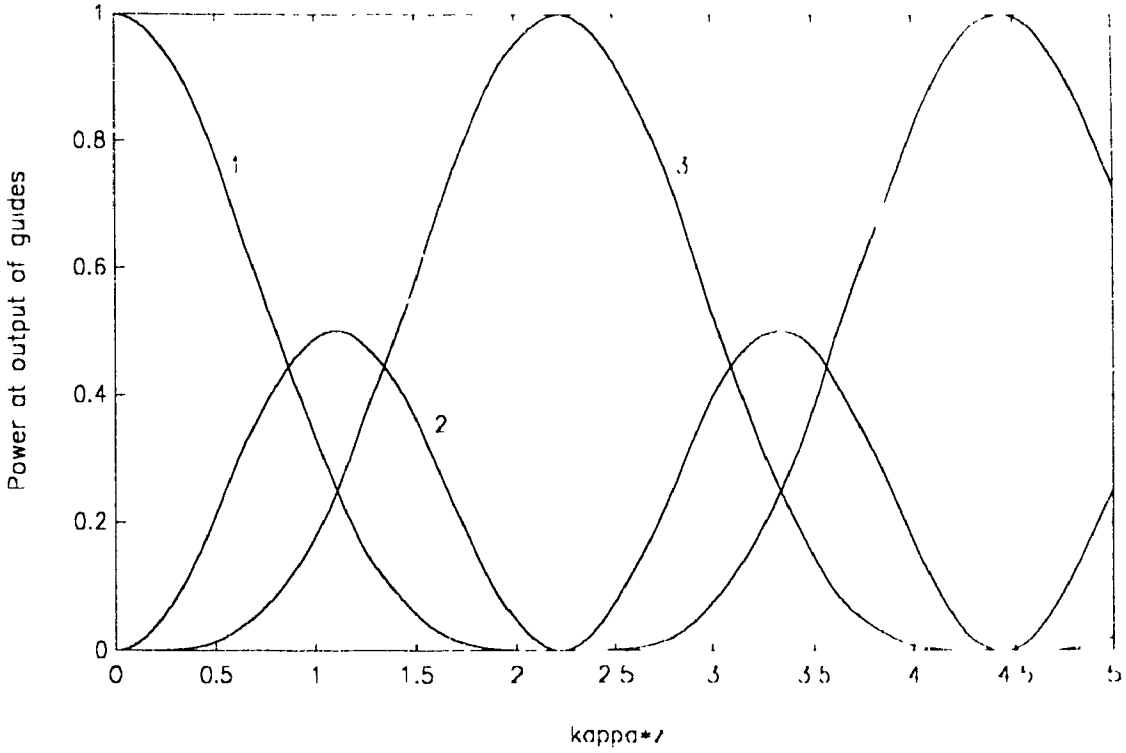

Figure 3.3: Transfer characteristic of the 3 × 3 coupler.

guides is neglected. To reinforce this point, consider the situation where the coupling between outside guides is no longer neglected. Assuming the coupling between neighboring guides to be 25 times that of the coupling between outer guides, the coupling matrix becomes

$$\mathbf{R} \quad \begin{bmatrix} \beta & \kappa & \frac{1}{25}\kappa \\ \kappa & \beta & \kappa \\ \frac{1}{25}\kappa & \kappa & \beta \end{bmatrix} \tag{3.12}$$

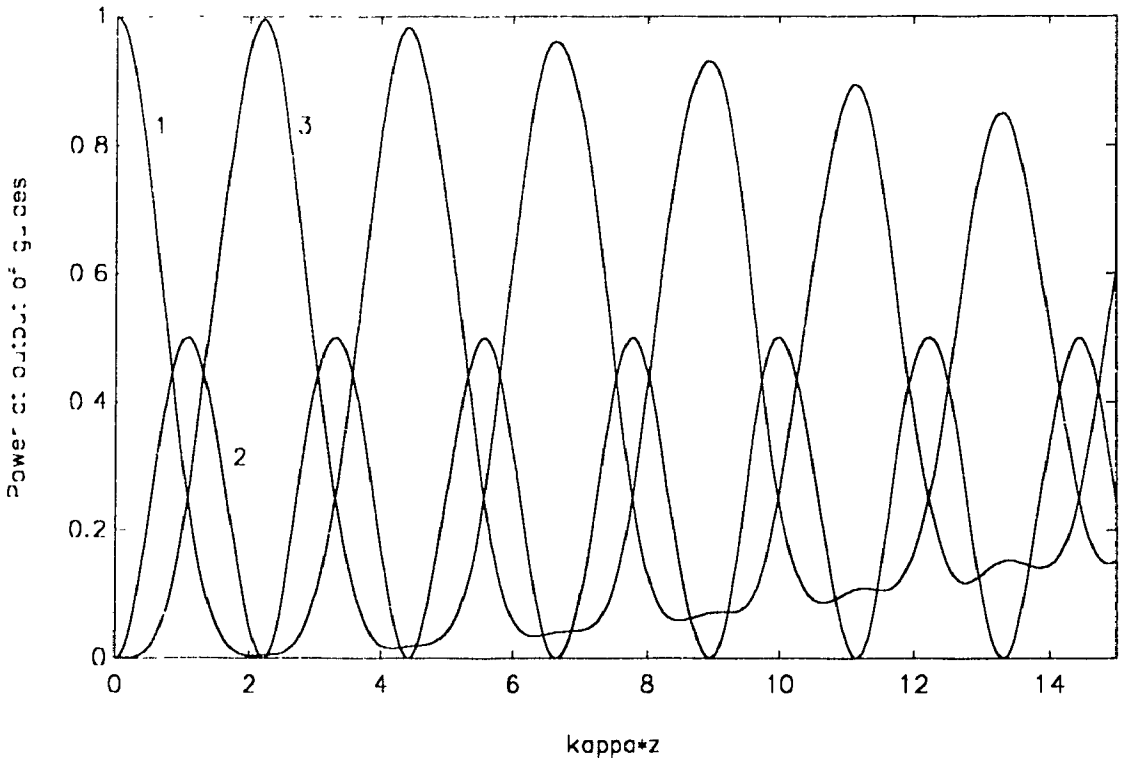

Figure 3.4: Transfer characteristic of the 3×3 coupler with $\kappa_{1,3} = 25\kappa$.

The transfer characteristic of this device can be determined numerically by evaluating (3.26), resulting in Fig. 3.4. It shows that although an exchange of power among the three guides still occurs, power is not transferred entirely to any one of the guides. Thus, the non-zero $\kappa_{1,3}$ limits the switching capability of the device.

Let us now consider power combining in a 3×3 coupler characterized by coupling and transfer matrices given by (3.21) and (3.32) respectively.

Assume an input excitation

$$E(0) \quad \begin{bmatrix} 1 & 0 & 1 \\ \sqrt{2} & & \sqrt{2} \end{bmatrix}^{t} \tag{3.13}$$

i. e. , identical signals are applied to the outer guides, and no input is fed into the center guide. The output of the device is given by (3.35), resulting in

$$E_1(L) \qquad E_3(L) \quad \frac{1}{\sqrt{2}} \cos(\sqrt{2}\kappa L) \tag{3.14}$$

$$E_2(L) \qquad j \sin(\sqrt{2}\kappa L) \tag{3.15}$$

These results are illustrated in Fig. 3.5, and show that a complete transfer of power from the outside guides into the center guide occurs at half the conversion length, i. e. at $l \quad \pi/2\sqrt{2}\kappa$.

The usefulness of the 3×3 coupler as a power combiner is limited by the fact that the signals to be combined must be of equal magnitude and phase. To illustrate this point, consider the case where the input signals are of the same amplitude but have a phase difference of ϕ. The input vector can be represented by

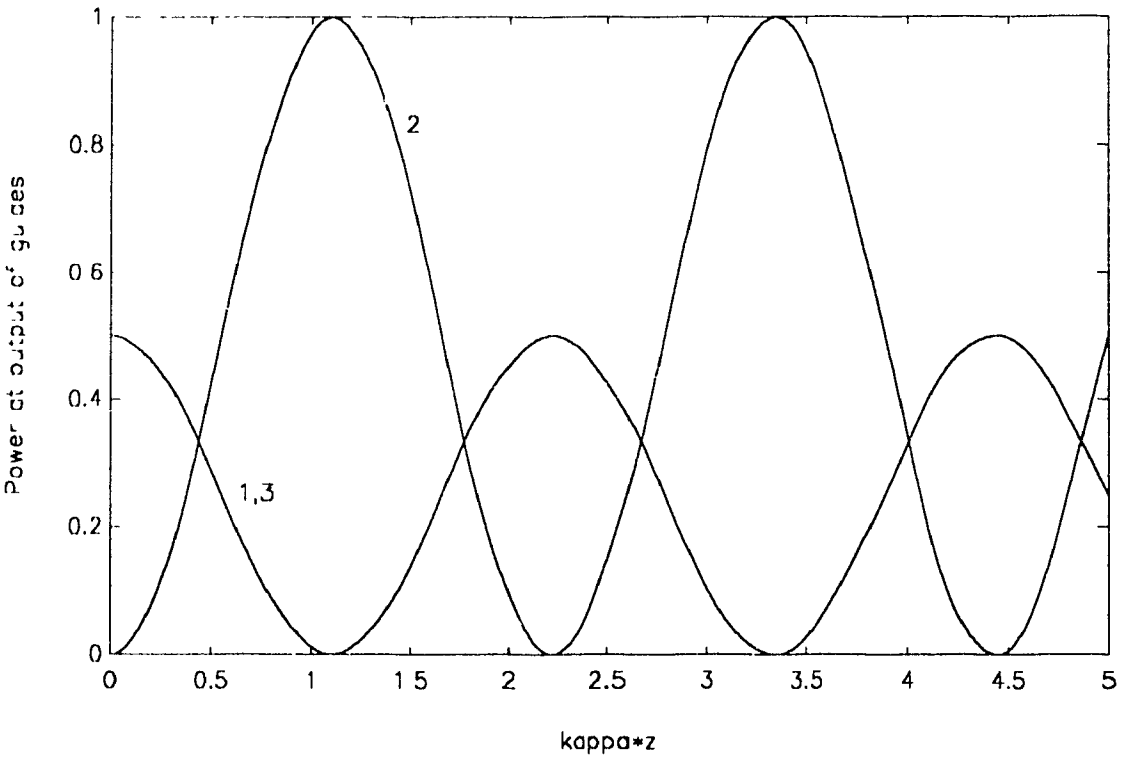

Figure 3.5: Transfer characteristic of the 3 × 3 coupler used as a power combiner for applied signals in guides 1 and 3 of equal magnitude and phase.

$$E(0) = \left[\frac{1}{\sqrt{2}} \quad 0 \quad \frac{1}{\sqrt{2}}\angle\phi^{o}\right]^{t} \tag{3.46}$$

When the phase of the input signals differs by 180°, for example, substituting (3.46) into (3.35) results in

$$E_1(L) \qquad E_1(0) \tag{3.17}$$

$$E_2(L) \qquad 0 \tag{3.18}$$

$$E_3(L) \qquad E_3(0) \tag{3.19}$$

This demonstrates that no power is transferred between the guides when a phase shift of 180° exists between the input signals. To consider the effect of other values of phase shift, the value of ϕ in (3.46) was varied, and substituted into (3.35) to study the resulting signals in all three guides. Fig. 3.6 plots the percentage of total power coupled into the center guide as a function of the phase difference between the equal magnitude signals applied to the inputs of guides 1 and 3. Complete power transfer occurs only when the phase shift is zero. Thus, when a phase difference exists between the input signals $E_1(0)$ and $E_2(0)$, an external device to eliminate this phase difference would be required.

A similar analysis can be effected for the case where the magnitude of the signals applied to guides 1 and 3 differs. In this case, it may be shown that the percentage of total power coupled into the center guide would decrease with the difference in magnitude between the two input signals and that total power transfer occurs only with identical input signals.

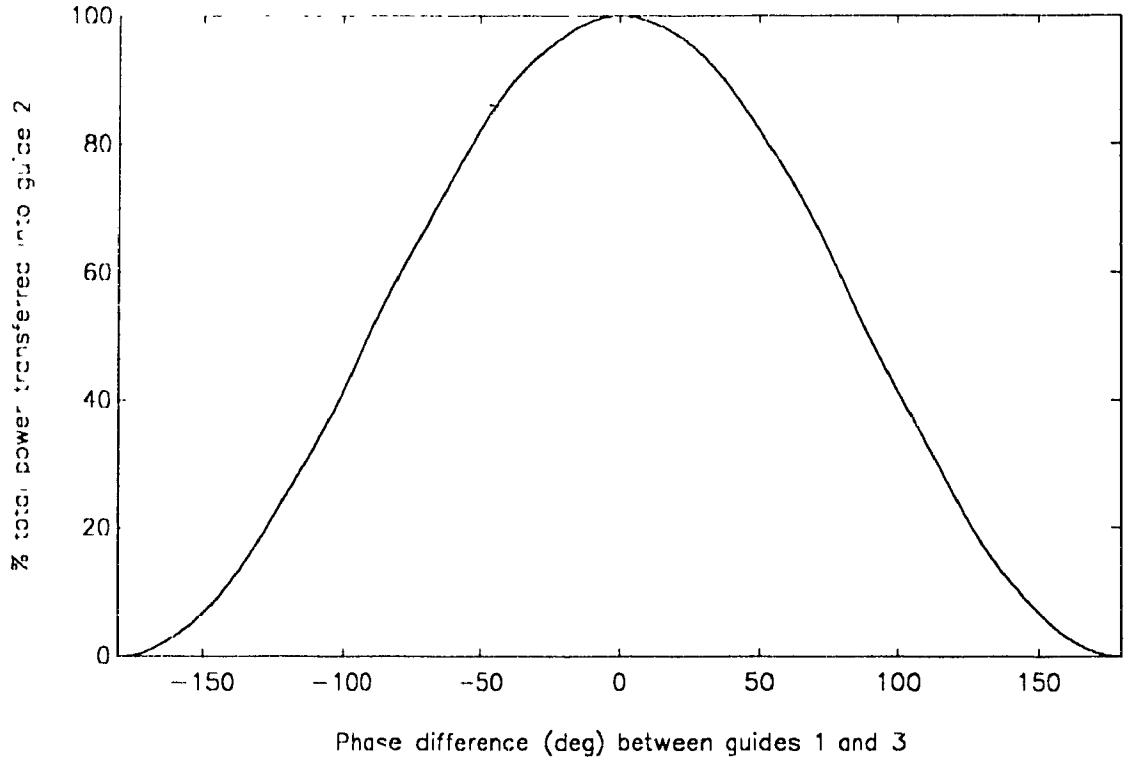

Figure 3.6: Percent of total power transferred into guide 2 of a 3×3 coupler with guides 1 and 3 excited by signals of equal magnitude and varying phase.

Up to this point, we have used graphs that plot the amplitude and phase of signals as they propagate through the three guides of a device in order to analyze the characteristics of a coupler. In what follows we introduce a novel method of graphically animating the complex wave amplitudes as they evolve along the length of the device. A computer program was developed to compute eigensolutions of the system, which are then depicted using circular plots.

Consider the eigenmodes of the 3 × 3 device. To each eigenmode or eigenvector $\bar{u}_i$ there corresponds an eigenvalue, $\exp(-jp_i z)$, where the p_i is an eigenvalue of the coupling matrix, **R**. The eigenmodes rotate at the rate $\exp(-jp_i z)$ as the signal propagates along the coupler. Since the eigenvectors represent a complete set, any excitation can be represented as a linear combination of the eigensolutions.

For a general input excitation of

$$\bar{E}(0) = c_1 u_1 + c_2 u_2 + c_3 u_3 \tag{3.50}$$

the output of the coupler is

$$\bar{E}(z) = c_1 \exp(-jp_1 z)\bar{u}_1 + c_2 \exp(-jp_2 z)u_2 + c_3 \exp(-jp_3 z)u_3 \tag{3.51}$$

In matrix form:

$$\begin{bmatrix} E_1(0) \\ E_2(0) \\ E_3(0) \end{bmatrix} = \mathbf{U} \begin{bmatrix} c_1 \\ c_2 \\ c_3 \end{bmatrix} \tag{3.52}$$

and

$$\begin{bmatrix} E_1(z) \\ E_2(z) \\ E_3(z) \end{bmatrix} \quad \mathbf{U} \begin{bmatrix} \exp(\ jp_1 z) & 0 & 0 \\ 0 & \exp(\ jp_2 z) & 0 \\ 0 & 0 & \exp(-jp_3 z) \end{bmatrix} \begin{bmatrix} c_1 \\ c_2 \\ c_3 \end{bmatrix} \tag{3.53}$$

where **U** is a matrix whose columns are the eigenvectors of the system and the c_i's are the modal amplitudes, or weight coefficients. The c_i's are determined from the initial condition which can be obtained from (3.52), namely

$$\begin{bmatrix} c_1 \\ c_2 \\ c_3 \end{bmatrix} = \mathbf{U}^{-1} \begin{bmatrix} E_1(0) \\ E_2(0) \\ E_3(0) \end{bmatrix} \tag{3.54}$$

A computer program, CLOCKS.M listed in the Appendix, has been developed to aid the user in visualizing the eigensolutions as they evolve with their respective propagation constants. The program plots both the amplitude and phase for the three elements of the eigensolutions; that is, the individual eigenvectors multiplied by their respective weight coefficients derived from (3.54) as they vary along the length of the device. Also, the sum of the eigensolutions in each guide is plotted to illustrate the complex wave amplitude and phase at that position within the device.

To better illustrate how a graphical approach can be helpful in analyzing these devices, the example at the beginning of this section will be used, where unity input was applied to guide 1, and no input was applied to the other

two guides. The coupling matrix provided in (3.31) can be put in the form of a reduced coupling matrix according to (3.29)

$$\mathbf{R}_{reduced} \quad \begin{bmatrix} 0 & \kappa & 0 \\ \kappa & 0 & \kappa \\ 0 & \kappa & 0 \end{bmatrix} \tag{3.55}$$

The eigenvalues are

$$p_1 \qquad \sqrt{2}\kappa \tag{3.56}$$

$$p_2 \qquad 0 \tag{3.57}$$

$$p_3 \qquad \sqrt{2}\kappa \tag{3.58}$$

and the matrix consisting of the eigenvectors is

$$\mathbf{U} \quad \frac{1}{2}\begin{bmatrix} 1 & \sqrt{2} & 1 \\ \sqrt{2} & 0 & \sqrt{2} \\ 1 & \sqrt{2} & 1 \end{bmatrix} \tag{3.59}$$

The inverse of (3.59) is

$$\mathbf{U}^{-1} \quad \frac{1}{2}\begin{bmatrix} 1 & \sqrt{2} & 1 \\ \sqrt{2} & 0 & \sqrt{2} \\ 1 & \sqrt{2} & 1 \end{bmatrix} \tag{3.60}$$

and the weight coefficients corresponding to the initial condition given in (3.36) are

$$c = \frac{1}{2}\begin{bmatrix} 1 & \sqrt{2} & 1 \\ -\sqrt{2} & 0 & \sqrt{2} \\ 1 & \sqrt{2} & -1 \end{bmatrix}\begin{bmatrix} 1 \\ 0 \\ 0 \end{bmatrix} = \frac{1}{2}\begin{bmatrix} 1 \\ -\sqrt{2} \\ -1 \end{bmatrix} \tag{3.61}$$

The top of Fig. 3.7 shows the complex modal amplitudes for each of the coupled guides at $z = 0$. These amplitudes are obtained from (3.54) using $E(0) = [1\ 0\ 0]^t$, signifying that unit amplitude with zero phase reference is applied to guide 1 at $z = 0$. The three 'clocks' in the first row, denoted by 'Line 1', show the values of the eigensolutions $U_{11}c_1$, $U_{12}c_2$ and $U_{13}c_3$, respectively, the sum total of which is $E_1(0) = 1$. Similarly, the amplitude that appears in the $ijth$ clock is given by $U_{ij}c_j$, so that their sum over j, namely

$$\sum_{j}^{ij} U_{ij}c_j = E_i(0) \tag{3.62}$$

is the excitation amplitude in line i at $z = 0$. At an arbitrary point z along the coupler, the three clocks in the first row show the values of $U_{11}\exp(-jp_1z)c_1$, $U_{12}\exp(-jp_2z)c_2$ and $U_{13}\exp(-jp_2z)c_3$, the sum total of which is $E_1(z)$. The amplitude that appears in the $ijth$ clock is given by $U_{ij}\exp(-jp_jz)c_j$, so that

their sum over j is

$$\sum_{j}^{3} U_{ij} \exp(-jp_j z) c_j \quad E_i(z) \tag{3.63}$$

which is the signal amplitude in guide i at z.

As z progresses, the complex amplitudes evolve in magnitude and phase, the arms of the clocks rotate and vary in length. Partial waves with positive and negative propagation constants will rotate in the clockwise and counterclockwise directions respectively, since the rotation depends on the phase factor $\exp(-jp_i z)$. This rotation represents the phase shift with respect to the moving reference β_o, the average propagation constant. A clock that corresponds to $p_2 = 0$ will not rotate at all.

The central part of Fig. 3.7 illustrates the eigensolutions at a distance z in the guide, after the clocks corresponding to non-zero eigenvalues have rotated $\pm 90^o$. The figure shows that at this point the field amplitudes in all three guides are non-zero. Since our aim is to determine the position, z, where all the power is transferred into guide three, it is necessary to determine the location of z where the eigensolutions in guides 1 and 2 cancel out, indicating that power flow exists at that point in guide 3 only. The bottom part of Fig. 3.7 shows that this occurs after a phase delay of $p_{1,3}z \quad \pm\pi$ indicated on the clock diagram by a $\pm 180^o$ rotation of the arms with respect to their

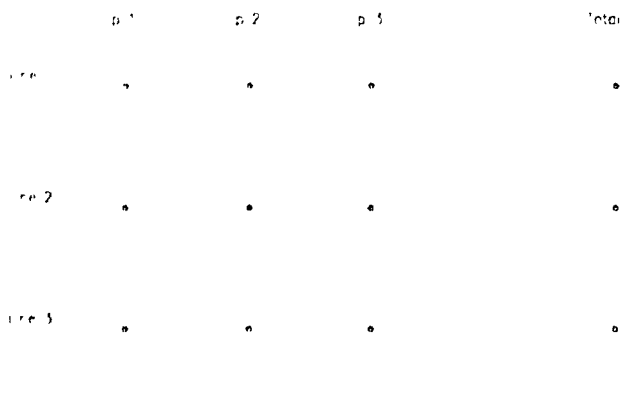

$z = 0$

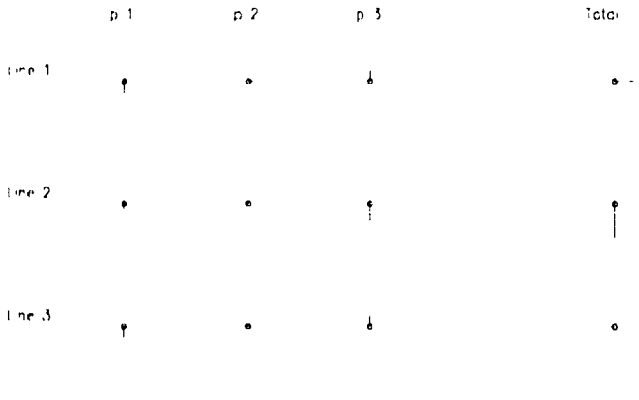

$z = \pi/2\sqrt{2}\kappa$

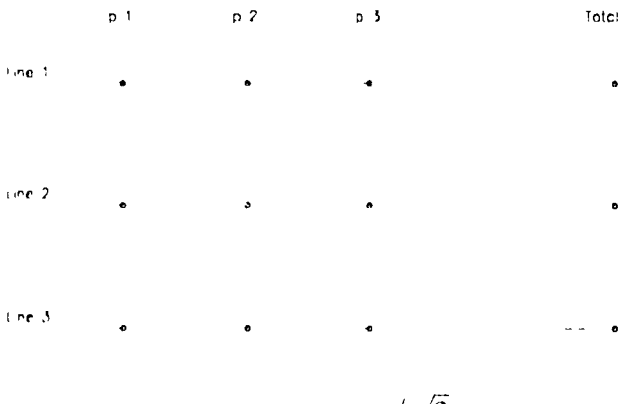

$z = \pi/\sqrt{2}\kappa$

Figure 3.7: Eigensolutions of a symmetric 3 × 3 coupler that result from unity input into guide 1. Graphical results determined using CLOCK.M program provided in the Appendix, as described in Section 3.4

initial position at $z = 0$. This occurs at the conversion length

$$z = l \frac{\pi}{\sqrt{2}\kappa} \tag{3.64}$$

Since this device exhibits transverse symmetry, applying a unit input into guide 3 would result in complete power transfer into guide 1 at the same conversion length.

This graphical method of monitoring eigenmodes provides simple, visual means of predicting how a particular device performs subject to a given input. For example, by comparing the 'Total' clock from the initial and final states depicted in Fig. 3.7, it can be noted that a phase shift of 180° occurred as the signal was completely transferred from one outside guide to the other. Also, Fig. 3.7 allows one to anticipate that if an input is applied to the center guide in addition to the signal already applied to guide 1, the output of the center guide will be identical to its input with a 180° phase shift. Testing this hypothesis, consider a normalized input of

$$E(0) = \begin{bmatrix} .8 & .6 & 0 \end{bmatrix}^t \tag{3.65}$$

This results in

$$E(l) \quad 0 \quad .6 \quad .8\ ^{t} \tag{3.66}$$

at $z \quad l$, confirming that the signal in guide 2 maintained its amplitude but was shifted by 180°.

A similar analysis may be effected to show how this device can act as a splitter. Applying unity input to the center guide:

$$E(0) \quad ^{t}0 \quad 1 \quad 0\ ^{t} \tag{3.67}$$

As shown in Fig. 3.8, at one-half the conversion length, $z \quad l/2 \quad \pi\ ^{t}/2\sqrt{2}\kappa$, the signal splits equally between the two outside guides; while at $z \quad l \quad \pi \ \backslash\ 2\kappa$, the signals will recombine in the center guide. Thus, the 3 · 3 coupler may effectively act as a splitter or a combiner.

This method may be used to better illustrate an earlier example where guides 1 and 3 of the coupler were excited by signals of equal magnitude, but with a phase difference of 180°:

$$E(0) \quad \left[\begin{matrix} 1 & 0 & 1 \\ \backslash\ 2 & & \backslash\ 2 \end{matrix}\right]^{t} \tag{3.68}$$

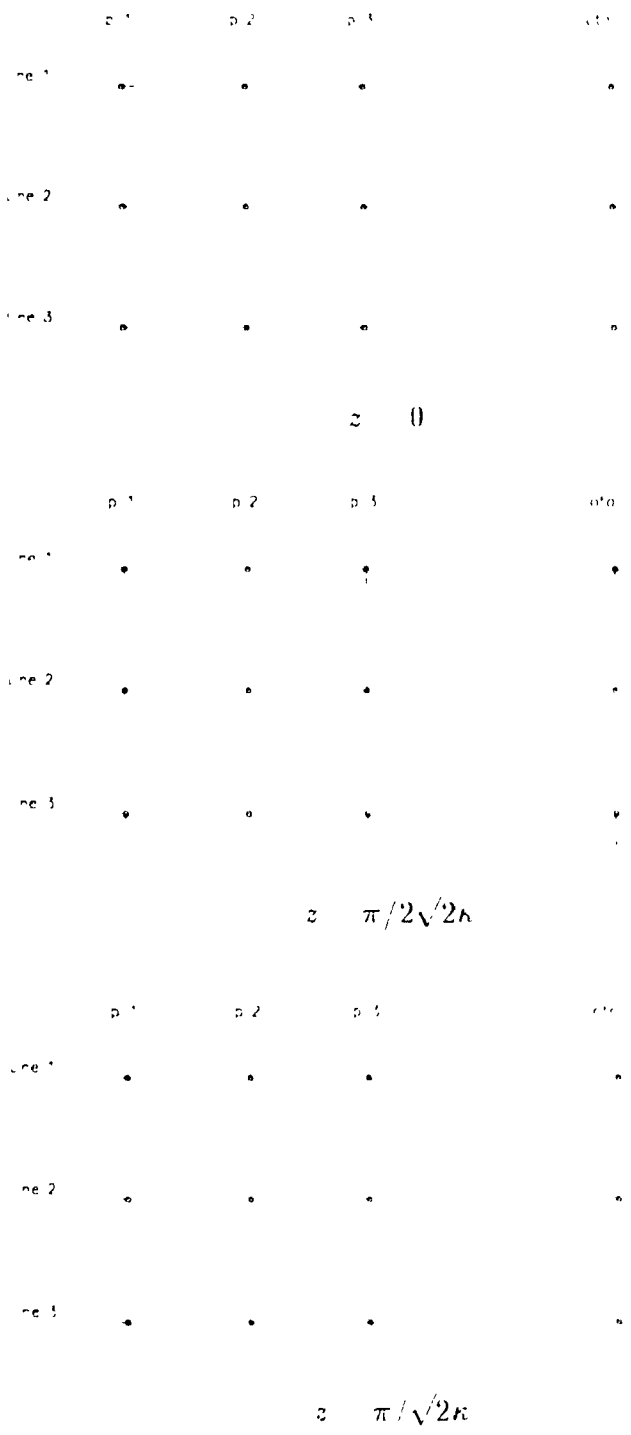

Figure 3.8: Eigensolutions of a symmetric 3 × 3 coupler that result form unity input into the center guide. Graphical results determined using CLOCK M program provided in the Appendix, as described in Section 3.4

The input signal has been normalized to represent unit power. Since (3.68) is an eigenvector corresponding to p_2 in (3.59), the signal will propagate through the coupler unchanged, and the clocks depicted by Fig. 3.9 will remain in their original position as z is incremented.

The graphical "clocks" method of analyzing coupling devices developed and introduced in this study is a useful tool for determining the required geometrical and material parameters for achieving a particular result. Given a set of input signals, the device length, L, and the coupling coefficient, κ, necessary for the 3×3 coupler to act as a combiner or splitter according to desired signal proportions may be easily calculated.

3.5 Implementation of a 3×3 coupler

A 3×3 coupler can be implemented as an integrated device in the planar configuration using titanium indiffusion on a lithium niobate substrate. $LiNbO_3$ is often used for integrated optical devices because of its excellent electrooptic properties. Details of the fabrication process of Ti-indiffused optical waveguides and their characteristics can be found in [39] and [44].

The material and geometrical parameters of a 3×3 coupler realized on X cut Y propagating Ti-indiffused $LiNbO_3$ are shown in Fig. 3.10, where

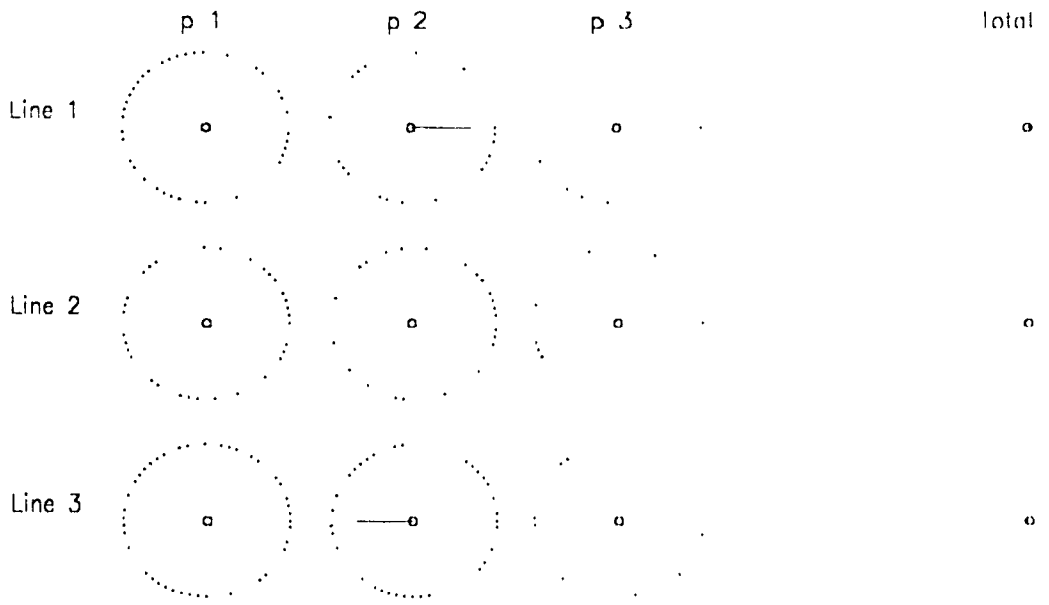

Figure 3.9: Eigensolutions of a 3 × 3 coupler that result from an excitation of signals of equal magnitude and a phase difference of 180°, for all z.

the laboratory and crystal coordinates of the device are given in lower and upper case letters respectively. The elements of the coupling matrix of the device can be determined using coupled mode theory as described in Section 2.1. The coupling between any two guides is evaluated using (2.5) Although, strictly speaking, the electric fields in the guides have both x and y variation, matters will be simplified here by showing results one can expect in the case where one dimensional slab waveguides with no y variation are used. This

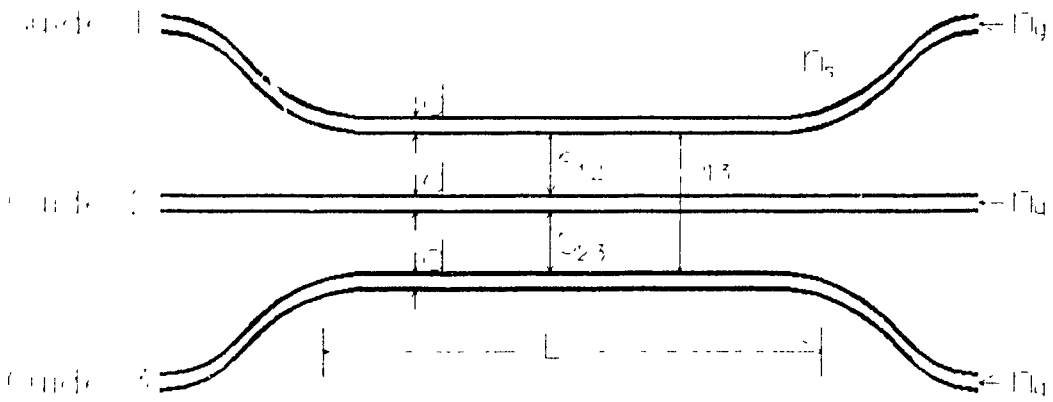

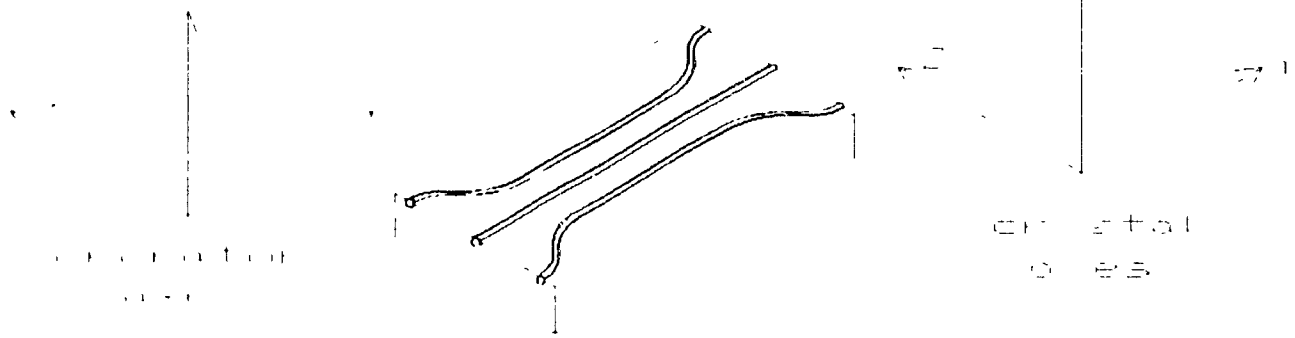

Figure 3.10: Schematic of the 3 × 3 coupler indicating physical and material parameters.

approach sufficiently describes the theory while reducing the complexity of determining the coupling coefficients.

The x components of the wavenumbers in the core and cladding, respectively, are determined from:

$$k_{2i} \quad \sqrt{\omega^2 \mu_o \epsilon_o n_g^2 \quad k_z^2} \tag{3.69}$$

and

$$\alpha_i \quad \sqrt{k_z^2 \quad \omega^2 \mu_o \epsilon_o n_s^2} \tag{3.70}$$

where n_g and n_s are the refractive indices of the guide and the substrate, ω is the frequency, $\mu_o = 4\pi \times 10^{-7}\ H/m$ and $\epsilon_o \quad 8.854 \cdot 10^{-1}\ F/m$ are the permeability and permittivity of free space, and k is the propagation constant in the z direction of an isolated line. The transverse resonance condition is used to obtain the characteristic equation that links α_i to k_{2i}:

$$\tan\left(\frac{k_{2i}d}{2}\right) \quad \frac{\alpha_i}{k_{2i}} \tag{3.71}$$

k_{2i} can be solved for by rewriting (3.70) in terms of k_{2i}, and substituting

into (3.71):

$$\tan\left(\frac{k_{2i}d}{2}\right) = \sqrt{\frac{\omega^2\mu_o(n_g^2 - n_s^2) - k_{2i}^2}{k_{2i}^2}} \tag{3.72}$$

The relationship between the propagation constant in the z direction and k_{2i} is given by

$$k_z = \sqrt{\omega^2\mu_o\epsilon_o n_g^2 - k_{2i}^2} \tag{3.73}$$

As stated in Section 2.1, the propagation constant of a coupled line is approximately that of the uncoupled case, thus the β_i's in the coupling matrix $\mathbf{R}$ can be approximated by

$$\beta_i \approx k_z \tag{3.74}$$

The expression for the coupling coefficient κ_{ij} can be determined using the methods outlined in Section 2.1, resulting in

$$\kappa_{ij} = \frac{2\omega^2\mu_o\epsilon_o(n_g^2 - n_s^2)\alpha_i\cos^2(k_{2i}d/2)}{k_z d\left(1 + \frac{1}{\alpha_i d}\right)(\alpha_i^2 + k_{2i}^2)}\exp(-\alpha_i s_{ij}) \tag{3.75}$$

A complete derivation of the above equations can be found in [31].

Using the fabrication parameters illustrated in Fig. 3.10, the coupling matrix, **R**, of the 3 × 3 coupler can be evaluated using (3.71) and (3.75)

$$\mathbf{R} = \begin{bmatrix} 2.199 \times 10^{7} & 382.0 & 1.194 \\ 382.0 & 2.199 \times 10^{7} & 382.0 \\ 1.194 & 382.0 & 2.199 \times 10^{7} \end{bmatrix} \frac{1}{m} \tag{3.76}$$

The transfer matrix of this device can be determined using (2.16). Fig. 3.11 illustrates the output of the three guides as the length of the device is varied for a coupler with unity power applied only to the first guide. For this example, a vacuum wavelength of $\lambda_o = .63 \cdot 10^{-6}\ m$, corresponding to an angular frequency of $\omega = 2.99 \times 10^{15}\ rad/s$, was used. Evaluating (3.41), we find that complete transfer of power occurs for a device of length $L = 5.81\ mm$.

The wavelength dependence and filter characteristics of the device can be examined by observing the transfer characteristics as the wavelength (or frequency) of the signal is varied. Fig. 3.12 illustrates the output of the first guide when a device length of $L = 11.63\ mm$ is chosen. These results show that the device has a FWHM bandwidth of approximately $30 \cdot 10^{-4}\ \mu m$ around the operating wavelength of $\lambda_o = .63\ \mu m$, i. e. a relative bandwidth of 5%.

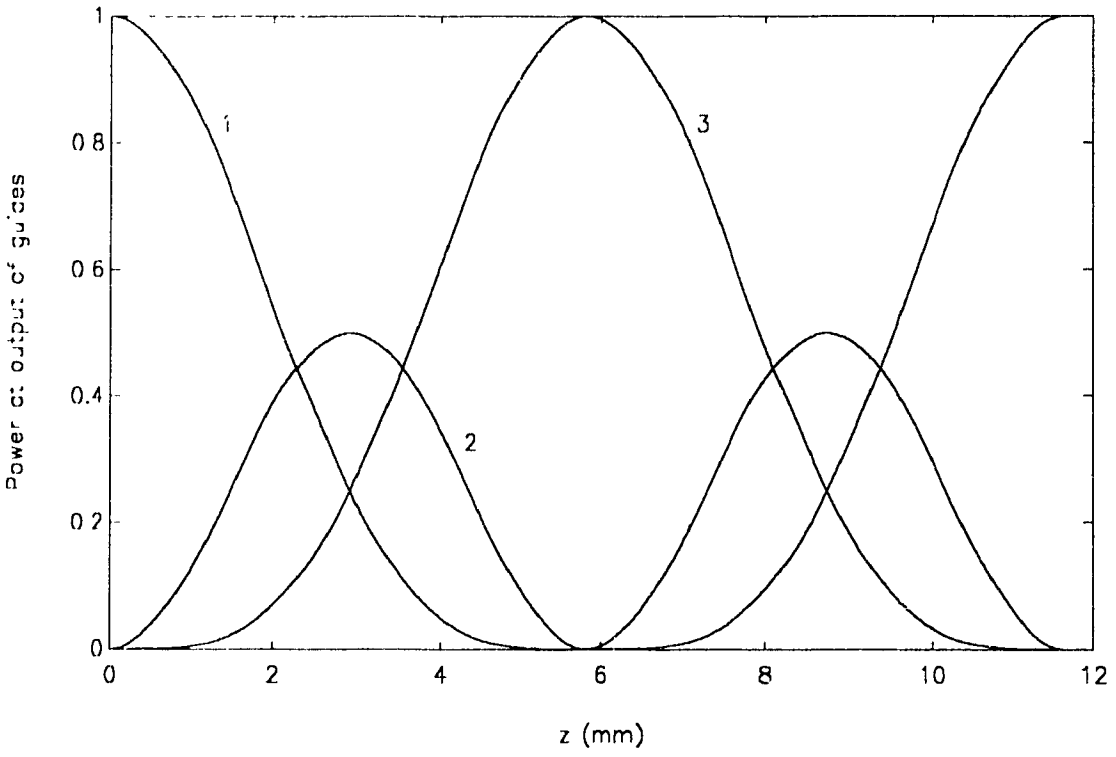

Figure 3.11: Transfer characteristic of the 3×3 coupler at $\lambda_o = .63\ \mu m$

3.6 Switched directional 3×3 couplers

Chapter 2 discussed how a 2×2 switched directional coupler can be made to switch from the bar state to the cross state by using sections of alternating phase mismatch. A $\Delta\beta$ coupler can form part of a large switching system used to network many communication channels. However, the number of switches and stages of switches increases with the number of communication channels required. These numbers can be dramatically reduced if the indi-

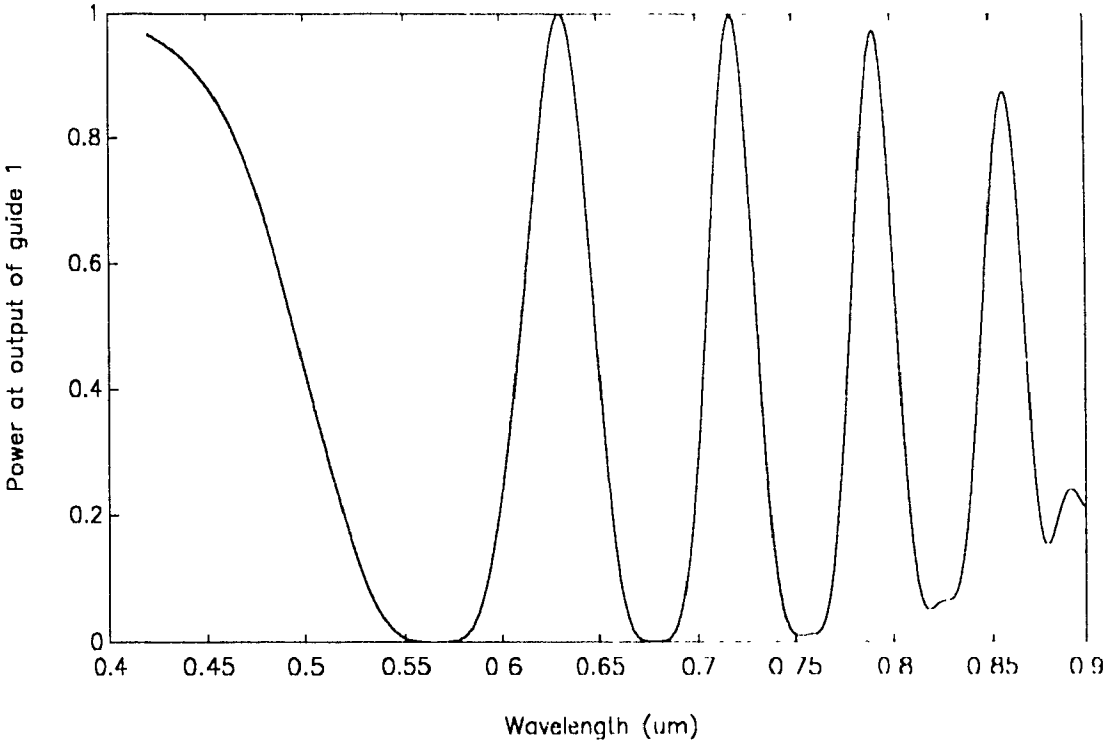

Figure 3.12: Wavelength dependence of the 3 × 3 coupler.

vidual switches used are capable of switching between three channels instead of two.

Consider the two switching configurations depicted in Fig. 3.13. The top of the figure shows that three stages each consisting of four 2 × 2 switches are needed to switch between eight channels, whereas the bottom of the figure illustrates how only two stages of three 3 × 3 switches allow switching between nine channels. Advantages of using less switches include reduced device size,

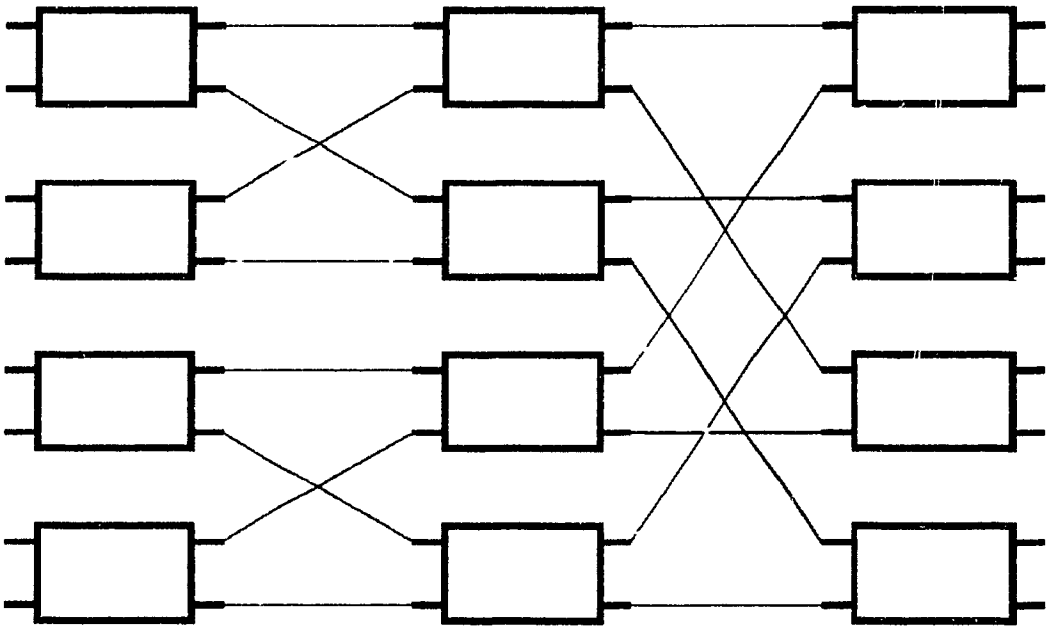

(a)

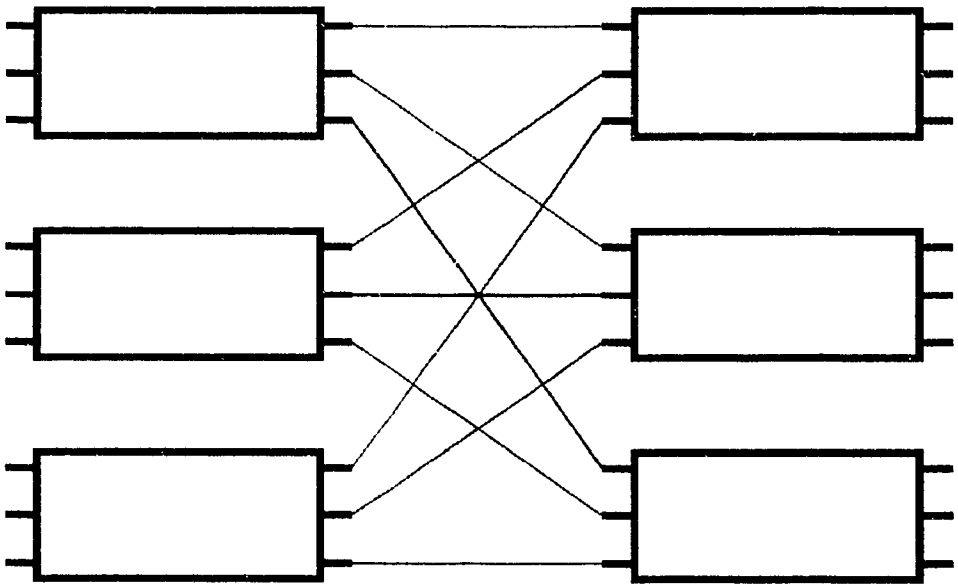

(b)

Figure 3.13: Typical switching configurations using (a) 2×2 and (b) 3×3 switches

cost savings and reduced transmission loss. Since most of the losses in large switching systems occur at interconnections, a decrease in the number of stages results in a substantial decrease in the total system loss.

A 3 × 3 switch can be realized by placing three 2 × 2 switches on a single substrate as illustrated by Fig. 3.14. However, this approach is impractical because building a relatively small device would require curved interconnections with small radii of curvature. Since the radiation loss of curved guides increases with decreasing radius of curvature, this type of device would have to be either very large or very lossy. As an alternative to using three 2 2 elements on a single substrate, Ogiwara suggests implementing a 3 3 switch using a single 3 × 3 coupler with alternating sections of phase mismatch [45,46].

As illustrated by Fig. 3.15, the 3 × 3 switching device is operated by adjusting four separate voltages. These voltages induce the requisite phase mismatch in the manner discussed in Section 2.5 . The purpose of the device is to achieve any input/output combination possible with a 3 × 3 device, as shown in Fig. 3.16. In this section, the methods for analyzing couplers previously presented in Chapters 2 and 3 are used to determine how the six states of the 3 × 3 switch can be realized.

Consider first the example described at the beginning of Section 3.4 It has been shown that a symmetric device whose coupling matrix is described

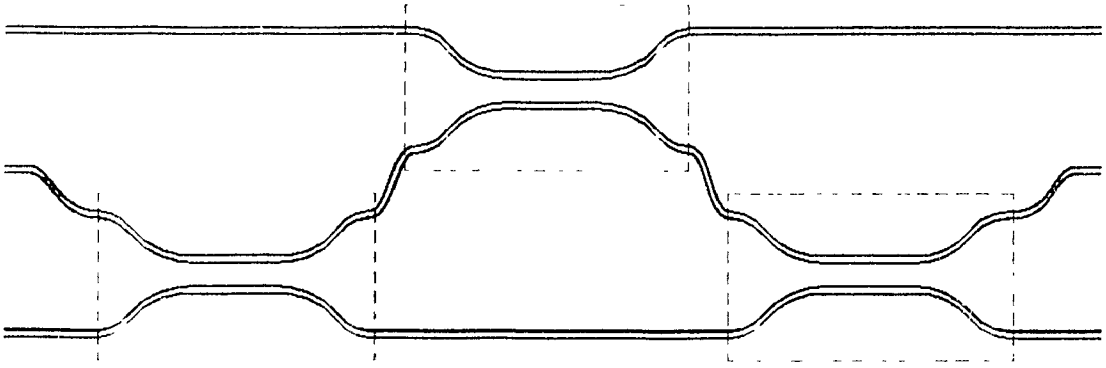

Figure 3.14: The 3 × 3 switch using 2 × 2 switching elements.

by (3.31) can be used to transfer power from guide 1 to 3, or from guide 3 to 1, when the device length equals $\pi/\sqrt{2}\kappa$. Also, any signal fed into guide 2 will exit from that same guide. Thus, state (1) in Fig. 3.16 can be realized without employing detuning, so all electrodes must be grounded. This can be implemented using the Ti-indiffused $LiNbO_3$ coupler depicted by Fig. 3.10 in Section 3.5. The coupling matrix of the device was provided by (3.76). Since the coupling between outside guides is much less than that of adjacent

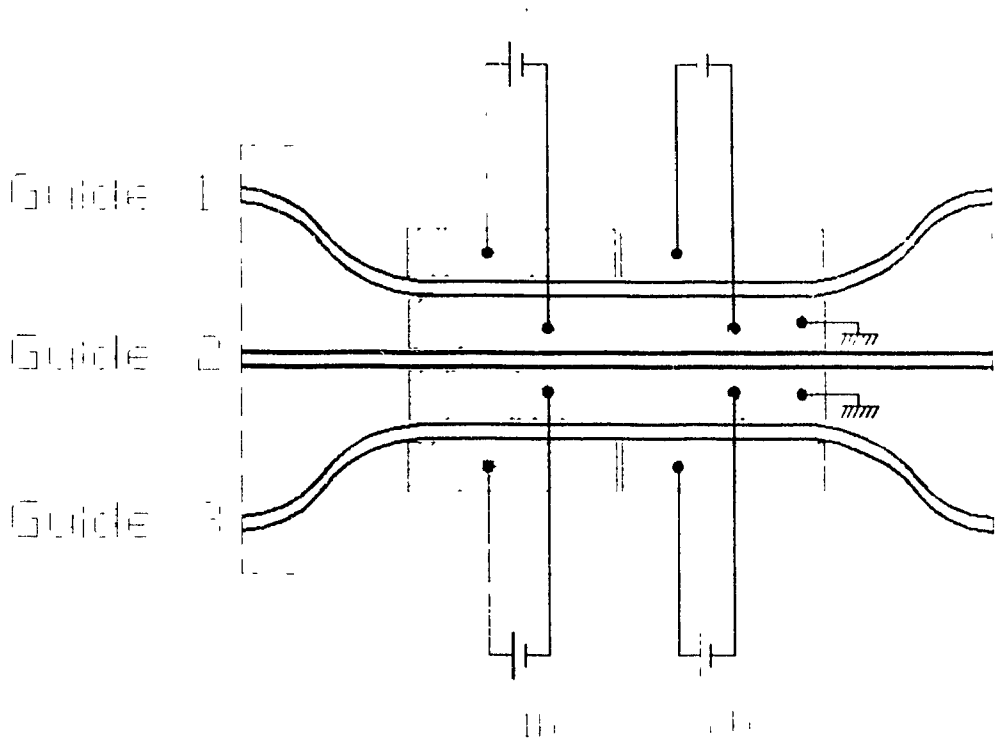

Figure 3.15: Implementation of the 3 × 3 switch using two sections of phase mismatch.

guides, it can be ignored, and state (1) of the 3 × 3 switch can be realized by setting the length of the coupler to $L = \pi/\sqrt{2}\kappa_1 = \pi/\sqrt{2}(3820) = 5.81\ mm$

State (2) can be achieved if the device is detuned so as to prevent any depletion or crossover. In order to determine how this can be done, the system eigensolutions must be examined. If the control voltages in Fig. 3.15 are adjusted such that

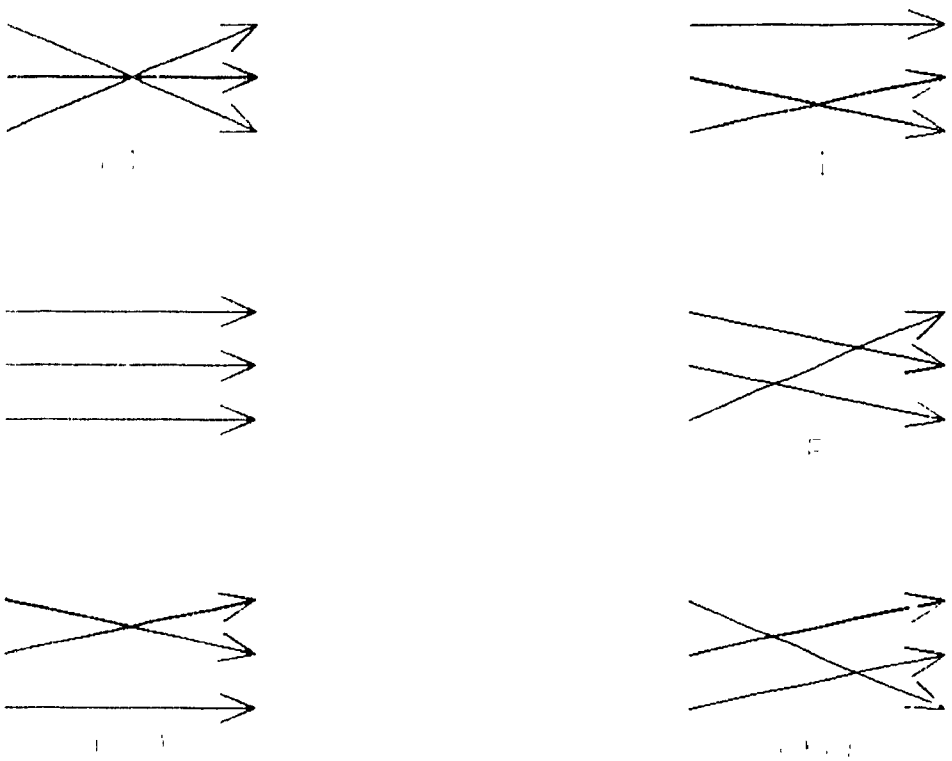

Figure 3.16: The six connecting states offered by a 3 × 3 switch.

$$V_{1a} \quad V_{2a} \qquad V_{1b} \quad V_{2b} \tag{3.77}$$

then the two sections of Fig. 3.16 are biased identically and the resulting reduced coupling matrix applicable to both sections becomes

$$\mathbf{R}_{reduced} \quad \begin{bmatrix} \Delta\beta & \kappa & 0 \\ \kappa & 0 & \kappa \\ 0 & \kappa & \Delta\beta \end{bmatrix} \tag{3.78}$$

The eigenvalues of this detuned system are

$$\begin{aligned} p_1 &= -\sqrt{\Delta\beta^2 + 2\kappa^2} \\ p_2 &= 0 \\ p_3 &= \sqrt{\Delta\beta^2 + 2\kappa^2} \end{aligned} \tag{3.79}$$

The objective is to detune the guides so as to prevent any power transfer in a device with a fixed length of $L = \pi/\sqrt{2}\kappa$ ($L = 5.81\ mm$). This is the total coupler length previously determined to be the requisite for state (1). This objective is achieved if the eigensolutions of the system, which rotate at a rate of $\exp(-jp_iL)$, are the same at $z = L$ as they were at $z = 0$. That is, when

$$\exp(-jp_iL) = 1 \tag{3.80}$$

For eigenvalue p_2 this is always satisfied. For p_1 and p_3, this condition is satisfied when

$$\sqrt{\Delta\beta^2 + 2\kappa^2}L = 2n\pi \tag{3.81}$$

Using $L = \pi/\sqrt{2}\kappa$, solving for the lowest $\Delta\beta$ (and consequently the lowest control voltage) results in $\Delta\beta = \sqrt{6}\kappa$.

In determining the associated control voltage, we consider the electrooptic effect in order to establish a relationship between the voltage and propagation constant. A voltage V applied to the electrodes separated by a distance d creates a field $E_{bias} = V/d$. Applying an electric field across a waveguide built using an electrooptic material such as $LiNbO_3$ induces a change in the refractive index of the guide (n_g) according to

$$\Delta n_g = -\frac{1}{2} n_g^3 r E_{bias} \tag{3.82}$$

where r is the relevant electrooptic coefficient which depends upon the crystal orientation and the direction of the applied electrical field. The change in the propagation constants of the waveguides is related to the change in the refractive index by

$$\Delta\beta = \frac{2\pi \Delta n_g}{\lambda_o} \tag{3.83}$$

Substituting (3.82) into (3.83) provides a solution for the voltage required

for a specific $\Delta\beta$:

$$V = \frac{\Delta\beta\lambda_o d}{\pi n_f^3 r} \tag{3.84}$$

where r, the electrooptic coefficient for $LiNbO_3$, is $30.8 \times 10^{-12}\ m/V$.

Thus, a change in the propagation constant of $\Delta\beta = \pi \times 68.1 = 935.7\ m^{-1}$ can be induced in a waveguide fabricated on Ti indiffused X cut Y propagating $LiNbO_3$ using electrodes separated by a distance of 1 μm that are applied a voltage of 0.546 V. Thus, State (2) is realized by setting

$$V_{1a} = V_{2a} = V_{1b} = -V_{2b} = 0.546\ V \tag{3.85}$$

In states (3) and (4) of Fig. 3.16, interaction takes place only between two neighboring guides. Only state (3), switching between guides 1 and 2, will be discussed here, as similar results apply to state (1). It will be shown that the detuning voltages that are required to achieve state (3) are,

$$\begin{aligned} V_{1a} &= V_{2a} \\ V_{1b} &= -V_{2b} \end{aligned} \tag{3.86}$$

That is, the two sections of guide 1 are detuned using oppositely polarized voltages, while the two sections of guide 3 are either detuned by the same voltage or by equal but oppositely polarized voltages. As a result, the reduced coupling matrices of the first and second half sections of the coupler become

$$\mathbf{R}_{1reduced}\begin{bmatrix} \Delta\beta_1 & \kappa & 0 \\ \kappa & 0 & \kappa \\ 0 & \kappa & \Delta\beta_1 \end{bmatrix} \tag{3.87}$$

and

$$\mathbf{R}_{2reduced}\begin{bmatrix} \Delta\beta_1 & \kappa & 0 \\ \kappa & 0 & \kappa \\ 0 & \kappa & +\Delta\beta_1 \end{bmatrix} \tag{3.88}$$

Interaction between guide 3 and the rest of the system is reduced as the propagation constant of that guide is increasingly detuned. First, it will be assumed that guide 3 is detuned so much that it does not interact with guides 1 and 2; then, a method of transferring signals between 1 and 2 will be developed, and finally the results will be modified to consider the interaction with guide 3.

As the detuning of guide 3 goes to infinity ($\Delta\beta_1 \to +\infty$), the interaction between guide 3 and the other two guides reduces to zero and the transfer matrices of (3.87) and (3.88) become

$$\mathbf{T}_1(z) \quad \begin{bmatrix} A & jB & 0 \\ jB & A & 0 \\ 0 & 0 & \exp(-j\Delta\beta_1 z) \end{bmatrix} \tag{3.89}$$

and

$$\mathbf{T}_2(z) \quad \begin{bmatrix} A & jB & 0 \\ jB & A & 0 \\ 0 & 0 & \exp(+j\Delta\beta_1 z) \end{bmatrix} \tag{3.90}$$

respectively, where A and B are described by (2.40) and (2.41) respectively. The transfer matrix of the system consisting of two cascaded sections is,

$$\mathbf{T}_{system}(z) \quad \begin{bmatrix} |A|^2 & |B|^2 & j2BA & 0 \\ j2BA & |A|^2 & |B|^2 & 0 \\ 0 & 0 & \exp(+j\Delta\beta_1 + \Delta\beta_1 z) \end{bmatrix} \tag{3.91}$$

indicating that in the absence of any interaction with guide 3, guides 1 and 2 comprise a 2×2 coupler with two sections of alternating phase mismatch whose transfer matrix is given by (2.44) and whose condition for cross states is provided by (2.45). Substituting the fixed $L = \pi/\sqrt{2}\kappa$ into (2.44) reveals that cross states occur when $\Delta\beta_1 = 2\kappa$. This is achieved by setting $V_{1a} = -V_{2a} = 0.455\ V$.

At this point the interaction of guide 3 with the rest of the system must be considered. Unless guide 3 is completely isolated from guides 1 and 2,

unwanted power transfer between that guide and the rest of the system will take place. Complete isolation is impossible as it would require an excessively large voltage. Thus, the object is to maximize the isolation of guide 3 with the lowest possible control voltage. Alternatives to be considered include detuning both sections of the guide uniformly, or, detuning the two sections with equal voltages of opposite polarity. Fig. 3.17 illustrates the results for these two alternatives. The figure plots the output of guide 3 when the device is fed with unity input into guide 2. Line A represents the case where guide 3 is detuned with oppositely polarized voltages ($V_{1b} = -V_{2b}$), and line B represents the case of uniform detuning ($V_{1b} = V_{2b}$). The ordinate is a logarithmic scale, and the abcissa is the detuning voltage V_{1b}. These results indicate that crosstalk reduction is periodic with a decreasing slope of approximately 2.5 dB/V. For the case where oppositely polarized voltages are used, regions of extremely low crosstalk occur in this periodic fashion. Visual inspection and computer simulation lead to the result that the dips in Fig. 3.17 occur at approximately

$$\Delta\beta_1 L/2 = 2n\pi \tag{3.92}$$

Fig. 3.17 shows the output level in guide 3 when guide 2 of the 3 × 3 switch is excited. A similar analysis may be performed to determine the

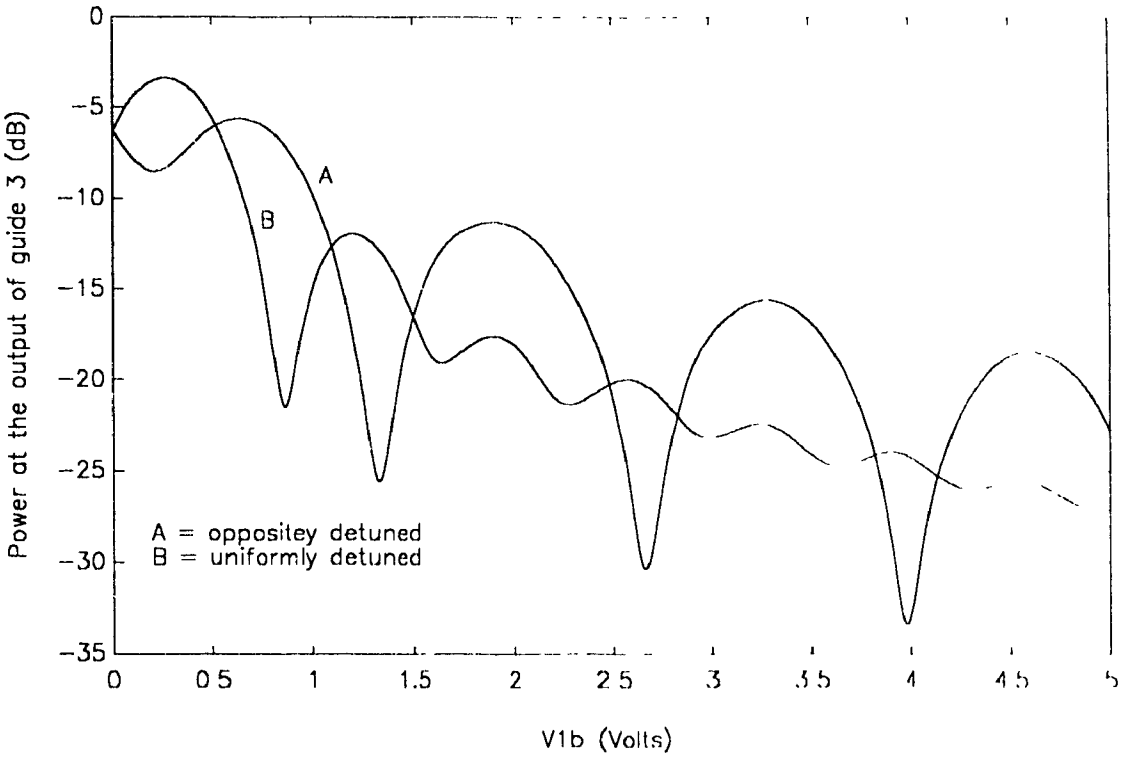

Figure 3.17: Crosstalk in guide 3 of a 3 × 3 switch that results from unity input into guide 2, for a coupler length of $L = 5.81mm$

levels of crosstalk when guide 1 is excited. In both cases it was found that minimum crosstalk occurred at the points shown in Fig. 3.17. Thus, states 3 and 4 are best implemented when the detuning voltage is set to correspond to a dip in crosstalk using oppositely polarized voltages (i. e. $V_{12} = -V_{32} = 1.25\ V, 2.6\ V, 4.0\ V, \ldots$).

States (5) and (6) of Fig. 3.16 can only be realized by cascading some combination of the first four. For example, to realize state (6), states (2) and

(3) are cascaded.

Thus, we have shown that adjusting the four detuning voltages of a 3×3 device with two sections of alternating phase mismatch provides a method of controlled switching between four distinct states; two additional switching states may be achieved by cascading two of the primary states.

Chapter 4

The 3×3 coupler with feedback

4.1 Reasons for using a 3×3 coupler with feedback

The signal processing capabilities of the 3×3 coupler can be significantly enhanced by the application of feedback [47]. A 3×3 coupler with feedback is realized by looping one of the outputs back into one of the inputs, thus reducing the system to a four port. Fig. 4.1 illustrates the five generic feedback configurations for a 3×3 coupler. This study will consider configuration (a), where the output of guide 3 is connected to its input. Similar analysis can be carried out on the remaining configurations, however they will not be documented in this thesis.

This novel device is useful in optical switching, power splitting/combining and wavelength filtering. In optical switching, power applied to one of the input guides of a 3×3 coupler with feedback can be distributed, in any

ratio, between the two output ports. The transfer ratio can be adjusted by varying the electrical length of the feedback line. In power combining, an adjustment of both the electrical length of the feedback line and the propagation constant of one of the three arms allows the device to combine two signals of arbitrary magnitude and phase. In wavelength filtering, the device can act as a wavelength division multiplexer or as a bandpass filter with extremely narrow bandwidth.

In this chapter we discuss the characteristics of the 3 × 3 coupler with a feedback path and contrast them with those of two and three guide couplers, which are briefly reviewed here. Although a symmetrical 2 × 2 coupler can be built to transfer a fixed fraction of power from one guide to the other, the relative phase difference between the output signals is 90°. By introducing alternating phase mismatch, it was shown that this transfer ratio is variable, but the relative phase between the output signals varies with the transfer ratio. In the case of a symmetrical 3 × 3 coupler with identical lines, complete power transfer between guides can be achieved, but only with an output phase shift of 180°. The conventional 3 × 3 coupler is also capable of combining two incoming signals, however, complete combination is restricted to the case where the input signals are equal in magnitude and phase, otherwise residual power remains on the source waveguides. In contrast, it will be shown that introducing feedback to a 3 × 3 coupler results in a device that

can transfer power in any ratio while maintaining a 0° phase shift between the output signals. It will also be shown that this device can combine two signals of arbitrary magnitude and phase. Finally, it will be shown that the requirements of identical lines and transverse symmetry are not required for this device to perform the above tasks.

Recall that $\mathbf{R}_{reduced}$ is obtained by factoring out the average β_0 term from the propagation constants of the three guides. Thus, analysis using $\mathbf{R}_{reduced}$ does not retain the average phase shift through the coupler which must be considered when using a feedback loop. For this reason, the analysis of circuits involving feedback loops in this chapter will use the full coupling matrix, $\mathbf{R}$, rather than $\mathbf{R}_{reduced}$ described in (3.29).

4.2 The 3×3 coupler with feedback used as a switch

In this section we discuss how the 3 × 3 coupler with a feedback loop placed around the third guide is used as a power divider. The objective of this device is to transfer any fraction of the incident power from one guide to another. As an example we design a divider with an output power ratio, ζ. For a normalized input of $E(0) = [1 \quad 0]^t$ we expect an output of

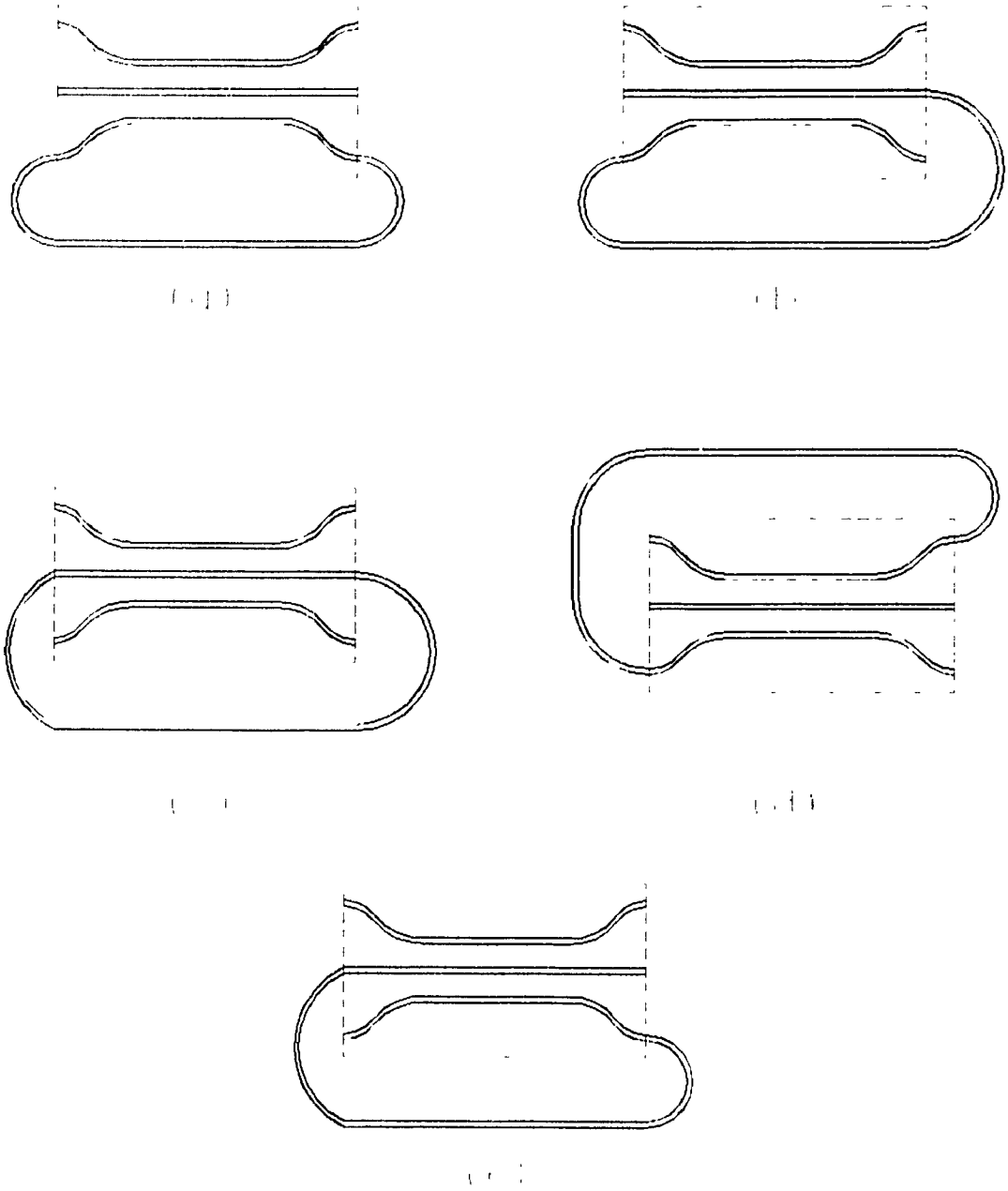

Figure 1.1: The five generic feedback configurations using a 3 × 3 coupler.

$$E(L) \quad \begin{bmatrix} \\ \\ \end{bmatrix} \tag{4.1}$$

The input and output of guide 3 are related by

$$E_3(0) \quad tE_3(L) \tag{4.2}$$

where $t = |t|\exp(-j\phi)$; ϕ represents the phase shift and t is the gain of the feedback line. Therefore

$$\begin{bmatrix} E_1(L) \\ E_2(L) \\ E_3(L) \end{bmatrix} \quad \mathbf{T}(z) \begin{bmatrix} E_1(0) \\ E_2(0) \\ E_3(L)t \end{bmatrix} \tag{4.3}$$

and $\mathbf{T}(z)$ is the transfer function of the coupler whose elements are given by (3.26). This can be reduced to a 2×2 form,

$$\begin{bmatrix} E_1(L) \\ E_2(L) \end{bmatrix} \quad \mathbf{T}_{fb} \begin{bmatrix} E_1(0) \\ E_2(0) \end{bmatrix} \tag{4.4}$$

where

$$\mathbf{T}_{fb} \quad \begin{bmatrix} T_{11} - \frac{t_{13}t_{31}t}{1-t_{33}t} & T_{12} - \frac{t_{13}t_{32}t}{1-t_{33}t} \\ T_{12} - \frac{t_{23}t_{31}t}{1-t_{33}t} & T_{22} - \frac{t_{23}t_{32}t}{1-t_{33}t} \end{bmatrix} \tag{4.5}$$

Consider a symmetric 3 × 3 coupler of the planar design where $\beta_1 = \beta_2 = \beta_3 = \beta$, $\kappa_{12} = \kappa_{23} = \kappa$ and $\kappa_{13} = 0$. For the coupler under consideration, $\mathbf{T}(z) = \mathbf{T}(z)^t$ and the coupling and transfer matrices are described by (3.31) and (3.32) respectively. The elements of (3.32) can be substituted into (4.5) to determine the transfer matrix of the four port device derived by adding the feedback line. When the electrical length of the coupler is chosen so that $\beta L = 2n\pi$, where n is an integer, then the transfer matrix of the reduced 2 × 2 coupler is

$$\mathbf{T}_{fb} = \frac{1}{1 - (X + .5)t} \begin{bmatrix} X(1 - 2t) + .5 & Y(1 - t) \\ Y(1 - t) & X(2 - 2Xt - t) + Y \end{bmatrix} \tag{4.6}$$

where the expressions for X and Y were given by (3.33) and (3.31).

With unity input at port 1, zero input at port 2, and a feedback loop attached to the third guide, the outputs at guide 1 and 2 of this device are

$$E_1(L) = \frac{X(1 - 2t) + .5}{1 - (X + .5)t} \tag{4.7}$$

$$E_2(L) = \frac{Y(1 - t)}{1 - (X + .5)t} \tag{4.8}$$

Choosing κL so that $X = \frac{1}{6}$, i. e. $\kappa L = 1.351$, the above equations can be reduced to

$$E_1\left(L, \quad\right) \quad \frac{1}{3}(1 + t) \quad 1 \quad \frac{1}{3}t \tag{4.9}$$

$$E_2\left(L, \quad\right) \quad \frac{j2}{3}(1 \quad t) \quad 1 \quad \frac{1}{3}t \tag{4.10}$$

Dividing (4.9) by (4.10) results in

$$\frac{E_1\left(L\right|_{\quad}\right)}{E_2\left(L\right|_{\quad}\right)} \quad \frac{j}{2}\left(\frac{1 + t}{1 - t}\right) \quad \frac{1}{2}\cot\left(\frac{\phi}{2}\right) \tag{4.11}$$

Equation (4.11) reveals that for a lossless feedback line ($|t| = 1$), the ratio between the output signals at guides 1 and 2 is always real, and as a result, their phase difference is either 0° or 180°. As ϕ in $t = |t|\exp(-j\phi)$ varies from 0 to π, the ratio $E_1(L)/E_2(l)$ varies from infinity to zero, i. e. $E_2(L)$ rises from zero to unity (complete crossover). During this period, the phase difference between output ports 1 and 2 remains identically zero. When ϕ is further varied from π to 2π, $E_2(L)$ varies from 1 back to 0, with a constant phase difference of π between the two output ports.

This result is illustrated in Figs. 4.2 and 4.3. The device length, l, as well as β and κ were chosen to satisfy the conditions $\beta L = 2n\pi$ and $\kappa l = 1.351$. In Fig. 4.2 the distribution of power is plotted as a function of the phase shift, ϕ, in the feedback line. Fig. 4.3 plots the phase difference between the output ports as it varies with ϕ. These graphs demonstrate that any ratio of power transfer can be achieved by varying the electrical length of the feedback line while a fixed phase shift between the output signals is maintained. The advantage of maintaining a constant phase is evident in test and measurement applications, where such a coupler may be used to extract a reference signal.

Let us consider the effect on the transfer characteristic if the feedback line is not lossless. Similar techniques used to produce the transfer characteristic for the lossless system are repeated for the specific case of a feedback line with 1dB loss. The resulting transfer characteristic shown in Fig. 4.4 illustrates that at $\phi = \pi$, the output power in guide 1 dips close to zero, and most of the total input power, minus the loss in the feedback line, is transferred to guide 2, as desired in a power divider. The phase characteristics in Fig. 4.5 also show acceptable results, since there exist regions of constant phase difference between guides 1 and 2; however, these regions occur for less values of ϕ than in the lossless case.

Similar analysis is performed to study the sensitivity of the device to

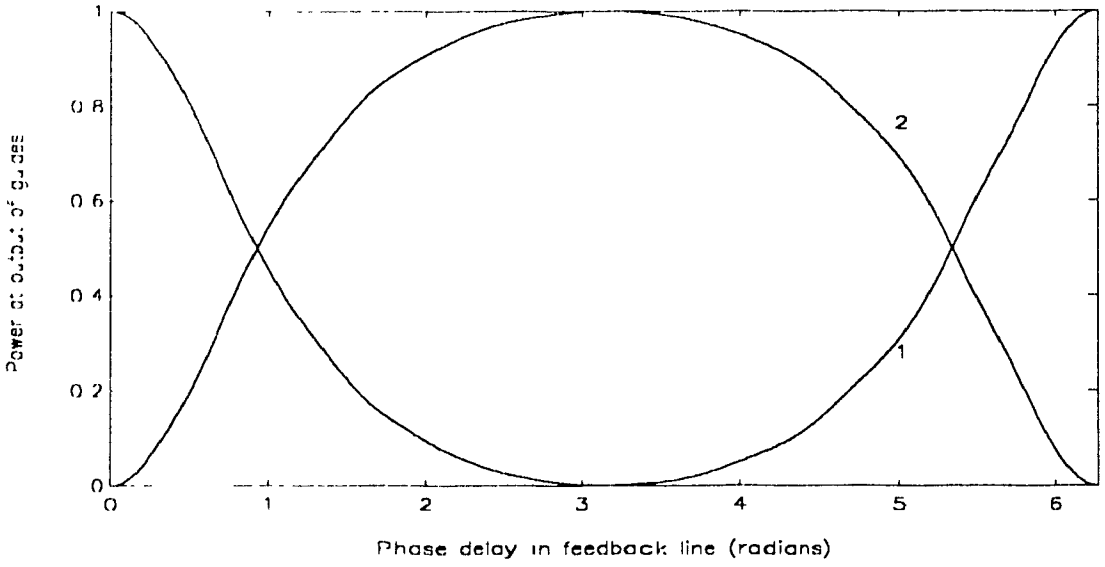

Figure 4.2: Transfer characteristics of a 3 × 3 coupler with feedback

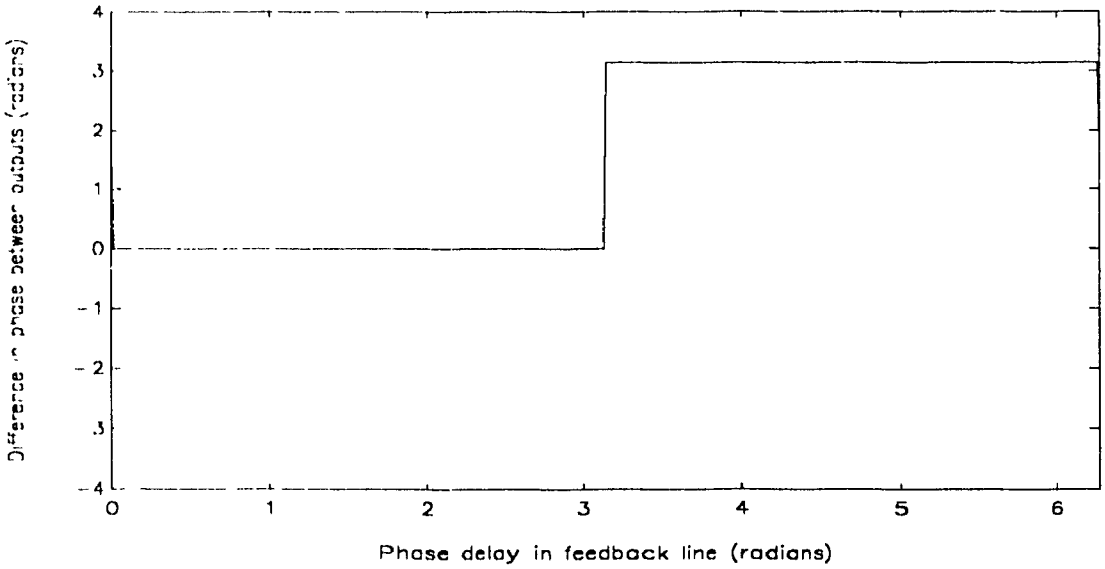

Figure 4.3: Phase difference between ports 1 & 2 for the device characterized in Figure 4.2

changes in κL. Given a device with κL 1.351, it can be shown that a reduction in κL by 5% will result in greater than 99% of the total power transferred to guide 2. Thus, the power transfer ratio exhibits low sensitivity to κL. However, the phase difference no longer remains constant, which is undesirable.

It is important to note that the realization of the power divider requires that the feedback loop does not resonate. This point may be illustrated by considering the two conditions for resonance:

$$|T_{33}(L)||t| \quad 1 \tag{4.12}$$

and

$$\phi_{33}(L) + \phi_{fb} \quad 2n\pi \tag{4.13}$$

where $|T_{33}(L)|$ is the magnitude of the transfer coefficient of guide 3, and, $\phi_{33}(L)$ and ϕ_{fb} are the phase shifts incurred by guide 3 and the feedback line respectively.

The first condition requires $T_{33}(L)$ $T_{33}(z)$ $\frac{1}{2}\cos(\sqrt{2}\kappa z) + \frac{1}{2}$ 1 when a lossless feedback loop is used. This in turn requires the device length to be $L = (2n\pi)/(\sqrt{2}\kappa)$. However, substituting this length into the transfer matrix (3.32) results in

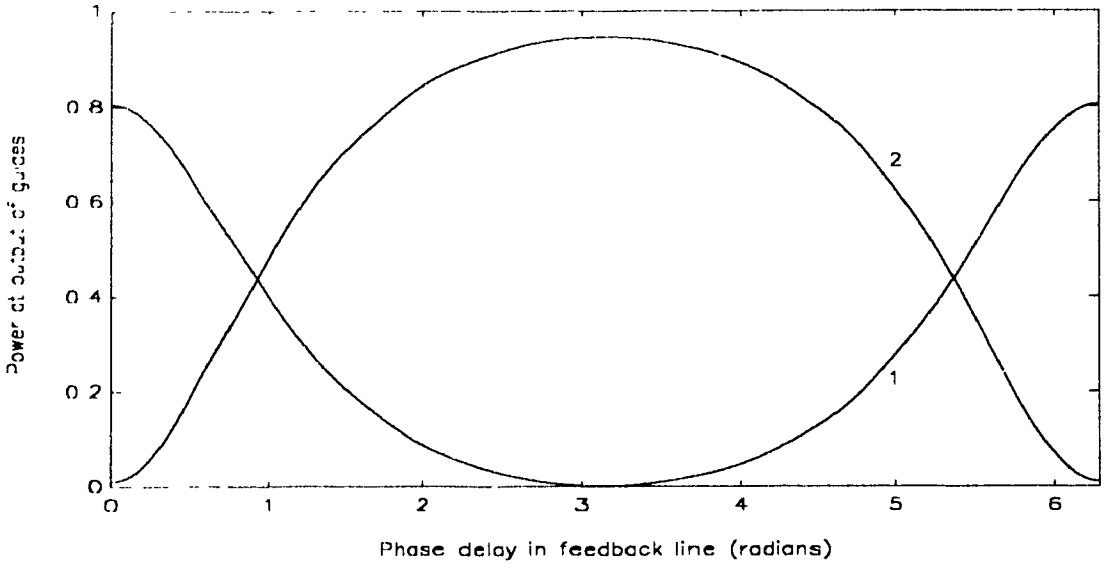

Figure 4.4: Transfer characteristics of a 3 × 3 coupler with 1 dB loss in feedback line

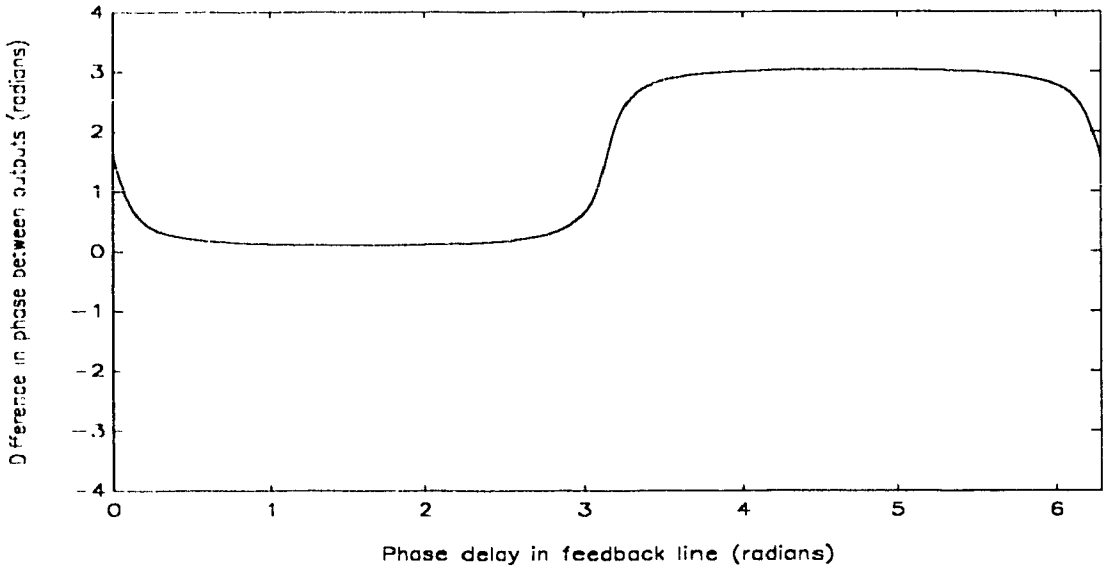

Figure 4.5: Phase difference between ports 1 & 2 for the device characterized in Figure 4.4 with 1 dB loss in feedback line.

$$\mathbf{T} \quad \exp\left(\quad j^{\backslash} \frac{2n3\pi}{\kappa} \right) \begin{bmatrix} 1 & 0 & 0 \\ 0 & 1 & 0 \\ 0 & 0 & 1 \end{bmatrix} \tag{4.14}$$

The reduced transfer matrix $\mathbf{T}_{fb}$ in (4.5) also reduces to the product of the identity matrix and a phase term, and is independent of the phase shift in the feedback line. Thus, a 3 × 3 coupler with feedback that has been built using a coupler length that allows resonance in the feedback loop cannot serve as a power divider, as it maintains a fixed power transfer ratio despite any variation of phase shift in the feedback line.

Note that the power divider analyzed at the beginning of this section was restricted to a symmetric design with identical guides, resulting in a simplified $\mathbf{R}$ matrix. In the general case, the coupling matrix is arbitrary, subject only to the condition of losslessness. A closed form derivation is rather cumbersome for this general case, therefore numerical methods are used for analysis.

Applying unity input to port 1 and zero input to port 2, a solution for the outputs can be determined from the four port transfer function (4.5). An additional condition, κ_{ij} real, has been used to maintain $\mathbf{T} \quad \mathbf{T}^{t}$, resulting in

$$E_1(L) \qquad T_{11} \quad \frac{T_{11}T_{33} \quad T_{13}^2\, t}{1 \quad T_{33}t} \tag{4.15}$$

$$E_2(L) \qquad T_{12} \quad \frac{T_{12}T_{33} \quad T_{23}T_{13}t}{1 \quad T_{33}t} \tag{4.16}$$

Total depletion of guide 1 ($E_1(L) \quad 0$) is achieved when the numerator of (4.15) is zero. Assuming $|t| \quad 1$, $E_1(L)$ can be set to zero by ensuring that

$$|T_{11}| \quad |T_{11}T_{33} \quad T_{13}^2| \tag{4.17}$$

and

$$\arg(T_{11}) \quad \arg([T_{11}T_{33} \quad T_{13}^2]t) \tag{4.18}$$

The first condition for total depletion, described by (4.17) can be met by choosing the appropriate coupler length, L. Holding L constant, the second condition (4.18) is met by varying the electrical length of the feedback line. This can be accomplished by varying the phase constant through mechanical or thermal stress, or through the electrooptic effect.

A computer program, ZPHLM, capable of determining the (L, ϕ) combination required to satisfy (4.17) and (4.18) has been written and is listed in the Appendix. As an example, consider a device with the following coupling matrix

$$\mathbf{R} \begin{bmatrix} 5.35 \times 10^{-7} & 300 & 30 \\ 300 & 5.35 \times 10^{-7} & 300 \\ 30 & 300 & 5.35 \times 10^{-7} \end{bmatrix} \begin{bmatrix} 1 \\ m \end{bmatrix} \qquad (4.19)$$

After the addition of the feedback loop, the program evaluates the shortest device length, L, that will satisfy (4.17). It then solves for the corresponding ϕ using (4.18). For this case, the solution is $L = 4.50\ mm$ with $\phi = 4.01\ rad$ Thus, a 3×3 feedback device with these parameters will function as a power divider. These results are illustrated in Figs. 4.6 and 4.7. Fig. 4.6 shows that the output power in the guides will vary from zero crossover at $\phi = 1.05\ rad$ to complete crossover at $\phi = 4.04\ rad$. Fig. 4.7 shows that although the phase difference between the two guides is slightly higher than 0 or π, it nevertheless remains constant as ϕ is varied. This result is important, as it illustrates that the 3×3 coupler with feedback can be used as a power divider, even for a transversely asymmetrical device with dissimilar waveguides.

The output characteristics shown in Fig. 4.6 indicate that a 3×3 coupler with feedback can also be used as a sensor. One such configuration is illustrated in Fig. 4.8 where the feedback line is placed in an environ

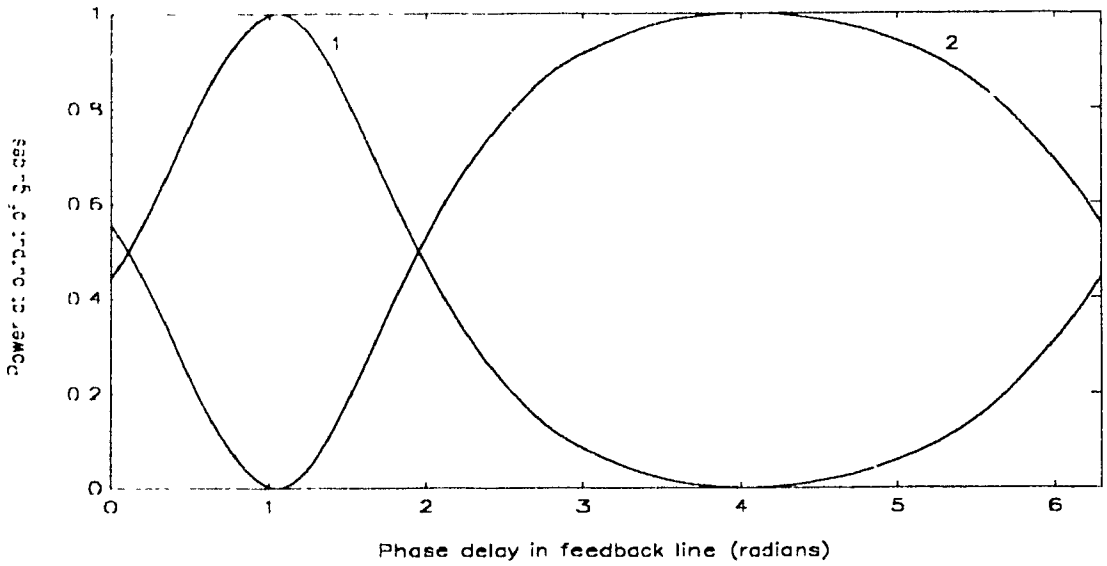

Figure 4.6: Transfer characteristics of a 3 × 3 coupler with feedback with an **R** matrix described by (4.19)

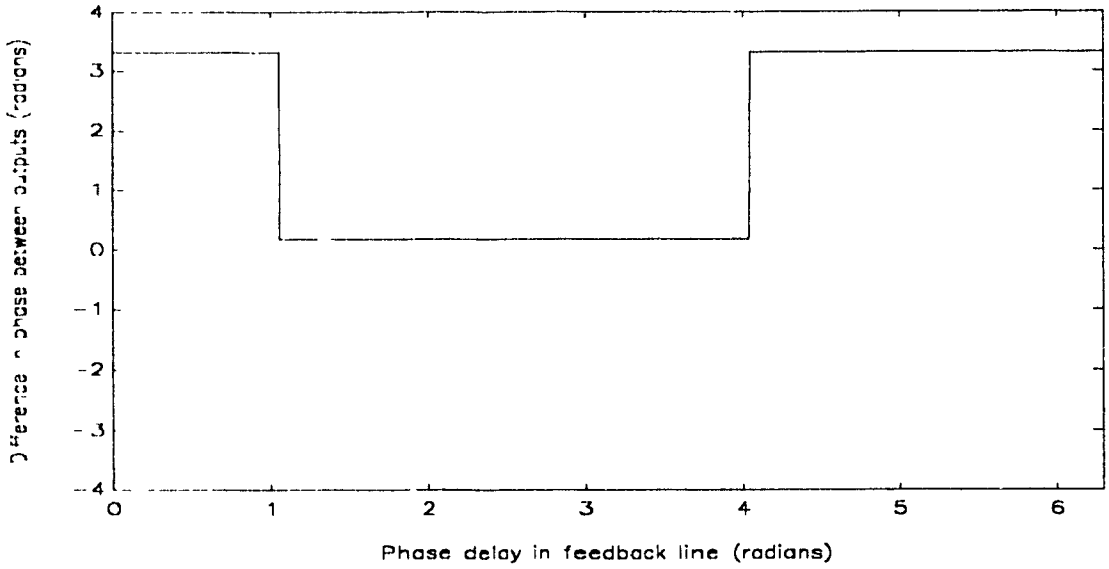

Figure 4.7: Phase difference between ports 1 & 2 for the device characterized in Figure 4.6.

ment of varying temperature. Since the electrical length of the feedback line $\phi = \beta_{fb} L_{fb}$ will be some function of temperature, detectors placed at the output ports of the coupler can be calibrated to measure the temperature variation sensed by the feedback line. Alternatively, the device can also be used as a sensor of large electric field strength, such as that found in the vicinity of high power transmission lines, by placing a fiber coil, serving as a feedback line, close to the high tension wire where the electric field through the electrooptic effect will influence the fiber refractive index and thereby the electrical length (ϕ). One important feature of this device is that since changes can be determined from the ratio of amplitudes exiting from the coupler, the amplitude of the input source (the laser) is not critical and can vary without affecting the results. The performance characteristics of fiber and integrated optical sensors utilizing directional couplers is investigated in [48].

4.3 3×3 coupler with feedback used as a combiner/splitter

In this section the application of the 3×3 coupler with feedback as a power combiner/splitter is discussed. The device is a power combiner when two

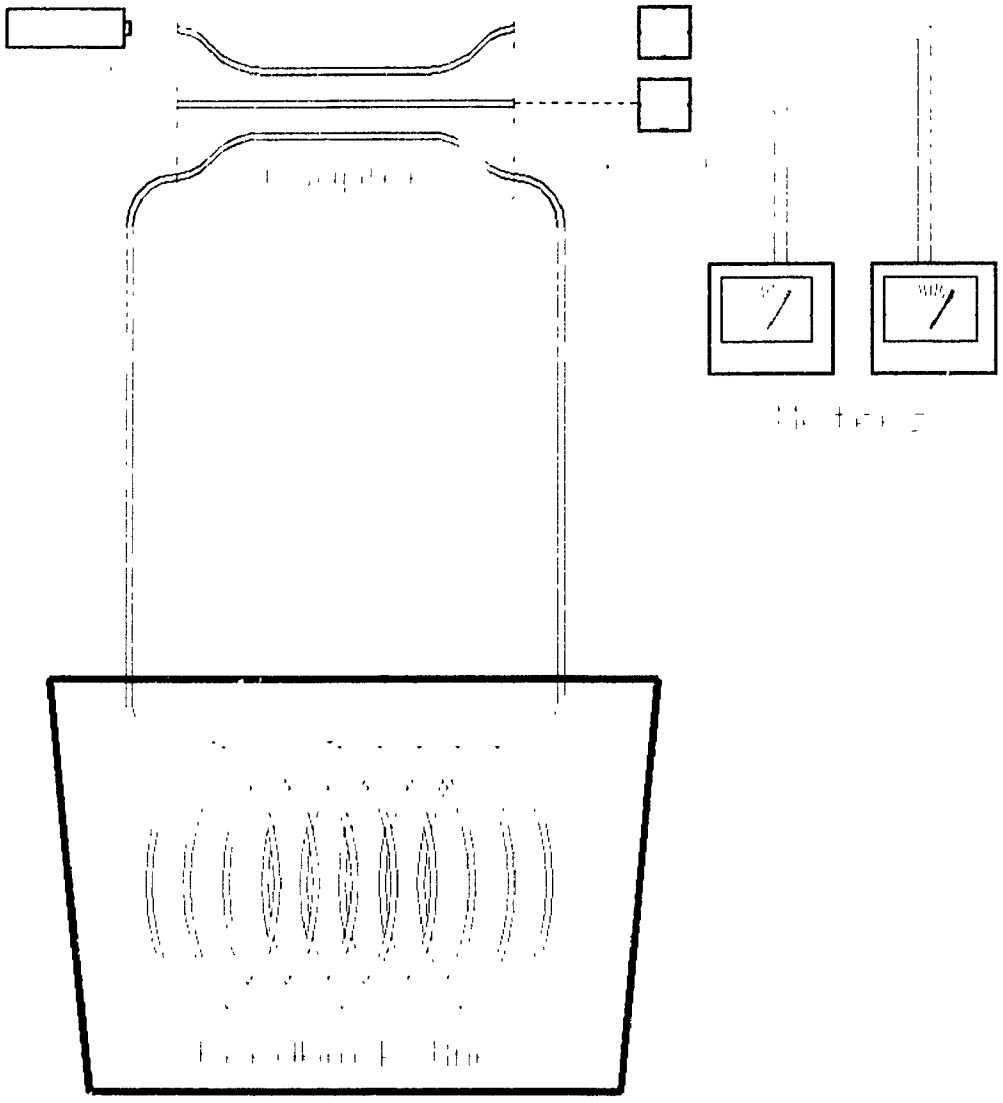

Figure 4.8: The 3 × 3 coupler used in sensor application to monitor changes in temperature.

signals fed into separate input ports exit from only one of the output ports, or it is a splitter when a signal applied to one input port is distributed in some ratio between the two output ports.

Consider the phase matched 3 × 3 device described at the beginning of Section 4.2. The transfer function for the coupler without the feedback loop was expressed by (3.32). Adding the feedback loop and satisfying the requirement $\beta L = 2n\pi$ resulted in the transfer function of (4.6). Choosing $\kappa L = 1.351$ so that $X = \frac{1}{6}$, we now consider the general case where arbitrary inputs are applied to guides 1 and 2. The outputs can be expressed as

$$E_1\left(L|_{X=\frac{1}{6}}\right) = \frac{\frac{1}{3}(1+t)}{1-\frac{1}{3}t}E_1(0) + \frac{\frac{t}{3}(1-t)}{1-\frac{1}{3}t}E_2(0) \qquad (4.20)$$

$$E_2\left(L|_{X=\frac{1}{6}}\right) = \frac{\frac{t^2}{3}(1-t)}{1-\frac{1}{3}t}E_1(0) + \frac{\frac{1}{3}(t-7)}{1-\frac{1}{3}t}E_2(0) \qquad (4.21)$$

This device is called a combiner if the inputs applied to guides 1 and 2 exit guide 2, for example, with zero power available at the output of guide 1. The value of t required for E_1 to equal zero can be found by setting (4.20) to zero and solving for t:

$$t \quad t\exp(\ j\phi) \qquad \begin{matrix} E_1(0) & j2E_2(0) \\ E_1(0) & j2E_2(0) \end{matrix} \tag{4.22}$$

In cases where $E_1(0)$ and $E_2(0)$ are in phase, the magnitude of the right side of (4.22) is unity; thus, a value of ϕ for a lossless feedback line can always be found, namely

$$\phi \quad 2\tan^{-1}\left(2\frac{E_2(0)}{E_1(0)}\right) \pi \tag{4.23}$$

Thus we have illustrated that a change in the ratio of magnitudes at the input may be compensated for by a change in ϕ. This is in contrast with the 3 3 combiner analyzed in Section 3.4 which required input signals of equal magnitude and phase. The characteristics of the combiner with the feedback loop are illustrated in Fig 4.9. The power at the output of guides 1 and 2 is plotted as a function of the phase delay, ϕ, in the feedback line. The arbitrarily chosen input conditions are: $E_1(0)$ .866 and $E_2(0)$ .5. Note that as the phase shift in the feedback line is varied, the ratio of coupled power between the outputs changes. At a phase shift of 4.856 *rad*, the total power in the system is combined and exits at the output of guide 2.

We shall now discuss how the constraint of phase matching the input signals can be eliminated. In the previous example, the requisite phase dif-

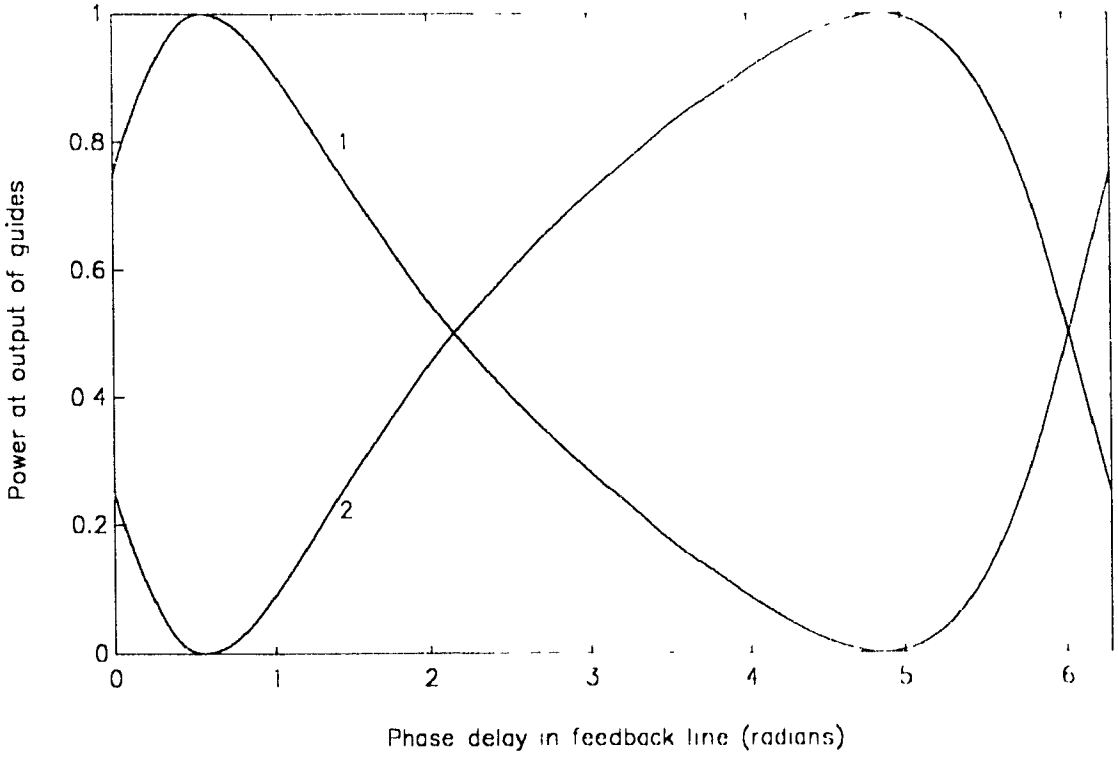

Figure 4.9: Transfer characteristics of a power combiner with $\beta_1 = \beta_2 = \beta_3 = \beta$, $\kappa_{12} = \kappa_{23} = \kappa$, and $\kappa_{13} \approx 0$.

ference between the two inputs was zero. It can be shown numerically that for other cases, a fixed, but not necessarily zero, differential phase between the two inputs is required for signal combining to be achieved. We will discuss how even this restriction on input phase differential can be eliminated by building a device which permits the propagation constant of one of the guides to be varied.

For the general case when the elements of the **R** matrix are arbitrary (κ is

real) and subject only to the condition of losslessness, the output of guide 1 for an arbitrary input can be expressed using the four port transfer function (4.5):

$$E_1(L) = \begin{pmatrix} T_{11} & [T_{11}T_{33} & T_{13}^2]t \\ & 1 & T_{33}t \end{pmatrix} E_1(0) + \begin{pmatrix} T_{12} & [T_{12}T_{33} & T_{23}T_{13}]t \\ & 1 & T_{33}t \end{pmatrix} E_2(0) \tag{4.24}$$

Let us assume all parameters including the length of the device to be fixed, with the exception of the propagation constant, β_1, for guide 1 and the phase shift, ϕ, in the feedback line. The first step in finding a (β_1, ϕ) pair that allows the device to combine the total incident power into guide 2 requires setting $E_1(L)$ in (4.24) to zero and solving for t,

$$t = |t| \exp(-j\phi) \frac{T_{11}E_1(0) + T_{12}E_2(0)}{[T_{11}T_{33} - T_{13}^2]E_1(0) + [T_{12}T_{33} - T_{23}T_{13}]E_2(0)} \tag{4.25}$$

A numerical solution is employed that varies β_1 such that the magnitude of the right side of (4.25) equals the magnitude of t, which, for an assumed lossless system, is unity. Once β_1 is found, the required ϕ to equate the phases of the equation must be calculated. A computer program, B1PHI. M, developed to find the (β_1, ϕ) pair is listed in the Appendix. Computer analyses

of these devices reveal that there exist ranges of coupler length, l, where (β_1, ϕ) points can be found for any input. Thus, this device is capable of combining two signals of arbitrary magnitude and arbitrary phase. Changes in either magnitude or phase can be compensated for by adjusting β_1 and ϕ. An extremely desirable feature of this device is that it can tolerate large deviations in propagation constants, coupling coefficients and device length, which often occur due to errors in the fabrication process, by compensating for them through varying β_1 and ϕ.

The following example illustrates these results using the Ti indiffused 3×3 coupler described in Section 3.5 with a coupling matrix described by (3.76) and an arbitrarily chosen device length of L 3 mm. The program finds the (β_1, ϕ) pair(s) that satisfy complete transfer of the arbitrarily chosen inputs $E_1(0)$ .5/35.5° and $E_2(0)$ .866/ 149.0°. Two results were found, but the least detuning corresponds to a change of the propagation constant of $\Delta\beta_1$ β_1 β_o 83.34 m^{-1} and ϕ 1.79 rad. Fig. 4.10 illustrates the power in both guides of the combiner as a function of ϕ, for a fixed $\Delta\beta_1 = 83.34\ m^{-1}$.

The corresponding voltage required to detune the first guide can be determined by substituting $\Delta\beta_1$ 83.34 m^{-1} and the operating wavelength λ_o .63 μm, into (3.84), resulting in V 50.27 mV.

As discussed earlier, the phase shift, ϕ, of the feedback line can be varied

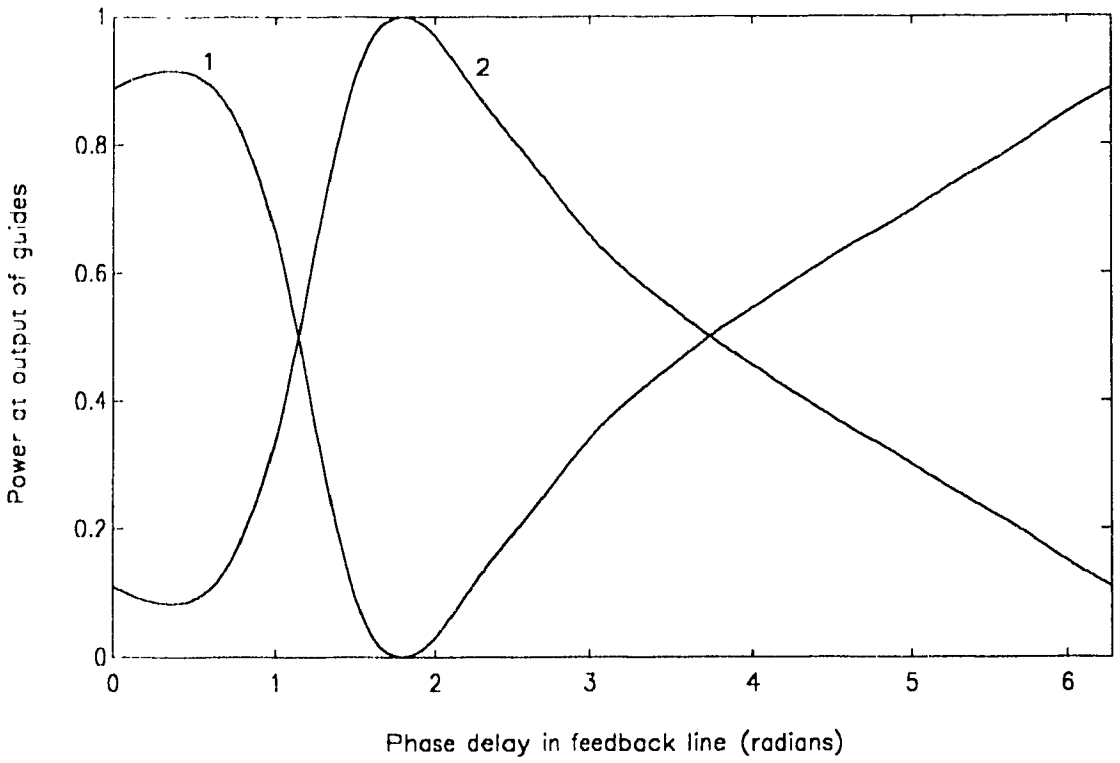

Figure 4.10: Transfer characteristics of a power combiner with **R** given by (3.76)

using the electrooptic effect by applying a voltage across electrodes placed on the feedback line. The voltages required to detune the feedback line can be determined by considering the relationship between the change in the refractive index of the feedback loop, n_g, described by (3.82), and the change in the phase shift of the feedback line,

$$\Delta\phi = \omega\sqrt{\mu_0\epsilon_0}\Delta n_g L_{electrode} \tag{4.26}$$

where $L_{electrode}$ is the length of the electrode. The voltage required to induce a $\pm\pi$ phase shift in the feedback loop can be determined by substituting (3.82), (3.83) and (4.26) into (3.84) with $\Delta\phi = \pm\pi$. The result is

$$V_\pi = \frac{\lambda_o d}{n_q^3 r L_{electrode}} \tag{4.27}$$

For this case, the voltage required to vary the phase shift in the feedback loop from 0 to 2π is 1.263 V. For detuning electrodes of length, $L_{electrode} = 3\ mm$, the necessary detuning voltage to set the phase shift in the feedback line to $\phi = 1.79\ rad$ is 361.0 mV. Once built, this device can combine two arbitrary signals. Note that as the magnitude or phase of either of the inputs changes, so does the required (β_1, ϕ) pair.

Fig. 4.11 shows the tuning characteristic of the device analyzed above. The abscissa indicates the voltages used to induce the phase shift in the feedback line, on the ordinate is the voltage used to detune the first guide. Contour lines indicate regions of equal power in Guide 2. Two points of maximum power where the signal is combined into guide 2 are indicated by asterisks. One point corresponds to the detuning voltages that achieved the (β_1, ϕ) pair calculated by the computer program. The second point corresponds to $\Delta\beta_{1,2} = -1700.0\ m^{-1}$, $\phi = 1.050\ rad$ and the resulting $V_2 = 1.025V$,

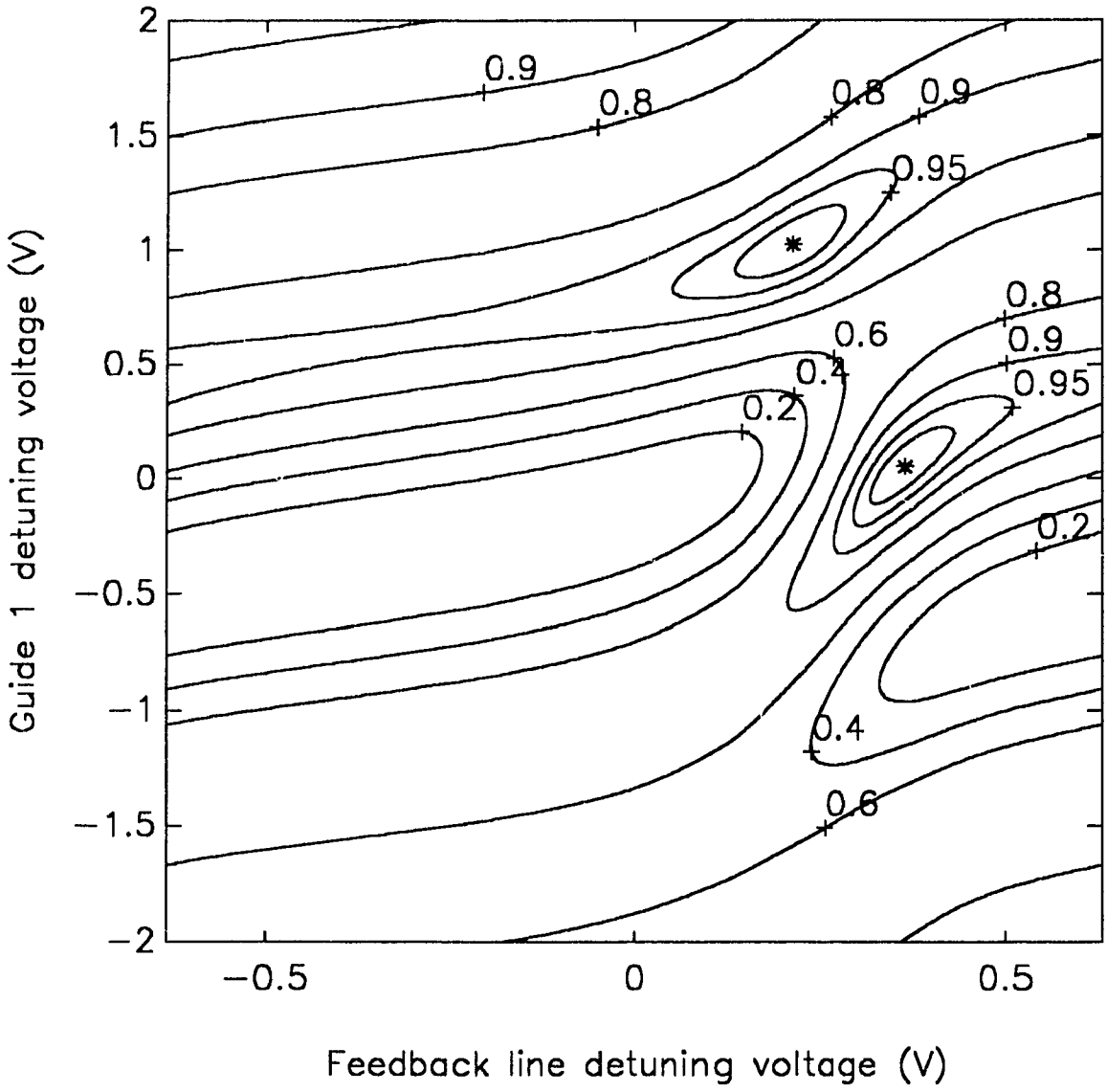

Figure 4.11: Tuning characteristics of a power combiner for $\bar{E}(0) = [0.5 < 35.5^{\circ} \quad 0.866 < -149.0^{\circ}]^{t}$. Curves represent points of equal power in guide 2; maximum power is denoted by an asterisk.

$V_0 = 211.1\ mV$. Note that as the ratio of magnitudes or difference in phase between the two input signals varies, the point where all the power combines will shift on the graph. This change must be compensated for by a change in the two detuning voltages, that in turn induce a change in $\Delta\beta_1$ and ϕ. A similar analysis can be effected using a coupler that is not transversely symmetric.

4.4 Wavelength dependence of a 3×3 coupler with feedback

This section examines the wavelength dependence of a 3 × 3 coupler with feedback and its usefulness as a wavelength selective filter and wavelength division multiplexer.

The phase delay of the feedback loop around guide 3 of the coupler portrayed in Fig. 3.10 is

$$\phi = \beta_{fb} L_{fb} \tag{4.28}$$

where L_{fb} is the length of the feedback loop and β_{fb} is the propagation constant of the waveguide that comprises the loop. If the feedback loop

is implemented by the same Ti-indiffusion process as the coupler and its width is identical to that of the waveguides in the coupler, then its propagation constant will be identical to those of the individual lines of the coupler (i. e. $\beta_o \quad \beta_{fb} \quad \beta$).

The length of the coupler and the phase delay incurred in the feedback line that are required so that a 3 × 3 coupler with feedback remains in the bar state (no transfer between guides 1 and 2) can be obtained using the program ZPIII. M that was described in Section 4.2. For the case of the coupler portrayed by Fig. 3.10, whose **R** matrix at $\lambda_o = 0.63\ \mu m$ was given in (3.76), the requisite parameters are $L = 3.536\ mm$ and $\phi = 0.691 + 2n\pi\ rad.$ The wavelength dependence of this device can be studied by examining the transfer function of the device as the wavelength is varied, while holding all other parameters fixed. Fig. 4.12 illustrates the output of guide 1 as a function of wavelength deviation from $\lambda_o = 0.63\ \mu m$. An input of $E(0) = [1 \ \ 0]'$ was applied. The results were obtained by recalculating the coupling matrix, using the method outlined in Section 3.5, for each wavelength. Points of zero power transfer into guide 2 occur periodically about the bias point $\Delta\lambda \quad 0$. This characteristic demonstrates the potential use of this device as a wavelength division multiplexer. For example, if the input to guide 1 consisted of signals with two wavelengths, $\lambda = 0.63\ \mu m$ and $\lambda = 0.63001\ \mu m$, then the former would exit from guide 1 and the latter from guide 2.

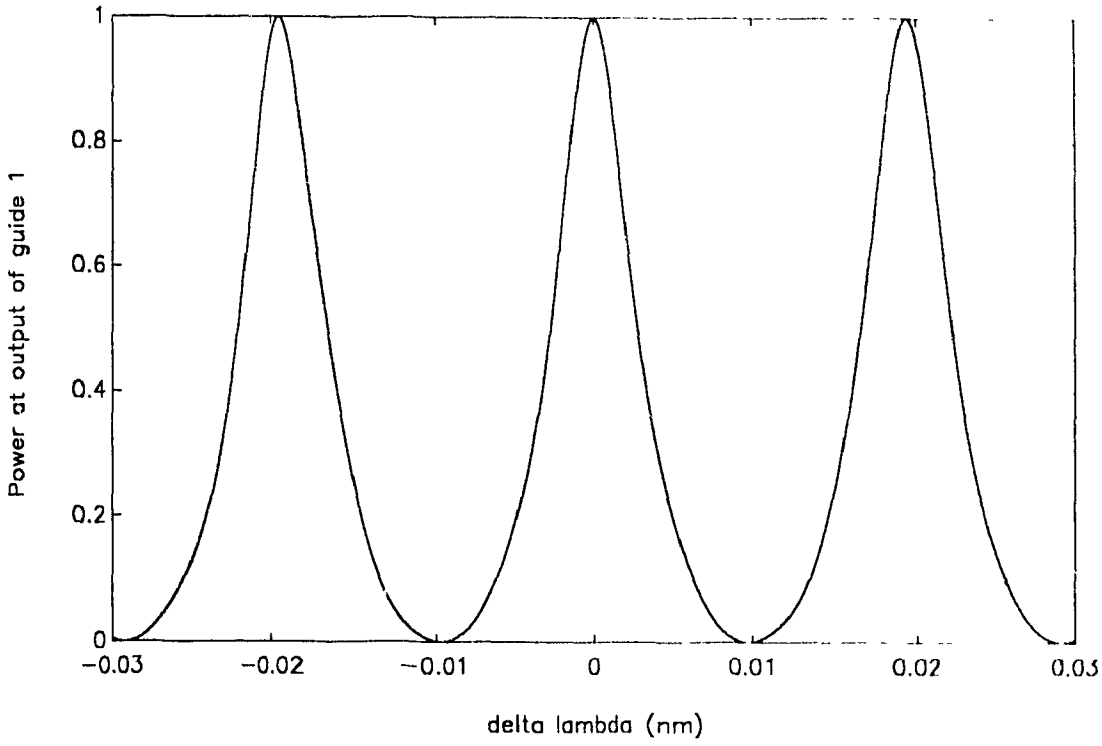

Figure 4.12: Wavelength dependence of the 3 × 3 coupler with feedback.

The quality of a comb filter is often assessed by its finesse, which is the free spectral range divided by the FWHM bandwidth. The free spectral range is defined as the wavelength separation of the transmission peaks. The characteristic of a comb filter with high finesse has narrow transmission peaks that are widely separated.

The finesse of the 3 × 3 coupler with feedback examined above can be increased dramatically if the separation between guides 2 and 3 is increased,

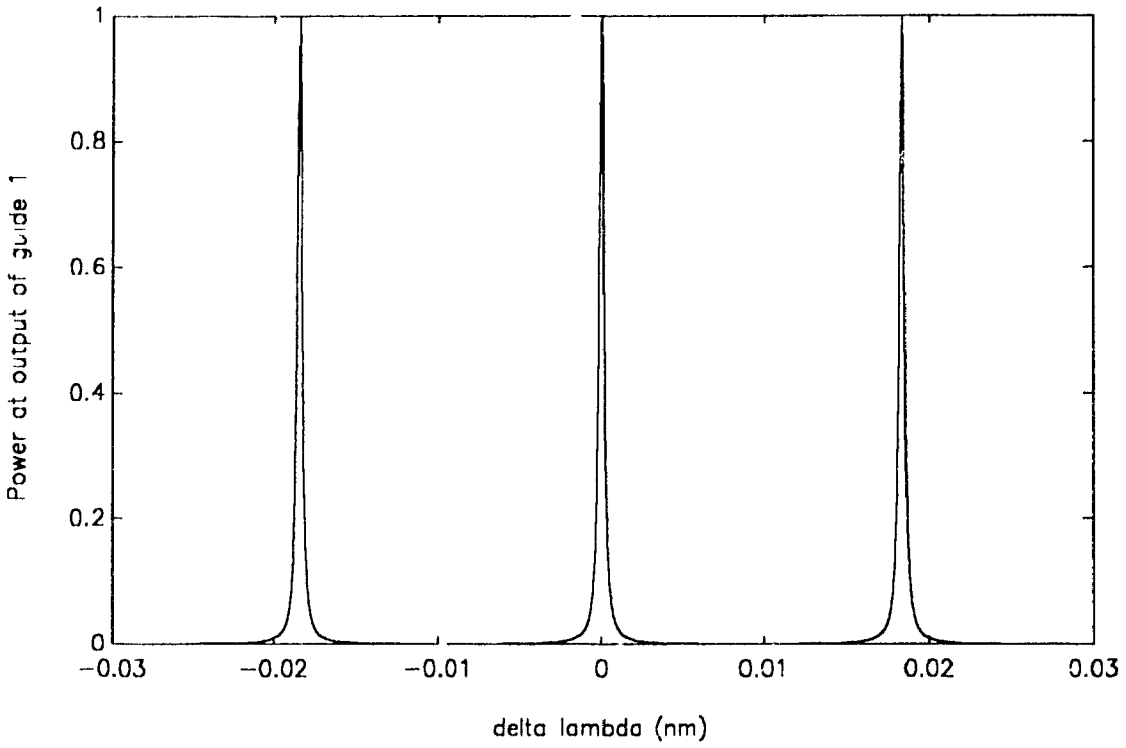

Figure 4.13: Wavelength dependence of the 3 × 3 coupler with increased separation between guides 2 and 3 .

e. g. from $s_{23} = 3\ \mu m$, as shown in Fig. 3.10, to $s_{23} = 4\ \mu m$. For this latter case, $L = 4.071\ mm$ and $\phi = 3.375\ rad$ are required for an input signal of $\lambda_0 = 0.63\ \mu m$ applied to guide 1 to exit completely from the same guide. The transfer characteristic of the modified device is illustrated in Fig. 4.13. The graph depicts that a small decrease in the spectral range and a large decrease in the bandwidth occurred, resulting in a increase in the finesse by approximately 15.

We shall now discuss the results depicted by Figs. 4.12 and 4.13 The free spectral range of this device is, to a very good approximation, given by

$$\Delta\lambda \quad \frac{\lambda^2}{n_{eff} L_{total}} \tag{4.29}$$

where L_{total} is the sum of the lengths of the coupler and the feedback line. n_{eff} is the effective refractive index of the guides given by

$$n_{eff} \quad \frac{\beta\lambda_o}{2\pi} \tag{4.30}$$

The bandwidth of each resonance is inversely proportional to the loaded quality factor of the resonator, Q_L. To increase the finesse one must either increase the Q_L, or decrease L_{total}, or both. The Q_L can be increased by reducing the coupling between the resonating guide and the rest of the coupler by increasing the separation s_{23}. This causes a significant narrowing of the bandwidth, but also necessitates a slight readjustment of the length of the coupler in order to maintain zero power transfer at the bias wavelength λ_o.

Finally, Fig. 4.14 demonstrates that the bias point of these filters or multiplexers can be moved by adjusting the phase delay in the feedback line. The figure depicts the same situation as Fig. 4.12, except that different values of ϕ were used. The characteristics are plotted with three different values

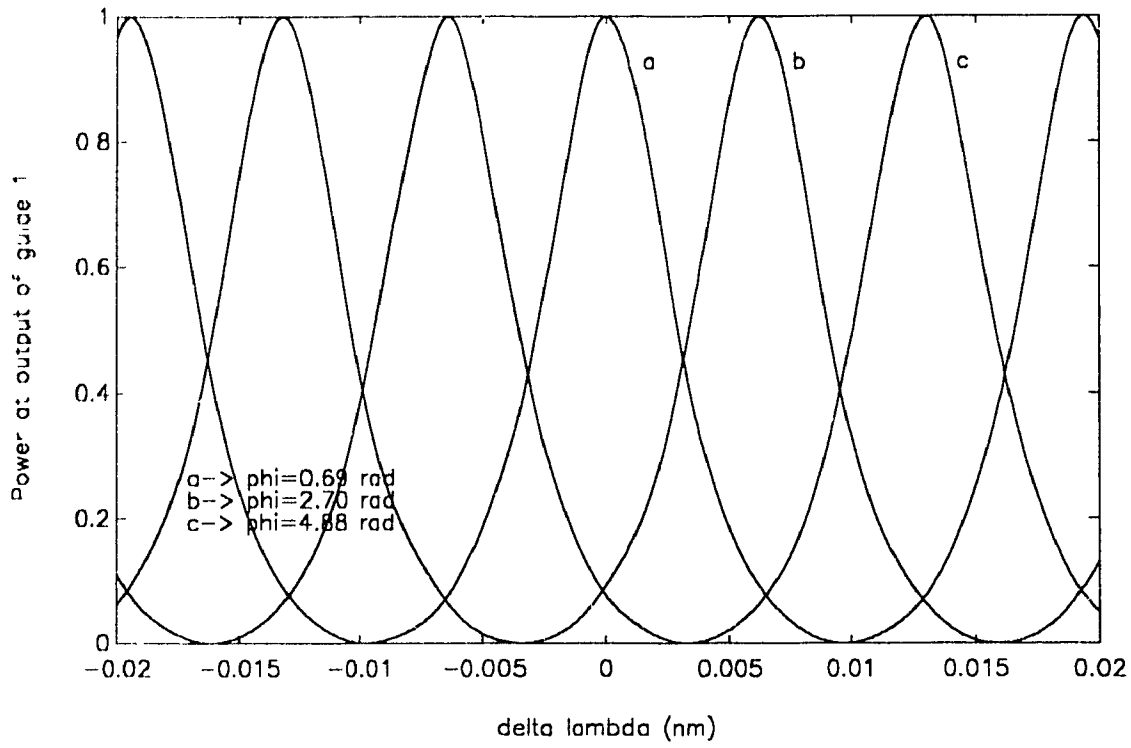

Figure 4.14: Wavelength dependence of the 3×3 coupler with varying phase delay in the feedback line.

of ϕ on the same graph. The first $\phi = 0.69\ rad$ illustrates the bias point at λ_o 0.63 μm. The other two curves, plotted with $\phi = 2.70\ rad$ and ϕ 1.88 rad show that the bias point can be shifted to either a higher or lower wavelength.

Chapter 5

$N \times N$ couplers

5.1 Introduction to $N \times N$ couplers

In this chapter we discuss how the analysis of two and three guide couplers can be extended to encompass devices containing an arbitrary number of coupled waveguides. Other methods of transferring power among N waveguides are discussed in [49,50]. It is demonstrated how the technique of eigensolution decomposition can be used to obtain specific transfer characteristics. Design examples are provided of interferometers, as well as of couplers capable of complete power transfer between designated channels.

5.2 Analysis of $N \times N$ couplers

Equation (2.13) can be used to describe, in matrix form, the complex amplitudes in N coupled waveguides. For the case of N guides, $E(z)$ is a column vector of length N containing the complex amplitudes of the signals. The coupling matrix is

$$\mathbf{R}_N = \begin{bmatrix} \beta_1 & \kappa_{12} & \kappa_{13} & \cdots & \kappa_{1N} \\ \kappa_{12} & \beta_2 & \kappa_{23} & \cdots & \kappa_{2N} \\ \kappa_{13} & \kappa_{23} & \beta_3 & & \kappa_{3N} \\ \vdots & \vdots & & \ddots & \\ \kappa_{1N} & \kappa_{2N} & \kappa_{3N} & \cdots & \beta_N \end{bmatrix} \tag{5.1}$$

and the terminal parameters of the coupler are related by the linear transformation given by (2.15). If the system is nondegenerate, it will consist of N distinct eigenvalues, and an arbitrary input excitation can be decomposed into the N eigenvectors, i. e. any excitation can be represented as a linear combination of the eigensolutions. For the general input excitation of

$$\begin{bmatrix} E_1(0) \\ E_2(0) \\ \vdots \\ E_N(0) \end{bmatrix} \quad \mathbf{U} \begin{bmatrix} c_1 \\ c_2 \\ \vdots \\ c_N \end{bmatrix} \tag{5.2}$$

the output of the coupler is

$$\begin{bmatrix} E_1(z) \\ E_2(z) \\ \vdots \\ E_N(z) \end{bmatrix} = \mathbf{U} \begin{bmatrix} \exp(-j\beta_1 z) & 0 & \cdots & 0 \\ 0 & \exp(-j\beta_2 z) & \cdots & 0 \\ \vdots & \vdots & \ddots & \vdots \\ 0 & 0 & \cdots & \exp(-j\beta_N z) \end{bmatrix} \begin{bmatrix} c_1 \\ c_2 \\ \vdots \\ c_N \end{bmatrix} \tag{5.3}$$

where $\mathbf{U}$ is an $N \times N$ matrix consisting of the eigenvectors of the system and the c_i's are the modal amplitudes, or weight coefficients that are determined from the initial condition of the system. Substituting the inverse of (5.2) into (5.3) results in the transfer matrix of the $N \times N$ coupler, namely

$$\mathbf{T}(z) = \mathbf{U}\mathbf{P}_{\mathbf{T}}(z)\mathbf{U}^t \tag{5.4}$$

where $\mathbf{P}_{\mathbf{T}}(z)$ is the diagonal matrix whose elements are $\exp(-j\beta_i z)$, $i = 1$ *to* N.

5.3 Coupling coefficients for a given power distribution

Haus and Molter-Orr have empirically developed the relationships between coupling coefficients required to design $N \times N$ couplers capable of complete

power transfer between outside guides [51,52,53]. For the case of couplers containing an odd number of waveguides, they have also developed the relationships between the coupling coefficients required to build an interferometer, which is a device that is capable of splitting an input signal into two signals of identical magnitude and phase. In this section, the technique of eigensolution decomposition will be used to verify their findings using the example of a 4 × 4 coupler. It will also be shown that the eigensolution method leads to alternate, undocumented, solutions, and demonstrates how an interferometer can be built using a coupler with an even, as well as an odd number of waveguides.

The general N guide coupler considered by Haus and Molter-Orr is illustrated in Fig. 5.1. Following their example, we shall assume that the device exhibits transverse symmetry, and only the coupling between adjacent guides is considered. Equations that allow the determination of the ratios of coupling coefficients required to transfer power between outside guides were described in [51] by the expression

$$\kappa_n^2 = Nn - n^2 \tag{5.5}$$

and the ratios of coefficients required to build an interferometer were given as

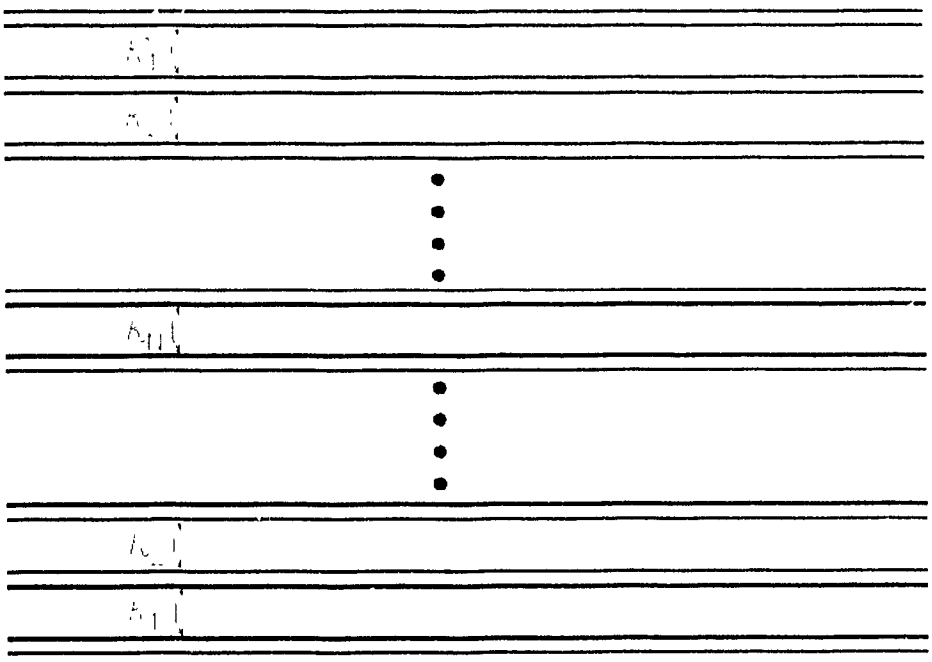

Figure 5.1: Schematic of a $N \times N$ coupler.

$$\kappa_n^2 \quad (N+1)n \quad 2n^2 \tag{5.6}$$

The convention assigns κ_1 to be the coupling coefficient between the outer most guides and their adjacent guides, as depicted by Fig. 5.1.

Applying the Haus and Molter-Orr method to a 4×4 coupler, (5.5) yields $\kappa_2/\kappa_1 = 2/\sqrt{3}$. This solution can be verified using the technique of

eigensolution decomposition. The reduced coupling matrix of this four guide coupler is

$$\mathbf{R}_{reduced} \quad \begin{bmatrix} 0 & \kappa_1 & 0 & 0 \\ \kappa_1 & 0 & \kappa_2 & 0 \\ 0 & \kappa_2 & 0 & \kappa_1 \\ 0 & 0 & \kappa_1 & 0 \end{bmatrix} \tag{5.7}$$

Four eigenwaves will rotate in this device at the rate of their corresponding eigenvalues. The eigenvalues are given by

$$p_1 \; - \; p_3 \; - \; \frac{\kappa_2}{2}(u \; + \; 1) \tag{5.8}$$

and

$$p_2 \; - \; p_3 \; = \; \frac{\kappa_2}{2}(u \; - \; 1) \tag{5.9}$$

where

$$u \quad \sqrt{1 \; + \; 4\frac{\kappa_1^2}{\kappa_2^2}} \tag{5.10}$$

Fig. 5.2 illustrates the eigensolutions for the 4×4 coupler. As in Section 3.5, the clocks represent the complex amplitude of each of the modes in each

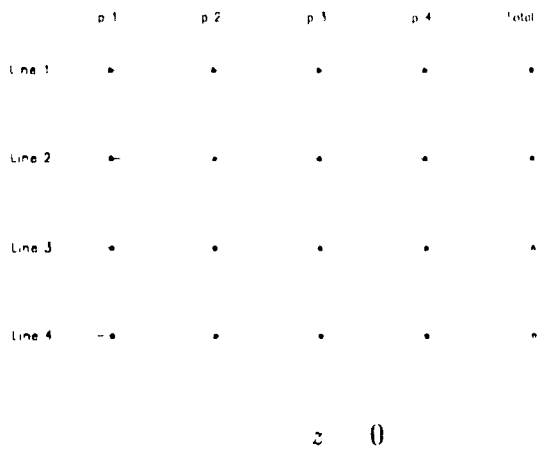

$z = 0$

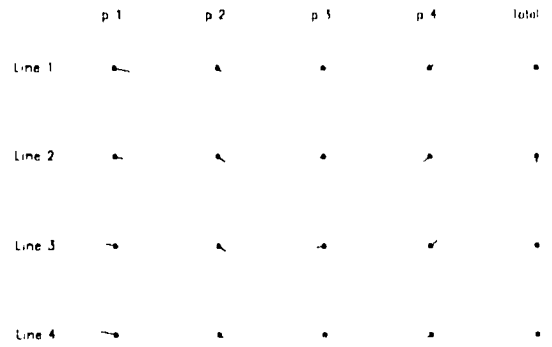

$z \ll \pi/2p_1$

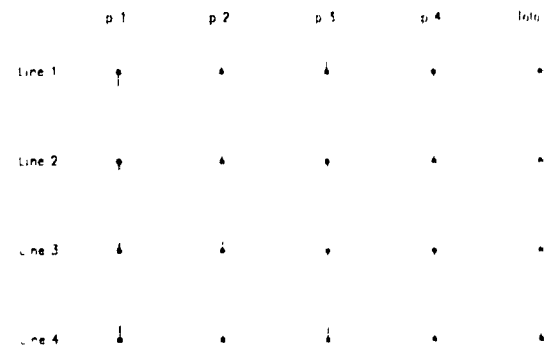

$z = \pi/2p_1 \quad 3\pi/2p_2$

Figure 5.2: Eigensolutions of a 4×4 coupler with $\kappa_2/\kappa_1 = 2/\sqrt{3}$

of the waveguides. The clocks in the right column represent the sum of the modes in each row corresponding to the amplitude and phase of the signal at position z. The eigensolutions for the modes at the input of the device are shown at the top of the figure. The eigensolutions after they have travelled a small distance z such that $z \ll \pi/2p_1$ are shown at the center, indicating the sense of rotation. Examination of the graphical representation of the eigensolutions reveals that they can be forced to cancel out in all guides, except the fourth, when the modes corresponding to p_2 and p_1 rotate by $\mp 3\pi/2$, and those corresponding to p_1 and p_3 rotate by $\mp\pi/2$. Determining the coupling coefficients, κ_1 and κ_2, are achieved by setting $p_2 = 3p_1$ and solving (5.8) and (5.9) for the required ratio. As expected, the result is $\kappa_2/\kappa_1 = 2/\sqrt{3}$. The length of the device that is necessary for complete transfer of power is found by setting

$$\exp(-jp_1 z) = \exp(-j\pi/2) \tag{5.11}$$

Thus, a device with a coupling ratio of $\kappa_2/\kappa_1 = 2/\sqrt{3}$ achieves the goal of transferring all power from guide 1 into guide 4 after propagating a distance of $z = \pi/2p_1 = 3\pi/2p_2$. This result is illustrated at the bottom of Fig. 5.2. A better illustration of how the power is distributed along the length of this device is provided in Fig. 5.3, where the power in each guide is plotted as a

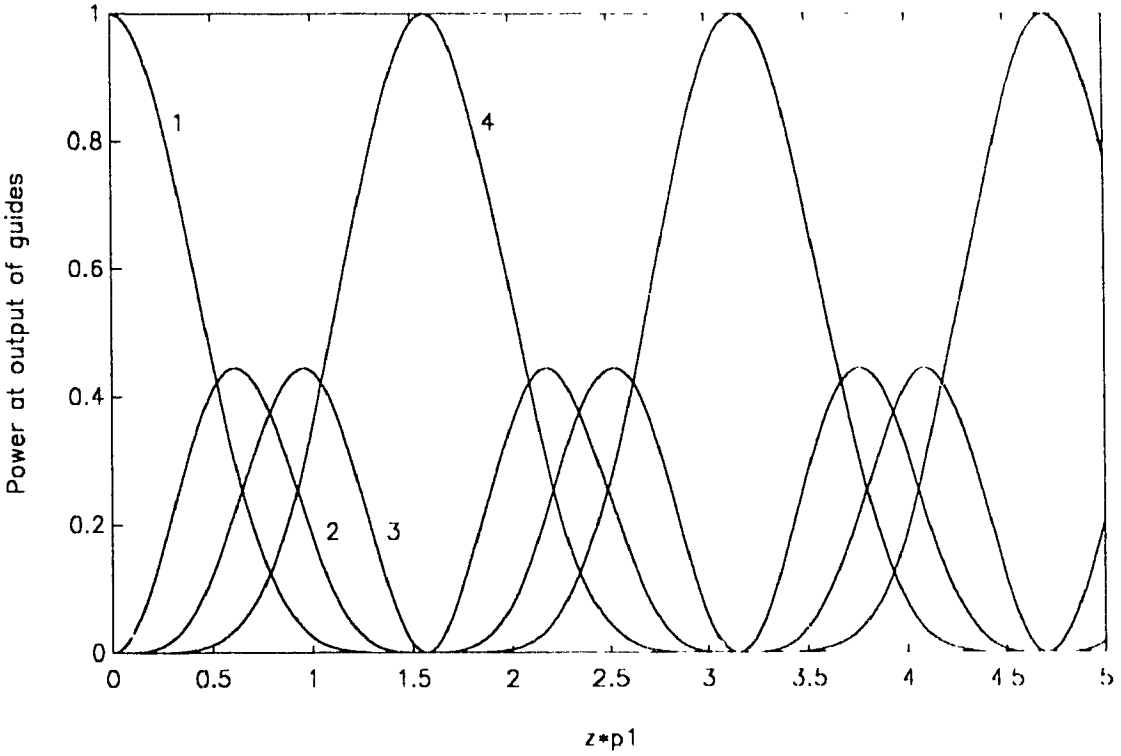

Figure 5.3: Transfer characteristics of a 4 × 4 coupler with $\kappa_2/\kappa_1 = 2/\sqrt{3}$.

function of device length.

Although the ratio of coupling coefficients calculated above achieves the desired goal, closer examination of the eigensolutions in Fig. 5.2 reveals that other solutions also exist. For example, coupling ratios that force the eigen solutions corresponding to p_2 and p_4 to rotate $\pm(4n-1)\pi/2$ while those corresponding to p_1 and p_3 to rotate $\pm\pi/2$ can be found. This results in $\kappa_2/\kappa_1 = 2/\sqrt{3}, 6/\sqrt{7}, 10/\sqrt{11}$ for $n = 1,2,3$ respectively. Fig. 5.4 illustrates

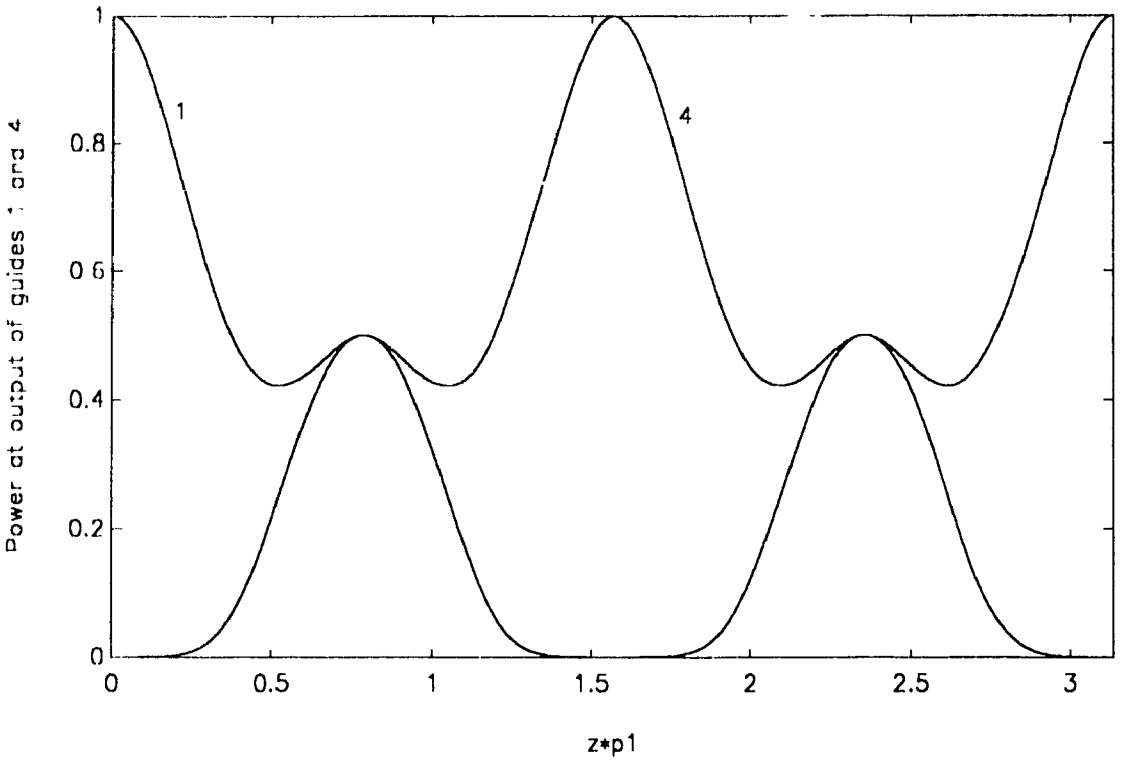

Figure 5.4: Transfer characteristics of a 4×4 coupler with $\kappa_2/\kappa_1 = 6/\sqrt{7}$.

the situation where p_2 and p_1 are forced to rotate $\pm 7\pi/2$ corresponding to $n = 2$ and $\kappa_2/\kappa_1 = 6/\sqrt{7}$. Although fluctuations occur in the transfer characteristic, it is clear that the goal of complete power transfer between guides 1 and 4 is still achieved. The transfer length is $z = \pi/2p_1 = 7\pi/2p_2$.

Examination of the eigensolutions will show how the four guide coupler can be used as an interferometer. Fig. 5.5(a) illustrates the eigensolutions that result when a signal is applied to guide 1 of a 1×4 coupler at $z = 0$.

The solutions after the signals have propagated a small distance $z = 2\pi / p_1$ is shown in Fig. 5.5(b). If the coupling coefficients were adjusted such that the modes corresponding the p_2 and p_1 rotate by $5\pi/4$ while those corresponding to p_1 and p_3 rotate by $3\pi/4$, then the eigensolutions in guides 1 and 3 would cancel out, leaving signals of equal magnitude at the outputs of guides 2 and 4. This result is illustrated in Fig. 5.5(c) where the signals were split after propagating a distance of $z = 3\pi/4p_1 = 5\pi/4p_2$. This example requires $\kappa_2/\kappa_1 = 2/\sqrt{15}$.

Finally, sections of alternating phase mismatch can be added to an $N \times N$ coupler. This provides the device with the ability to switch states, as well as tune out crosstalk induced by errors in coupling lengths. An analysis of these devices can be found in [52,54].

The method of eigensolution decomposition can be extended to any number of guides. As the number of guides increases, the complexity of closed form analysis grows dramatically, thus emphasizing the importance of graphical analysis. Coupling coefficients consistent with those described by (5.5) and (5.6), as well as others, can be found which aid in the design of interferometers and hybrid couplers.

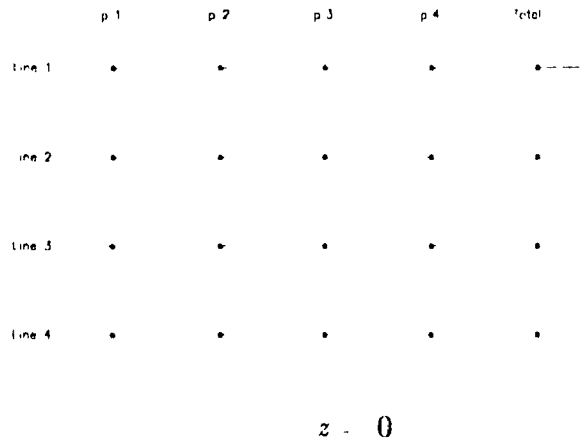

$z = 0$

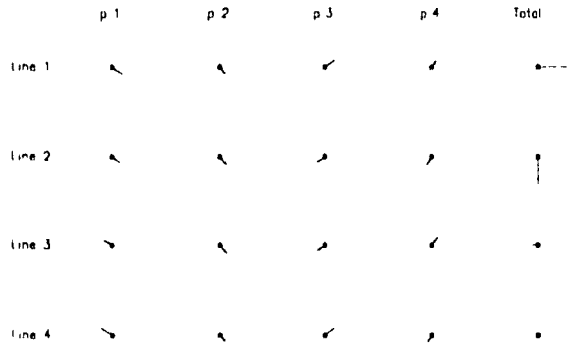

$z \ll 2\pi/p_1$

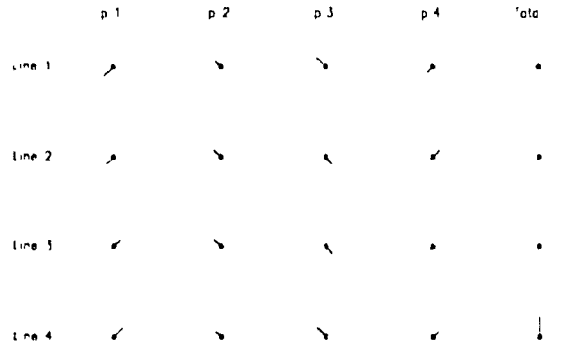

$z = 3\pi/4p_1 = 5\pi/4p_2$

Figure 5.5: Eigensolutions of a 4×4 interferometer with $\kappa_2/\kappa_1 = 2/\sqrt{15}$

Chapter 6

Conclusions

This thesis studied the transfer of power between guided modes of parallel open waveguides. The simple case of the two guide device was used to introduce the basic concepts of directional coupling. It was demonstrated how these devices can act as signal routers by inducing phase mismatches to allow an applied signal to be electrically switched between the crossover and straight-through states. Limitations of 2×2 devices were discussed, including the occurrence of a phase shift between the output signals when power is transferred between the guides.

The basic concepts of two guide couplers were then extended to devices consisting of three channels. Both analytical and numerical solutions for determining the 3×3 system transfer function were determined. The governing equations were cast into matrix form, and the matrices describing the coupling and transfer properties of the device were studied. A computer

program, developed in the course of this work, that graphically traced the eigensolutions of the three guide coupler was used to determine the geometrical and coupling parameters requisite for attaining a specific transfer characteristic. It was found that this method provides a good alternative to employing closed form analysis as it yields the same results but often reduces the complexity of evaluation. The application of the 3×3 coupler as a power combiner and a power divider was introduced, and some of the inherent limitations of 3×3 couplers were discussed. The design and implementation of a 3×3 switch using a three guide coupler with sections of alternating phase mismatch was presented and the six switching states were studied.

We have shown that reducing the 3×3 coupler to a 2×2 device by placing a feedback loop around one of the guides resulted in a device that overcame many of the limitations of both two and three guide couplers. Specifically, it was demonstrated that a 3×3 coupler with feedback is able to transfer any amount of power between two guides, while maintaining a constant phase difference between outgoing signals. Also, it was shown that varying the propagation constant in one of the guides in the 3×3 coupler with feedback allowed two input signals of arbitrary magnitude and phase to be combined. The wavelength dependence of the 3×3 coupler with feedback was also examined, and it was found that this device has the potential of being used as a filter or a wavelength division multiplexer.

Finally, the matrix method used throughout this thesis was extended to include devices with an arbitrary number of waveguides. Methods for determining the coupling coefficients required for the $N \times N$ coupler to act as a hybrid coupler or to transfer power between guides were discussed

Bibliography

1 E. Marcatili, "Dielectric rectangular waveguide and directional coupler for integrated optics," *Bell System Tech. J.*, pp. 2071–2102, Sept. 1969.

2 A. Milton and W. K. Burns, "Mode coupling in tapered optical waveguide structures and electro-optic switches," *IEEE Trans. Circ. and Sys.*, vol. CAS-26, pp. 1020–1028, Dec. 1979.

3 M. Vassel, "A theoretical analysis of mode-mixing in optical waveguides with nearest-neighbour mode coupling," *Opt. Quantum Electron*, vol. 8, pp. 23–30, 1976.

4 J.P. Donnelly, et al., "The extinction ratio in optical two-guide-coupler $\Delta\beta$ switches with asymmetric detuning," *IEEE J. Quantum Electron.*, vol. QE-26, no. 4, pp. 685–691, 1990.

5 S. K. Sheem, "Optical fiber interferometers with $[3 \times 3]$ directional couplers: analysis," *J. Appl. Phys.*, vol. 52, no. 6, pp. 3865–3872, 1981.

6 E. Udd, ed., *Fiber Optic Sensors*. New York: J. Wiley & Sons, 1991.

7 J. R. Pierce, "Coupling modes of propagation," *J. Appl. Phys.*, vol. 25, pp. 179–183, 1951.

8 M. C. Pease, "Generalized coupled mode theory," *J. Appl. Phys.*, vol. 32, pp. 1736–1743, Sept. 1961.

9 A. Yariv, "Coupled-mode theory for guided-wave optics," *IEEE J. Quantum Electron.*, vol. QE-26, pp. 919–933, Sept. 1973.

10 H. Kogelnik and C. V. Shank, "Coupled-wave theory of distributed feedback lasers," *J. Appl. Phys.*, vol. 43, pp. 2327–2335, May 1972.

[11] H. Kogelnik and R. V. Schmidt, "Switched directional couplers with alternating $\Delta\beta$," *IEEE J. Quantum Electron.*, vol. QE 12, pp. 396 401, July 1976.

[12] H. Haus and C. Fonstad, "Three-waveguide couplers for improved sampling and filtering," *IEEE J. Quantum Electron.*, vol. QE 17, no. 12, pp. 2321 2325, 1981.

[13] R. Priest, "Analysis of fiber interferometer utilizing 3 3 coupler," *IEEE J. Quantum Electron.*, vol. QE-18, no. 10, pp. 1601 1603, 1982.

[14] N. Tsukada, R. Tsujinishi, and K. Tomishima, "High efficiency coupling between phase-mismatched optical waveguides," *J. Appl. Phys.*, vol. 50, no. 7, pp. 4611 4615, 1979.

[15] S. Liping and Y. Peida, "General analysis of 3 3 optical fiber directional couplers," *Microwave Opt. Technol. Lett.*, vol. 2, pp. 52 54, 1989.

[16] E. Gottwald and J. Pietzsch, "Measurement method for the determination of optical phase shifts 3 · 3 fiber couplers," in *Proc. 12th Australian Cnf. Optical Fiber Tecnology*, pp. 197 200, 1987.

[17] H. Huang and C. Hung-Chun, "Vector coupled mode calculation of guided vector modes on an equilateral three core optical fiber," *IEEE Microwave and Guided Wave Letters*, vol. 1, pp. 57 59, March 1991.

[18] M. O. van Deventer, "Phase-diversity hybrid optimization in case of a two-detector receiver," *IEEE Photonics Tech. Lett.*, vol. 4, no. 9, pp. 1060 1062, 1992.

[19] S. K. Sheem, "Fiber-optic gyroscope with 3 · 3 directional coupler," *Appl. Phys. Lett.*, vol. 37, no. 10, pp. 869 871, 1980.

[20] W. Burns and A. Milton, "3 × 2 channel waveguide gyroscope couplers:theory," *IEEE J. Quantum Electron.*, vol. QE 18, no. 10, pp. 1790 1796, 1982.

[21] L. Solymar, "Some properties of three coupled waves," *IRE Trans. on Microwave Theory and Tech.*, pp. 284 291, May 1960.

[22] K. Iwasaki, S. Kurazono, and K. Itakura, "The coupling of modes in three dielectric slab waveguides," *Electronics and Communications in Japan*, vol. 58 C, no. 8, pp 100 108, 1975.

[23] J. P. Donnelly, N. DeMeo, and G. Ferrante, "Three-guide optical couplers in GaAs," *J. Lightwave Tech.*, vol. LT-1, no. 2, pp. 417-424, 1983.

[24] J. P. Donnelly, H. Haus, and N. Whitaker, "Symmetric three-guide optical coupler with nonidentical center and outside guides," *IEEE J. Quantum Electron.*, vol. QE-23, no. 4, pp. 401 406, 1987.

[25] J. P. Donnelly, "Limitations of power-transfer efficiency in three-guide optical couplers," *IEEE J. Quantum Electron.*, vol. QE-22, no. 5, pp. 610 616, 1986.

[26] R. R. A. Syms, "Resonant cavity sensor for integrated optics," *IEEE J. Quantum Electronics*, vol. QE-21, no. 4, pp. 322 328, 1985.

[27] H. A. Haus, W. P. Huang, S. Kawakami, and N. A. Whitaker, "Coupled-mode theory of optical waveguides," *J. Lightwave Tech.*, vol. LT-5, pp. 16 23, Jan. 1987.

[28] A. Hardy and W. Streifer, "Coupled mode theory of parallel waveguides," *J. Lightwave Tech.*, vol. LT-3, pp. 1135-1146, Oct. 1985.

[29] S. Chuang, "Application of the strongly coupled-mode theory to integrated optical devices," *IEEE J. Quantum Electron.*, vol. QE-23, pp. 499 509, May 1987.

[30] R. Peall and R. Syms, "Scalar strong coupled mode theory for slowly-varying waveguide arrays," *Optics Communications*, vol. 67, no. 6, pp. 421 421, 1988.

[31] R. Syms and R. Peall, "Explanation of asymmetric switch response of three arm directional couplers in $Ti : LiNbO_3$ using strong coupling theory," *Optics Communications*, vol. 66, no. 5,6, pp. 260-264, 1988.

[32] R. Peall and R. Syms, "Comparison between strong coupling theory and experiment for three-arm directional couplers in $Ti : LiNbO_3$," *J. Lightwave Tech.*, vol. 7, no. 3, pp. 510 554, 1989.

[33] R. Peall, "Further evidence of strong coupling effects in three arm $Ti : LiNbO_3$ directional couplers," *IEEE J. Quantum Electron*, vol. 25, no. 4, pp. 729-735, 1989.

[34] D. Lee, *Electromagnetic Principles of Integrated Optics*. New York: John Wily & Sons, 1986.

[35] M. C. Pease, ed., *Methods of Matrix Algebra*. New York: Academic Press, 1965.

[36] L. Storch, "The transmission matrix of N alike cascaded networks," *AIEEE*, no. 1, pp. 616-618, 1955.

[37] M. C. Pease, "Conservation laws of uniform linear homogeneous systems," *J. Appl. Phys.*, vol. 31, pp. 1988-1996, Nov. 1960.

[38] R. Kersten, "Phase sensitivity of directional couplers," *Optics Communications*, vol. 36, no. 6, pp. 444-448, 1981.

[39] R. V. Schmidt and R. C. Alferness, "Directional coupler switches, modulators, and filters using alternating $\Delta\beta$ techniques," *IEEE Trans. Circ. and Sys.*, vol. CAS-26, pp. 1099-1108, Dec. 1979.

[40] J. Pietzsch, "Scattering matrix analysis of 3 - 3 fiber couplers," *J. Lightwave Tech.*, vol. 7, no. 2, pp. 303-307, 1989.

[41] A. W. Snyder, "Coupled-mode theory for optical fibers," *J. Opt. Soc Am.*, vol. 62, pp. 1267-1277, Feb. 1972.

[42] MATLAB is a registered trademark of The MathWorks, Inc., 21 Eliot St., South Natick, MA, 01760-9889.

[43] G. H. Golub and C. F. Van Loan, *Matrix Computations*. Maryland: The John Hopkins University Press, 1989.

[44] R. Alferness, R. Schmidt, and E. Turner, "Characteristics of Ti diffused $LiNbO_3$ optical directional couplers," *Applied Optics*, vol. 18, pp. 4012-4016, Dec. 1979.

[45] H. Ogiwara and H. Yamamoto, "Optical waveguide switch (3 - 3) for an optical switching system," *Applied Optics*, vol. 17, pp. 1182-1186, April 1978.

[46] H. Ogiwara, "Optical waveguide 3 × 3 switch: theory of tuning and control," *Applied Optics*, vol. 18, pp. 510 515, Feb. 1979.

[47] Y. Ja, "Analysis of four-port optical fiber ring and loop resonators using 3 × 3 fiber coupler and degenerate two-wave mixing," *IEEE J. Quantum Electron.*, vol. 28, no. 12, pp. 2749 2757, 1982.

[48] E. Milczarek and O. Schwelb, "Optical sensors for displacement, vibration and refractive index modulation," in *Proc. Canadian Conference on Electrical and Computer Engineering*, pp. 52.3.1 -52.3.4, 1991.

[49] K. Okamoto, et al., "Fabrication of large scale integrated-optic $N \times N$ star couplers," *IEEE Photonics Tech. Lett.*, vol. 4, no. 9, pp. 1032-1034, 1992.

[50] G. Yun and M. Kavehrad, "$N \times N$ passive star coupler using grating degeneration and sandwich structures," *IEEE Photonics Tech. Lett.*, vol. 1, no. 9, pp. 1035 1037, 1992.

[51] H. A. Haus and L. Molter-Orr, "Coupled multiple waveguide systems," *IEEE J. Quantum Electron.*, vol. QE-19, no. 5, pp. 840-844, 1983.

[52] L. Molter-Orr and H. A. Haus, "Multiple coupled waveguide switches using alternating $\Delta\beta$ phase mismatch," *Applied Optics*, vol. 24, no. 9, pp. 1260 1264, 1985.

[53] L. Molter-Orr and H. A. Haus, "Multiple waveguide lens," *Appl. Phys. Lett.*, vol. 45, no. 2, pp. 19 21, 1984.

[54] L. A. Molter-Orr and H. Haus, "$N \times N$ coupled waveguide switch," *Optics Letters*, vol. 9, no. 10, pp. 466 -467, 1984.

Appendix

The following programs were written in MATLAB [42]. Explanations of each are given as part of the preamble.

- CLOCKS. M
- ZPHI. M
- BIPHI. M
- TUNE. M

```
%  PROGRAM CLOCKS.M                Last Revision: April 30, 1992
%
%  This program, described in Sec. 3.4 of the thesis plots the
%  eigensolutions of a 3X3 coupler as the independent variable
(z)
%  is varied.
%
%        Uses - Subprogram PSETUP.M
%             - Function PPOINT.M
%
%
clear
clg
hold on
result=zeros(12,2);
%
global depvarmax depvar depvarmin erpoint
```

```
%

%
% ENTER THE FOLLOWING PARAMETERS
% Enter 'depvar' for the variable to be varied
%
depvarmin=   0                    ; % Independent variable minimum
depvarstep=  pi/sqrt(2)/.25/20    ; % Independent variable step
depvarmax=   pi/sqrt(2)/.25       ; % Independent variable maximum
%
psetup          % Draw setup screen
for depvar=depvarmin:depvarstep:depvarmax
%                                 ;
beta1=0                           ; % The coupling matrix
parameters
beta2=0                           ;
beta3=0                           ;
k12=.25                           ;
k13=0                             ;
k23=.25                           ;
z=depvar                          ; % The device length
Ain=[1;0;0]                       ; % The input
%
%
R=[beta1 k12 k13 ; ...
   k12 beta2 k23 ; ...
   k13 k23 beta3 ];
%
[u,v]=eig(R)       ; % Calculating eigenvals & eigenvecs resp.
c=u^(-1)*Ain       ; % Solving for c's
%
erpoint=1          ; % Erase last point
ppoint(result)     ; %
%
%  Calculate the eigensolutions
for n=1:3
  sol(:,n)=u(:,n)*c(n)*exp(-j*v(n,n)*z);
```

```
end
%
%  Calculate total field in the line
for n=1:3
  total(n)=sum(sol(n,:));
  sol(n,4)=sum(sol(n,1:3)); % storing total in 4th col. of sol
end
%
% Storing values into a matrix to transfer data to plotting prog.
for n=1:3
  for k=0:3
    result(k+4*(n-1)+1,1)=real(sol(n,k+1));
    result(k+4*(n-1)+1,2)=imag(sol(n,k+1));
  end
end
%
erpoint=0       ; % Plot the vectors
ppoint(result)  ;
pause
end ; % end outside loop
hold off
%
%
-----------------------------------------------------------------
%
%   SUBPROGRAM PSETUP          Last Revision: April 30, 1992
%
%
%  This subprogram, used by CLOCKS sets up the circles on the
%  graphics screen where the eigensolutions will be plotted
%
%
global base

axis([0 12.5 0 8.75]),axis('normal')
hold on;
clg
```

```
text(.3,8.7,'p 1');
text(2.8,8.7,'p 2');
text(5.3,8.7,'p 3');
text(10.4,8.7,'Total');
text(-1.5,7.5,'Line 1');
text(-1.5,4.9,'Line 2');
text(-1.5,2.3,'Line 3');

% Setting up the center points for the circles
for k=1:4
 for n=0:2
  base(k+4*n,1)=1+(k-1)*2.5;
  base(k+4*n,2)=7.5-n*2.6;
   if k==4;base(k+4*n,1)=1+k*2.5;end
 end
end
%
% Plotting the center dots
for n=1:12
  plot(base(n,1),base(n,2),'o')
end
%
% Plotting the circles
for a=0:.1:2*pi
  x=real(exp(j*a));
  y=imag(exp(j*a));
  for n=1:12
    plot(base(n,1)+x,base(n,2)+y,'.g')
  end
end
%
%
% Creating the legend
p1=sprintf('Min. = %g',depvarmin);
p2=sprintf('Max. = %g',depvarmax);
text(0,.1,p1,'sc');
```

```
text(.5,.1,p2,'sc');
text(0,0.046,'o','sc');
text(.125,0.046,'o','sc');
text(.375,0.046,'o','sc');
text(.5,0.046,'o','sc');
text(.25,0.046,'o','sc');
%
%
%
---------------------------------------------------------------
%
%
%  FUNCTION PPOINT.M        Last Revision: April 30, 1992
%
%  This function is used by CLOCKS to plot the vectors stored in
%  "result" onto the graphics screen.
%
function ppoint=ppoint(result)
%
% Plot or erase last line
for n=1:12
  if erpoint==0
   plot([base(n,1) result(n,1)+base(n,1)], ...
        [base(n,2) result(n,2)+base(n,2)],'w')
  else
   plot([base(n,1) result(n,1)+base(n,1)], ...
        [base(n,2) result(n,2)+base(n,2)],'i')
end
%
text(depvar/depvarmax*.5,0.05,'.','sc');
end
%
%
***************************************************************
%

%
%  PROGRAM ZPHI.M                Last Revision: May 4, 1992
```

```
%
% This program finds a pair (z,phi) that will result
% in complete crossover
%
clear
% USES - teigb1 to find the z
%      - r33phi to find the phi with the corresponding z
%
clear
%
firstgpi=3 ; % Initial guess for pi
firstgz=1  ; % Initial guess for z
%
%
global beta1 beta2 beta3 k12 k13 k23
%
beta1=1   ; % Coupling matrix parameters
beta2=.9  ;
beta3=.8  ;
k12=1.2   ;
k13=.1    ;
k23=.8    ;
fz=fzero('teigb1',firstgz,1e-14,1); % Find the z
z=fz;
global z;
fphi=fzero('r33phi',firstgpi,1e-8,1);
b1=beta1;b2=beta2;b3=beta3;kk12=k12;kk13=k13;kk23=k23;zz=z;
test=r33phi(fphi);
clc
test
zphi=[z fphi]
%
% ------------------------------------------------------------
%
% FUNCTION TEIGB1                Last Revision: May 4, 1992
%
function teigb1=teigb1(z)
```

```
%
% This function finds a length z where complete crossover
% can occur
%
R=[beta1 k12 k13;k12 beta2 k23 ; k13 k23 beta3];
teig=expm(-j*R*z);
teigb1=abs(teig(1,1)) - abs(teig(1,1)*teig(3,3)-teig(1,3)^2);
%
%
% ------------------------------------------------------------
%
% FUNCTION R33PHI.M                Last Revision: May 4, 1992
%
function r33phi=r33phi(phi)
%
% finds the phi with the corresponding z
%
a(1)=1;
a(2)=0;
x=exp(-j*phi);
%
R=[beta1 k12 k13;k12 beta2 k23 ; k13 k23 beta3];
T=expm(-j*R*z);
ff(3)=(T(1,3)*a(1)+T(2,3)*a(2))/(1-T(3,3)*x);
ff(1:2)=T(1:2,1:3)*[a(1);a(2);ff(3)*x];
r33phi=real(ff(1));
%
% ************************************************************
%

%
% PROGRAM BPHI.M               Last Revision: May 2, 1992
%
% This program finds the beta1-phi pair needed to acheive proper
% combiner properties (i.e. Output only out of guide 2)
%
%   Uses - TFBDB
clear
```

```
global R E1 E z
%
E=[ .5*exp(-j* 62); .866*exp(j*2.6)];
E=E/sqrt(abs(E(1)^2)+abs(E(2)^2));
z=1.8;
R=[8.1 1.2 .3;...    % For R(1,1) enter initial guess value
    1.2 9. .9;...
    .3 .9  8.8];
%
beta1=fzero('tfbdb',R(1,1),1e-14,1)
%
R(1,1)=beta1;
T=expm(-j*R*z);
phi=(E(1)*T(1,1)+E(2)*T(1,2)) / ...
    ((T(1,1)*T(3,3)-T(1,3)^2)*E(1)+...
    (T(1,2)*T(3,3)-T(2,3)*T(1,3))*E(2) );
phi=log(phi)/(-j)+2*pi;
%
clc
beta1
phi
%
% ------------------------------------------------------------
%
%
% FUNCTION TFBDB.M                    Last Revision: May 2, 1992
%
%
function tfbdb=tfbdb(db1)
% This function is used to evaluate the difference
% in magnitudes of equation 4.22
Rp=R;
Rp(1,1)=db1;
T=expm(-j*Rp*z);
tfbdb=abs(     (E(1)*T(1,1)+E(2)*T(1,2)) / ...
      ((T(1,1)*T(3,3)-T(1,3)^2)*E(1)+(T(1,2)*T(3,3)-...
      T(2,3)*T(1,3))*E(2) ))-1;
```

```
%
% ****************************************************************
%

%
%  PROGRAM TUNE.M    Last Revision. May 1, 1992
%
% This program creates a contour plots showing how the
% combiner output given by 4.22
%
%  Uses T2.M
%
clear
nopts=100               ; % number of subdivisions
beta=10:-4/nopts:6      ; % The range of beta1 values
phi=0:2*pi/nopts:2*pi   ; % Phi range
%
beta2=9;
beta3=8.8;
k12=1.2;
k13= .3;
k23=.9;
Ain=[.5*exp(-j*.62);.866*exp(j*2.6)];
Ain=Ain/sqrt(abs(Ain(1)^2)+abs(Ain(2)^2));
z=1.8;
for nnn=1:nopts+1
 for mmm=1:nopts+1
   beta1=beta(nnn);
   phi1=phi(mmm);
%
   e=t2(beta1,beta2,beta3,k12,k13,k23,z,phi1)*Ain;
   eddy(nnn,mmm)=abs(e(2))^2;
 end
end
%
V=[0,.2,.4,.6,.8,.9,.95,.98,1]
%
axis('square')
```

```
cs=contour(eddy,V,phi(1:nopts+1),beta(nopts+1:-1:1));
clabel(cs)
xlabel('Phase delay in feedback line (radians)')
ylabel('Beta 1')
%
% ------------------------------------------------------------------
%
% FUNCTION T2 M          Last Revision: Feb. 12, 1992
%
%  This function evaluates the transfer matix of 3x3
%  coupler reduced by a feedback line
%
function t2=t2(beta1,beta2,beta3,k12,k13,k23,z,phi)
%
x=exp(-j*phi);
%
R=[beta1 k12 k13;k12 beta2 k23 ; k13 k23 beta3];
T=expm(-j*R*z);
t2(1,1)=T(1,1)+T(1,3)^2*x/(1-T(3,3)*x);
t2(1,2)=T(1,2)+T(1,3)*T(2,3)*x/(1-T(3,3)*x);
t2(2,1)=T(1,2)+T(1,3)*T(2,3)*x/(1-T(3,3)*x);
t2(2,2)=T(2,2)+T(2,3)^2*x/(1-T(3,3)*x);
%
% ******************************************************************
%
```